Year : 2014

Fibroblastic Reticular Cells during Immune Response in Activated Lymph Node and Gut Lamina Propria

Yang Chen-Ying

UNIL | Université de Lausanne

Faculté de biologie et de médecine

Département de Biochimie

**Fibroblastic Reticular Cells during Immune Response
in Activated Lymph Node and Gut Lamina Propria**

Thèse de Doctorat ès Sciences de la Vie (PhD)

présentée à la

Faculté de Biologie et de Médecine
de l'Université de Lausanne

par

Chen-Ying Yang

Maîtrise ès Sciences
National Yang-Ming University, Taiwan

Jury

Prof. Benjamin Marsland : Président
Prof. Sanjiv A Luther : Directeur de Thèse
Prof. Fabienne Tacchini-Cottier : Expert et Représentant du PhD Programme
Prof. Dietmar Zehn : Expert interne
Prof. Christopher Buckley : Expert externe

Lausanne 2014

Ecole Doctorale

Doctorat ès sciences de la vie

Imprimatur

Vu le rapport présenté par le jury d'examen, composé de

Président	Monsieur	Prof. Benjamin	**Marsland**
Directeur de thèse	Monsieur	Prof. Sanjiv	**Luther**
Experts	Madame	Prof. Fabienne	**Tacchini-Cottier**
	Monsieur	Prof. Dietmar	**Zehn**
	Monsieur	Prof. Christopher	**Buckley**

le Conseil de Faculté autorise l'impression de la thèse de

Madame Chen-Ying Yang

Master of Science National Yang Ming University, Taïwan

intitulée

Fibroblastic Reticular Cells during Immune Response in Activated Lymph Node and Gut Lamina Propria

Lausanne, le 10 octobre 2014

pour La Doyenne
de la Faculté de Biologie et de Médecine

Prof.   Benjamin Marsland

Acknowledge

Table of contents

Abstract

Fibroblasts are in close contact with lymphocytes both in lymphoid organs and in peripheral tissues. In lymphoid organs, fibroblasts have been reported to regulate the development, tolerance, survival, and migration of lymphocytes besides their role in maintaining the organ structure. However, how these fibroblasts react to lymph node swelling and whether they maintain their original function is not yet fully understood. In this thesis, we investigated the phenotype and function of fibroblasts at two sites of ongoing immune response, in acutely inflamed lymph nodes (LN) and in the intestinal lamina propria were immune responses are constantly ongoing.

Adaptive immunity is initiated in T cell zones of secondary lymphoid organs where dendritic cells and recirculating T cells meet and where T cell activation and differentiation occur. These zones are organized by a rigid 3-dimensional network of fibroblastic reticular cells (FRC) that are a rich cytokine source. In response to lymph-borne antigens, draining LN expand several fold in size but the fate and role of the FRC network during immune response is not fully understood. Here we show that T cell responses are accompanied by the rapid activation and growth of FRC, leading to an expanded but similarly organized network of T zone FRC that maintains its vital function for lymphocyte trafficking and survival. In addition, new FRC-rich environments were observed in the expanded medullary cords. FRC get activated within hours after onset of inflammation in the periphery. Surprisingly, FRC expansion depends mainly on trapping of naïve lymphocytes that is induced by both migratory and resident dendritic cells. Inflammatory signals are not required as homeostatic T cell proliferation was sufficient to trigger FRC expansion. Activated lymphocytes are also dispensable for this process but can enhance the later growth phase. Thus, this study documents the surprising plasticity but also the complex regulation of FRC networks allowing rapid LN hyperplasia that is critical for mounting efficient adaptive immunity.

The second study looked at the lamina propria (LP) of the small and large intestine which are sites constantly exposed to microbiota and therefore harbor many effector cells. However, these immune cells are scattered and therefore organized very differently than inside LN. In addition, there needs to be a stromal microenvironment which dampens reactivity of immune cells toward the normal flora while allowing their response to pathogenic microorganisms. Currently we have a poor understanding of the stromal cells that may act as organizing principle of the LP, and that may influence the balance between tolerance and immunity. To that end I investigated the frequency, phenotype, organization and function of fibroblasts in the LP. We found collagen and gp38 to mark a dense fibroblast network throughout all parts of the gut lamina propria. A digestion protocol for isolating intestinal fibroblasts was established and sorted cells were found

to express COX-1, COX-2, APRIL, BAFF, and CXCL12, and therefore could contribute to immune tolerance or plasma cell function in the intestines during homeostasis.

In conclusion, FRC networks develop at sites rich in lymphocytes and dendritic cells. They are not restricted to tissues containing naïve T cells like in secondary lymphoid organs but can be also observed in tissues rich in effector lymphocytes like in activated LN and the gut LP. Besides serving most likely as scaffold for adhesion and migration, I propose that FRC also influence adaptive immunity in several ways which still need further exploration.

Résumé

Les fibroblastes sont en contact étroit avec des lymphocytes, à la fois dans les organes lymphoïdes et dans les tissus périphériques. Dans les organes lymphoïdes, les fibroblastes, en plus de leur rôle dans le maintient de la structure de l'organe, agiraient comme régulateurs du développement, de la tolérance, de la survie et de la migration des lymphocytes. Cependant, la façon, dont ces fibroblastes réagissent à un gonflement des ganglions lymphatiques et qu'ils conservent leur fonction d'origine n'est pas encore entièrement comprise. Dans cette thèse, nous avons étudié le phénotype et la fonction des fibroblastes au niveau de deux sites: les ganglions lymphatiques (lymph node en anglais, LN) lors d'une inflammation aiguë et la lamina propria intestinale, où des réponses immunitaires sont constamment en cours.

L'immunité adaptative est initiée dans les zones T des organes lymphoïdes secondaires, où les cellules dendritiques et les cellules T recirculantes se rencontrent et où l'activation et la différenciation des cellules T se produisent. Ces zones sont formées d'un réseau tridimentionnel rigide de cellules réticulaires fibroblastiques (fibroblastic reticular cells en anglais, FRC), qui constituent une source importante de cytokines. En réponse à des antigènes qui sont drainés par la lymphe dans un LN particulier, le LN va fortement accroître sa taille, mais le sort et le rôle du réseau de FRC pendant la réponse immunitaire ne sont pas entièrement compris. Ici nous montrons que les réponses des cellules T sont accompagnées par l'activation rapide et la croissance des FRC, aboutissant à un réseau élargi des FRC de la zone T, mais organise de manière similaire, qui conserve sa fonction vitale pour le traffic et la survie des lymphocytes. En plus, nous avons observe de nouveaux environnements riches en FRC dans les cordons médullaires élargis. Les FRC se sont activés dans les heures suivant l'apparition de l'inflammation en périphérie. De manière surprenante, l'expansion des FRC dépend principalement de la capture des lymphocytes naïfs, qui est induite par les cellules dendritiques résidentes et migratrices. Les signaux inflammatoires ne sont pas indispensables car la prolifération homéostatique des cellules T est suffisante pour déclencher l'expansion des FRC. Les lymphocytes activés ne sont pas nécessaires pour ce processus, mais peuvent améliorer la phase de croissance ultérieure. Ainsi, cette étude documente l'étonnante plasticité, mais aussi la complexité de la régulation du réseau FRC permettant l'hyperplasie rapide du LN, qui est essentielle pour la mise en place d'une immunité adaptative efficace.

La deuxième étude a examiné la lamina propria (LP) du petit et du grand intestin qui sont des sites constamment exposés aux bactéries commensales et donc arborant de nombreuses cellules effectrices. Cependant, dans la LP ces cellules immunitaires sont dispersées et présentent donc une organisation très différente de celle observée à l'intérieur des LN. En outre, il est nécessaire d'avoir un micro-environnement stromal qui limite la réactivité des cellules immunitaires envers la flore normale, tout en permettant leur réponse contre les micro-organismes pathogènes. Actuellement, nous avons une compréhension insuffisante du rôle des

cellules stromales en tant que principe organisateur de la LP, ainsi que leur rôle dans l'établissement de l'équilibre entre la tolérance et de l'immunité. C'est pour celà que j'ai étudié la fréquence, le phénotype, l'organisation et la fonction des fibroblastes dans le LP. Nous avons identifié le collagène et gp38 qui permettent de marquer un réseau dense de fibroblastes dans toutes les parties de l'intestin. Un protocole de digestion pour isoler les fibroblastes intestinaux a été établi et les cellules identifiées ont montré une expression de COX-1, COX-2, APRIL, BAFF, et CXCL12, et donc pourraient être susceptibles de contribuer à la tolérance immunitaire, ou à la fonction des cellules de plasma dans l'intestin au cours de l'homéostasie.

En résumé, les réseaux de FRC se développent aux endroits riches en lymphocytes et cellules dendritiques. Ils ne sont pas limités aux tissus qui contiennent beaucoup de lymphocytes T naïfes comes des organes lymphoïdes secondaires, mais sont aussi retrouvés dans les tissus contenant beaucoup de lymphocytes effecteurs, comme dans un ganglion activé ou la LP intestinale. En plus de leur fonctionnement probable comme échaffaudage pour l'adhésion et la migration des lymphocytes, je propose que les FRC influencent l'immunité adaptative par plusieurs voies qui nécessitent des études supplémentaires.

1. Introduction

The immune system is a very complex system dedicated to the defense against invasion of the body by foreign organisms. While the innate immunity evolved very early and can be seen in almost every species, the more sophisticated adaptive immunity can only be seen in higher vertebrates and is characterized by its diversity, specificity, self-recognition, and memory. Except for some immune-privileged sites, including cornea, central nervous system, testicles, and placenta/fetus, the whole body is guarded by immune cells against pathogen invasion. Some are tissue resident while some circulate through the blood and lymph stream to search for foreign antigens (Ag) or danger signals.

The immune system comprises various types of cells and organs/tissues to establish multiple layers of protection. The primary lymphoid organs are sites where immune cells are generated, including bone marrow (BM) and thymus. The secondary lymphoid organs (SLOs) are sites where adaptive immune responses are elicited, including lymph nodes (LN), spleen, and various mucosal-associated lymphoid tissues (MALT), such as Peyer's patches (PP) in the small intestine. Although they localize differently, all SLO have similar structures and function to sustain the survival of immune cells and to facilitate their encounter with antigens (Junt et al., 2008). All SLO are composed of B cell-rich zones and T cell-rich zones that are surrounded by an antigen-sampling zone. The first part of the thesis is focusing on the LN and the second part on the intestine. The stromal cells of these two organs will be discussed in more details.

Secondary lymphoid organs develop during embryogenesis or in the early postnatal period and this process occurs independently of antigen or pathogen recognition at predetermined sites throughout the body as a result of complex interactions between various hematopoietic, mesenchymal, and endothelial cells (Randall et al., 2008). Development of different SLO starts at different time point in mice, as mesenteric LN start at E9 - 10, PP between E12.5 - 15.5, and popliteal LN at E17, etc. (Randall et al., 2008). The development of LN occurs concurrently with the process of lymphatic vascularization since LN are encapsulated by lymphatic endothelium. The lymphatic endothelial cells (LEC) form lymph sacs which buds from veins and differentiate in this process from blood endothelial cells (BEC) to LEC under the control of the master transcription factor, Prox-1 (prospero homeobox protein 1) (Wilting et al., 2002). Retinoic acid (RA) is produced around the sac, probably due to the stimulation by neurons (van de Pavert et al., 2009), and thereby induces CXCL13 expression on a specific population of mensenchymal cells named lymphoid tissue organizer cells (LTo cells) that express VCAM-1, ICAM-1, and lymphotoxin beta receptor (LTβR). The CXCL13 produced by LTo cells attract a population of CD45$^+$CD4$^+$CD3$^-$IL-7Rα^+ROR$\gamma\tau^+$CXCR5$^+$ cells, named lymphoid tissue inducer cells (LTi cells) to aggregate around the LTo cells and in turn induce LTo cells or mesenchymal cells to express

other chemokines and adhesion molecules needed for further retention and attraction of hematopoietic cells (Roozendaal and Mebius, 2011). IL-7, RANKL (receptor activator of nuclear factor kappa-B ligand) and lymphotoxin αβ (LTαβ) are key factors in this interaction with IL-7 and TRANCE from LTo cells up-regulating LTαβ expression on LTi cells, which then trigger LTβR$^+$ LTo cells to produce more CXCL13, CCL19/21 and adhesion molecules like vascular cell-adhesion molecule 1 (VCAM-1) and Intercellular Adhesion Molecule 1 (ICAM-1) that attract and possibly retain more LTi cells and later on T and B cells. Gene defects in these signaling pathways as well as transcription factors essential for LTi cell development, like RORγτ, will impair the development of SLO to different degrees (Figure 1.1) (Junt et al., 2008) (Randall et al., 2008).
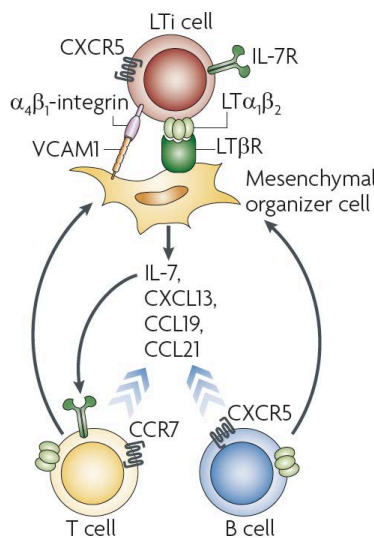
Figure 1.1 mechanism of SLO organogenesis

Lymphoid organogenesis is initiated by the interaction of RORγτ$^+$CD3$^-$ CD4$^+$CD45$^+$ IL-7Rα$^+$ LTi cells with mesenchymal organizer cells. As a first step, LTi cells are attracted to mesenchymal LTo through CXCR5 and they adhere to the inductive sites through interactions between VCAM-1 and α4β1 integrin. As a consequence, inductive interactions are formed, in which LTαβ expressed by LTi cells ligates LTβR expressed by LTo cells. This induces the local expression of CCL19, CCL21 and CXCL13, which, in turn, attract B and T cells to the activation site. As B and T cells also express LTαβ, a positive feedback loop is generated that leads to the local accumulation of more B cells and T cells, and eventually to the formation of the defined microenvironments in secondary lymphoid organs. (Junt et al., 2008)

1.1 Stromal compartment in the peripheral LN

LN are secondary lymphoid organs where primary T and B cell responses against lymph-borne pathogens or tumor antigens are induced most efficiently. LN contain three compartments (T zone, B zone, and medulla) that are characterized by distinct hematopoietic cells and resident stromal cells (Mueller and Germain, 2009) (Turley et al., 2010). The B cell zone (cortex, follicle) is composed of follicular dendritic cells (FDC) that produce CXCL13 to attract B cells. The T cell zone (paracortex) is rich in gp38$^+$ fibroblastic reticular cells (FRC), known as T zone FRC (TRC) that express CCL19 and CCL21 to attract naive T cells and dendritic cells (DC) (Link et al., 2007). Under the subcapsular sinus (SCS), there are also gp38$^+$ FRC named marginal reticular cells (MRC) that selectively express CXCL13, RANKL, and MAdCAM-1 (Katakai et al., 2008). Both FRC and MRC form the conduit system in the T zone and to a limited extent inside the outer B zone, respectively (Figure 1.2) (Mueller and Germain, 2009). Blood endothelial cells (BEC), including the high endothelial venules (HEV), are also located mostly in the outer T zone. Finally, the medulla is rich in efferent lymphatic vessels and serves as the exit zone of naive and

activated lymphocytes. It expands during immune response to accommodate short-lived plasma cells (Angeli et al., 2006) (Mohr et al., 2009) (Abe et al., 2012).
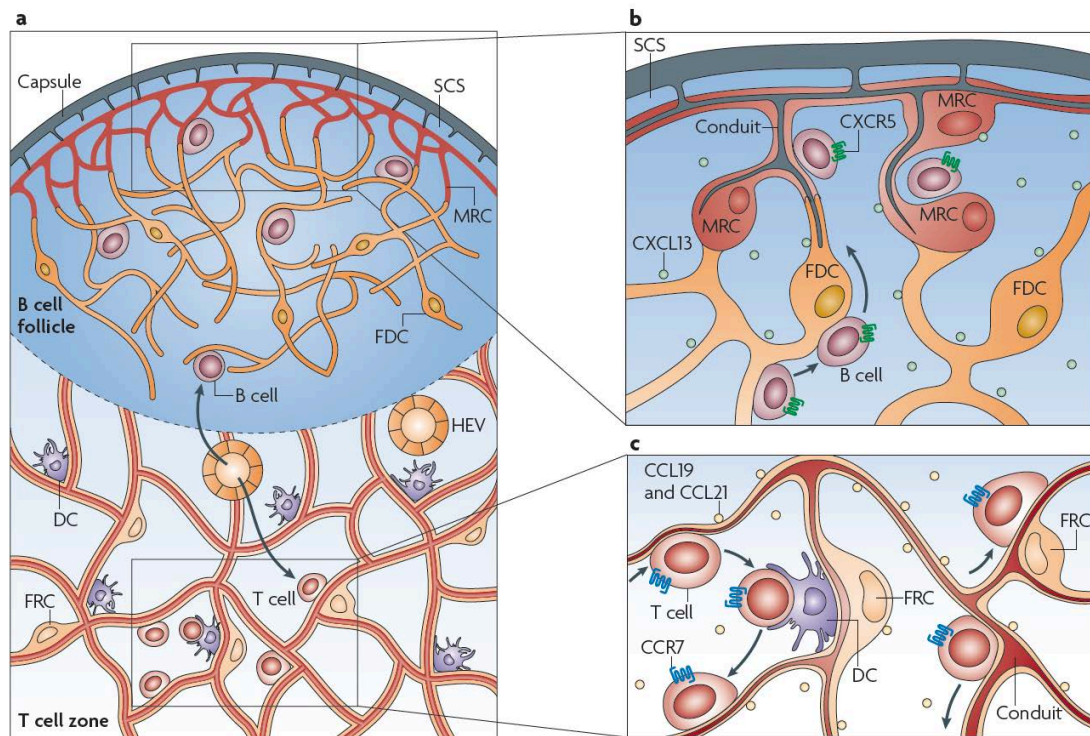
Figure. 1.2 Lymphocyte migration on stromal networks in secondary lymphoid organs.

(a) B and T cells enter lymph nodes through high endothelial venules (HEV) and immediately contact the (FRC) stromal network. B cells migrate along FRC at the edge of B cell follicles and traffic into these regions in response to CXCL13. T cells move along the FRC conduit network into the T cell zone of the lymph node paracortex. Resident and recently arrived DC attach themselves to the FRC network near HEV and deeper in T cell zones. (b) On entering B cell follicles, B cells expressing CXCR5 make their way into the CXCL13-rich FDC network, where they migrate along the stromal network in search of cognate antigen (arrows). B cells also traffic towards the periphery of B cell follicles, where MRC stromal networks form under the subcapsular sinus (SCS). MRC also express CXCL13. Antigen can enter B cell follicles through conduits formed by the MRC and be delivered to the FDC network. (c) In T cell zones, T cells traffic along FRC networks that are rich in CCL19 and CCL21 and interact with DC that adhere to FRC. The DC can then present antigens to T cells as they migrate past. Antigens can enter the conduit network from the lymph or blood and drain through the T cell zones. DC can sample antigens from the conduits and present them to T cells. (Mueller and Germain, 2009)

1.1.1 Blood endothelial cells

LN are connected to both blood and lymph circulation that are channeled by blood and lymphatic vessels, respectively. The blood capillaries inside the LN are composed of a single layer of blood endothelial cells (BEC) that express CD31 and some of them differentiated into a special structure called high endothelial venules (HEV) that serve as the entry site of naïve lymphocytes to the LN (von Andrian and Mempel, 2003). The BEC of HEV are characterized by their cuboidal morphology compared to the usual flat shape of regular BEC and their expression of different adhesion molecule for lymphocyte interaction. HEV express PNAd (peripheral node addressin; which includes molecules like CD34) and ICAM-1 (intercellular adhesion molecule 1) that interact with CD62L and $\alpha L\beta 2$, respectively, on lymphocytes to facilitate their extravasation. HEV can be found in all SLO except the spleen. In different tissues, BEC express either

MAdCAM-1 (in GALT and urogenital tract; binds $\alpha 4\beta 7$) or VCAM-1 (such as BALT, bone marrow, and skin; binds $\alpha 4\beta 1$) or both (mammary gland) which contribute to the homing of effecter cells to different organs (Kunkel and Butcher, 2003). BEC also produce CCL21, and to a less extent CCL19, CXCL12, and CXCL13 to attract lymphocytes and to induce the arrest of rolling lymphocytes (Miyasaka and Tanaka, 2004) (Stein et al., 2000).

DC have been reported to be important in modulating HEV function, T cell homing and LN size (Girard et al., 2012). It seems that DC can express vascular endothelial growth factor (VEGF) to induce the proliferation of HEV cells, similar to TRC (Webster et al., 2006) (Wendland et al., 2011). On the other hand, DC are also required for maintenance of the HEV phenotype as CD11c^{+} DC depletion causes the loss of the MECA-79 ligand GlyCAM-1, and the enzymes GlcNAc6ST2 and FuT7 but up-regulates MAdCAM-1 on LN HEV. LT$\alpha\beta$ signals provided by DC were proposed to be important for this function (Moussion and Girard, 2011).

1.1.2 Lymphatic endothelial cells

Lymphatic vessels are lined by a single layer of lymphatic endothelial cells (LEC) with valves that collect lymph throughout the whole body and eventually drain it back to the blood circulation via thoracic duct. The afferent lymphatic vessels are open-end capillaries draining interstitial fluid of a defined area and transport it passively to the local LN. Besides interstitial fluid, lymph can also contain soluble antigens and intact pathogens as well as signaling molecules like inflammatory cytokines produced in the periphery (Randolph et al., 2005). LEC in the periphery can express CCL21 to attract local CCR7^{+} DC to enter the lymphatics (Randolph et al., 2008). The drained lymph enters the LN via afferent lymphatics in the subcapsular sinus (SCS) of the LN, where the lymph is prevented from freely entering the LN parenchyma and either enters the conduit system or flows toward the medullary sinus through intranodal and subcapsular lymphatics (Cyster, 2005) (Cyster and Schwab, 2012a).

Efferent lymphatics are abundant in the medullary zone which is the exit site of LN for lymphocytes. The efferent lymphatics either later link up with another LN or connect to a larger lymphatic vessel or join to the vein (via thoracic duct). The exit of both T and B cells is controlled by sphingosine-1-phosphate (S1P) and its G protein-coupled receptor S1PR1. S1P is abundant in blood and efferent lymph (Cyster, 2005). S1P is generated in vivo by sphingosine kinases and mice deficient in one of these kinases in LEC showed significant loss of S1P in the lymph and impaired exit of lymphocytes from LN (Pham et al., 2010). Naïve lymphocytes express S1PR1 to sense and migrate towards the high concentration of S1P in the medulla. T cells seem to cross the lymphatics and enter the cortical sinus at multiple locations while B cells migrate directly

from follicle to adjacent cortical sinuses (Girard et al., 2012). Binding of S1P to S1PR1 probably counteracts the retention signal mediated by Gαi-coupled receptors, CCR7 and CXCR5. Indeed, pertussis toxin treatment that inactivates Gαi restores the egress of lymphocytes in the absence of S1P-S1PR1 signaling (Sinha et al., 2009) (Pham et al., 2008).

Besides the endothelial marker, CD31, LEC also express gp38, Lyve (lymphatic vessel endothelial hyaluronan receptor) -1, and Prox-1. Prox1 is a master transcriptional factor regulating LEC differentiation. Gp38 (also called podoplanin) also contributes to the proliferation, migration, and tube formation of LEC in vitro (Navarro et al., 2008) (Navarro et al., 2011). CLEC-2, ligand of gp48, is expressed on platelets and has bee shown to mediate proper lymphatic vessel formation the migration, proliferation, and in vitro tube formation of LEC (Osada et al., 2012).

1.1.3 Follicular dendritic cells (FDC)

Follicular dendritic cells are the major stromal cells in the B zone and play a fundamental role in B cell immune response. They produce CXCL13 to attract CXCR5^{+} B cells and thus form the B cell zone. During homeostasis, FDC also provide BAFF to support B cell survival (Aguzzi et al., 2014). FDC can capture and retain immune complexes on their surface via complement receptor 1/2 (CD35/21) or Fc receptors and then present the antigens to activate cognate B cells (Tew et al., 2001). Upon TLR signals and retinoic acid (RA) stimulation, FDC up-regulate the expression of CXCL13, BAFF and TGFβ that enhance the recruitment, survival, and class-switch of germinal center B cells (GCB), respectively (Aguzzi et al., 2014). FDC produce a molecule called milk fat globule-EGF factor 8 (Mfge8) that binds to phosphatidylserine (PS) on the surface of apoptotic cells as an 'eat-me' signal. These Mfge8-opsonized apoptotic cells are then recognized and cleared by tingible body macrophages (TBM) (Hanayama et al., 2002) (Kranich et al., 2008). FDC thus may avoid autoimmunity by contributing to rapid clearance of dying cells (Hanayama et al., 2004).

FDC has been shown to express intracellular adhesion molecule (ICAM)-1, vascular cell adhesion molecule (VCAM)-1, mucosal addressin-cell adhesion molecule (MAdCAM)-1, LTβR, and tumor necrosis factor receptor (TNFR)-1 (Aguzzi et al., 2014). During spleen homeostasis, FDC are differentiated from a population of ubiquitous perivascular precursors that express PDGFRβ, Mfge8, CXCL13, ICAM-1, MAdCAM-1, but not CD21/35. Their development to mature FDC depends on lymphoid tissue inducer cells and lymphotoxin (Krautler et al., 2012). Other papers have shown that B cells expressing TNFα and LTαβ are required for mesenchymal cells to differentiate into FDC (Roozendaal and Mebius, 2011) (Gonzalez et al.,

1998) (Endres et al., 1999) (Fu et al., 1998). Recently, Jarjour et al. showed by means of a multicolor fate mapping system that LN FDC which get newly generated either during inflammation or B cell reconstitution in RAG KO mice, differentiate from proliferating marginal reticular cells (MRC) that line the follicular side of the SCS (Jarjour et al., 2014).

1.1.4 Marginal reticular cells (MRC)

Marginal reticular cells (MRC) were first described by Katakai et al. and form a thin layer of reticular structure in the outer follicular region immediately underneath the subcapsular sinus of lymph nodes (Katakai et al., 2008). MRC express ICAM-1 and VCAM-1, but unlike other FRC also MAdCAM-1 and RANKL, a phenotype reminiscent of LTo cells during LN organogenesis. However, they don't express CCL21 or CD21/35, indicating they are distinct from FRC or FDC (Katakai, 2012). Reticular cells similar to MRCs are also found in the back the B cell follicle in the spleen and in the subepithelial dome (SED) region just under the basement membrane of the follicle-associated epithelium (FAE) in mucosal-associated lymphoid tissue (MALT) (Katakai et al., 2008).

The immune functions of MRC are still poorly understood. However, the conduit network constructed by MRC has been shown to transport soluble antigens from SCS to central B zones where FDC reside and where antigen can get deposited (Bajenoff and Germain, 2009) (Roozendaal et al., 2009). MRC might serve as a local FDC progenitor cells during acute LN swelling as shown by Jarjour et al. (Jarjour et al., 2014). Indeed, besides their similar expression of markers to LTo cells, Katakai et al. also showed that LTo cells are more concentrated in marginal zone of LN anlagen and this layer of LTo cells later expands outward with growth of the anlagen to become the MRC layer (Katakai et al., 2008). This data suggests that MRC are the direct descendants of LTo cells that preserve LTo markers such as MAdCAM-1 and RANKL (Katakai, 2012). Furthermore, RAG KO mice still exhibit a subcapsular MRC layer in atrophic LN and shrunken periarterial MRC sheaths in the spleen, indicating that MRC development occurs independently of B and T cells and is programmed before their colonization (Katakai et al., 2008).

1.1.5 Fibroblastic reticular cells (FRC)

The fibroblastic reticular cells in the T zone (TRC) as described by Anderson et al. (Anderson and Anderson, 1975), form a sponge-like reticular network throughout the T zone in the LN. With electron microscopy, microchannels were visualized within the network that are wrapped

by FRC and connect the subcapsular sinus (SCS) to the HEV (Gretz et al., 1997) (Ushiki et al., 1995). The so-called 'conduit system' consists of a core of collagen-I fibers that are surrounded by ECM including fibrillin-1, -2, and a component stained by antibody, ER-TR-7. These fibers are then wrapped by a layer of basement membrane composed of laminin, collagen-IV, and fibronectin. FRC tightly enwrap these ECM fibers and form the FRC network serving as a backbone in the T zone that eventually stabilizes the LN architecture (Sixt et al., 2005) (Kaldjian et al., 2001). The function of the conduit system is shown to allow for rapid transport of small soluble molecules (<70 kD), including antigens and cytokines, to the T zone and HEV (Gretz et al., 2000). Substances that are bigger cannot enter the conduit system and will be trapped by SCS macrophages instead. A similar conduit system is also found in the spleen that allows small molecules to enter the conduit of the white pulp via the marginal zone (Nolte et al., 2003).

Besides providing structural stability, FRC have been shown to produce CCL19 and 21 that attract CCR7^{+} naïve T cells and DC to the T zone (Luther et al., 2000). The production of these homeostatic chemokines is partially induced by LTβR and TNFR-I signaling (Ngo et al., 1999). Beyond just producing the chemokines that define the boundary of the T zone, the FRC network also serves as a highway for T cells to crawl on, as shown by two-photon laser scanning microscopy (Bajenoff et al., 2006). The motility of T cells seems at least partially dependent on CCL21-CCR7 interaction (Worbs et al., 2007) (Okada and Cyster, 2007) (Asperti-Boursin et al., 2007). On the other hand, antigen presenting cells (APC) have been shown to interact with the FRC network. In LN, resident DC, especially the CD8^{+} DC subset, adhere to the FRC and thus form a network closely associated with FRC network (Katakai et al., 2004a) (Sixt et al., 2005). Acton et al., showed that FRC and LEC interact with CLEC-2^{+} DC via gp38 (podoplanin) to promote DC mobility from peripheral sites through lymphatic vessels to the T zone of the LN (Acton et al., 2012). Local expression of CCL19/21 by FRC may help immune responses by promoting DC maturation (Marsland et al., 2005), endocytosis and antigen presentation (Yanagawa and Onoe, 2003), evoking their extension and probing of dendrites (Yanagawa and Onoe, 2002), increasing the probability of APC and T cell encounter (Friedman et al., 2006), and co-stimulating T cell activation (Flanagan et al., 2004).

FRC also contribute to T cell homeostasis by producing the T cell survival factor, IL-7 (Link et al., 2007). The population of T cells is maintained at a constant number that is balanced by newly generated T cells and the death of T cells in the periphery. The survival of T cells is controlled by competing for IL-7 and MHC complex recognition (Goldrath et al., 2000) (Schluns et al., 2000). Blocking the entry to the LN will reduce the life span of T cells, indicating the source of IL-7 is inside the LN. By isolating FRC from the LN, Link et al showed that FRC are the main source of IL-7 in the LN (Link et al., 2007). Besides TRC and MRC, LEC were also shown to be the possible source of IL-7 in the LN (Repass et al., 2009) (Onder et al., 2012).

FRC also contribute to peripheral tolerance during homeostasis. However, unlike DC that acquire self-antigens from tissues, FRC were shown to express the autoimmune regulator (AIRE) and a range of tissue-derived self-antigens (TSA), thus contributing to peripheral tolerance (Fletcher et al., 2010) (Magnusson et al., 2008) (Lee et al., 2007). However, the expression of TSA by FRC may not be controlled by AIRE (Cohen et al., 2010) and FRC express another transcriptional regulator, deformed epidermal autoregulatory factor 1 (DEAF1) that have been shown to up-regulate approximately 300 genes in pancreatic lymph nodes, 75% of which are classed as peripheral tissue-restricted antigens (Yip et al., 2009). AIRE and DEAF1 control distinct groups of TSA, which partially explains the differential expression of TSA in different stromal cells (Yip et al., 2009) (Cohen et al., 2010) (Fletcher et al., 2010). FRC could also promote tolerance by up-regulating programmed cell death ligand (PD-L1) after polyI:C treatment (Mueller et al., 2007). Comparison of FDC, FRC, and MRC are listed in Table 1.1 (Mueller and Germain, 2009).

Table 1.1 Stromal cell subsets in secondary lymphoid organs (Mueller and Germain, 2009)

Stromal cell subset	Tissue; location	Selected markers	Functions
Fibroblastic reticular cells	Lymph nodes, spleen, Peyer's patches, MALT and TLT; T cell zones	ER-TR7 antigen , podoplanin, laminin, desmin, fibrillin, fibronectin, α-SMA, LTβR, TNFR1, TNFR2, ICAM1, VCAM1, collagen I, collagen II, collagen IV, α1 integrin, α4 integrin, β1 integrin, MHC class I, VEGF, PDGFR, CCL21, CCL19, CXCL16 and IL-7	Structural support; production of reticular fibres; formation of conduit network; chemokine production and presentation; substrate for lymphocyte migration; APC adhesion; T cell homeostasis; antigen presentation
Follicular dendritic cells	Lymph nodes, spleen, Peyer's patches, MALT and TLT; B cell zones	CD16, CD21, CD23, CD32, CD35, C4, ICAM1, VCAM1, MADCAM1, laminin, desmin, CXCL12, CXCL13 and BAFF	Antigen capture; presentation of immune complexes; chemokine production and presentation; B cell homeostasis
Marginal reticular cells	Lymph nodes, spleen, Peyer's patches, MALT; SCS (in lymph nodes) and marginal zone (in the spleen)	ER-TR7 antigen, ICAM1, VCAM1, MADCAM1, RANKL, laminin, desmin, 1BL-11 antigen and CXCL13	Structural support; chemokine production; conduit function

1.2 Immune response and swelling of peripheral LN

1.2.1 Activation of lymphocytes and LN swelling

Speed is crucial to efficiently fight the spread of pathogens. Upon infection, the damaged epithelial cells will produce IFNα/β within minutes to recruit innate immune cells continuously patrolling the body. These cells have immediate effector function and generate a local inflammatory response that helps activating local APCs. At the same time, pathogens are taken up by skin-resident DC and digested into peptide fragment (8-15 amino acids in length) for presentation on MHCI or MHCII molecules at the APC surface. Upon antigen uptake and danger signal activation, APC become activated and mature to up-regulate surface CCR7 and start to migrate to the draining LN via afferent lymphatics. Matured migratory DC (mDC) can be detected in the LN starting from12-24 hours after infection and are very crucial for the induction of adaptive immune response.

However, it also has been shown that some small pathogen-derived molecules or viral particles (<200 nm) can be drained via the lymph to the SCS of LN and then be taken up by SCS macrophages, B cells, or further go into the T zone via the conduit system and be taken up by LN-resident DC. This can happen as early as 10 minutes after infection (Junt et al., 2008). The conduit system has also been shown to transport pro-inflammatory chemokines and cytokines from the peripheral site of inflammation to the T zone and the lumen of HEVs (Palframan et al., 2001). This may lead to the recruitment of inflammatory cells like monocytes to the LN, further enhancing inflammation.

The precursor frequency of antigen-specific T cells is actually extremely low. It is estimated that around 50-200 T cells with high affinity exist for a given antigen in an entire adult mouse (Moon et al., 2007). In order to increase the probability of successful encounters between naïve T cells and DC presenting their cognate antigen, the draining LN receives danger signals which starts a process named LN shutdown and HEV activation, that together cause the trapping of a large number of naïve lymphocytes thereby inducing LN swelling.

Shortly after infection, HEVs change their properties within hours with an increase in number and size in the following days (Soderberg et al., 2005) (Webster et al., 2006) (Chen et al., 2006). It was shown that the HEV diameter increases by 50% and the blood flow rate by 500% 3 days after infection (Hay and Hobbs, 1977) (Steeber et al., 1987) (Soderberg et al., 2005). Comparably, afferent lymphatic vessels proliferate, inducing increased recruitment of DCs from the periphery to the draining LN (Angeli et al., 2006). On the other hand, LN shutdown was achieved by blocking the exit of lymphocytes via IFNα/β which reduces the lymphocyte responsiveness to S1P as early as 6-18 hours after infection (Hall and Morris, 1965) (Matloubian et al., 2004) (Lo et al., 2005). Consequently, these events concentrate as many Ag-bearing APC and lymphocytes as possible in a single LN to facilitate the encounter of antigen and its cognate lymphocytes. How LN swelling is induced is only partially understood. Besides the S1P pathway, blocking of TNF or mast cells also partially reduced the LN hypertrophy (Jawdat et al., 2006) (McLachlan et al., 2003) suggesting their role in LN swelling. On the other hand, direct injection of TLR ligands, LPS and CpG, is sufficient to trigger LN swelling (Soderberg et al., 2005). However, LN swelling upon viral infection seems to be independent of TNF and MyD88 (Soderberg et al., 2005). These data suggests that multiple redundant pathways exist to induce LN swelling.

After recognizing cognate peptide-MHC complexes via their TCR, T cells become activated with the help of co-stimulatory signals provided by APC such as CD28 interactions with CD80/86. This Ag-MHC-TCR interaction is reinforced by cytokines and lead to full activation of T cells including up-regulation of CD69 and CD44. Later T cells (and DC) start to produce IL-2 and IFN-

γ to further stimulate T cells that have up-regulated the IL-2 receptor CD25. Finally, T cells dissociate from DC and undergo rapid proliferation and differentiation before leaving the LN (Mempel et al., 2004) (Henrickson and von Andrian, 2007). The clonal T cell expansion can be detected as early as 30 hours after activated DC arrived in the LN. Naïve CD8 T cells only require short interaction with antigen to initiate their proliferation and differentiation into cytotoxic T cells while naïve CD4 T cells need longer exposure to Ag to differentiate into different types of helper T cells, including T_H1, T_H2, T_H17, follicular T helper cells (T_{FH}) and induced regulatory T cells (iTreg). T_{FH} cells are unique for their expression of CXCR5 that drives them to migrate to the T-B border and assist T-dependent B cell activation.

B cells can be activated by antigens plus T cell help (T-dependent antigens) or just by repetitive antigens alone (T-independent antigens). Soluble antigens drained to the SCS of LN can be taken up directly by B cells or by SCS macrophages that later translocate the antigens into the follicle where B cells can capture it (Junt et al., 2007). Soluble antigen can also be drained to central B zones via MRC-associated conduits and be taken up directly by FDC to present it to B cells (Bajenoff and Germain, 2009) (Roozendaal et al., 2009). T-independent antigens activate B cells by cross-linking the BCR leading to B cell activation and differentiation into IgM-producing plasma cells (Shapiro-Shelef and Calame, 2005). In contrast, when BCR on B cells binds to T-dependent antigens, they up-regulate CCR7 and migrate to the T-B border and encounter CXCR5$^+$ antigen-specific T_{FH} cells. The T–B interaction in the periphery of the B-cell follicle results in the initiation of proliferation at the boundary. A small fraction of B cells proliferate at the interface and re-enter the follicle to initiate the germinal center (GC) while others continue their proliferation as plasmablasts and migrate towards the medulla where they fully differentiate into plasma cells. In the early stages of the GC response, activated B cells undergo extensive proliferation in the dark zone of the GC. The dark zone, which is proximal to the T-cell area, contains the majority of proliferating B cells, called centroblasts. It is also presumed that somatic hypermutation is restricted to centroblasts. Centroblasts migrate to the light zone after finishing their proliferation, become centrocytes but may return to dark zones to undergo repeated somatic hypermutation and affinity maturation. The centrocytes expressing high affinity receptors to foreign antigen will be positively selected by antigen-presenting FDCs and antigen-specific CD4$^+$ T cells. These B cells then become either memory cells or plasma cells (PC) producing high-affinity antibodies (Batista and Harwood, 2009) (Cyster, 2005). The centrocytes expressing low affinity receptors, however, will undergo apoptosis within the GC and be engulfed by macrophages.

While the short-lived PC remain for several days in the medullary region of the LN before dying locally, the long-lived plasma cells frequently travel to the bone marrow (BM). In humans and mice, around 0.1 -1% of the bone marrow cells are PC (Terstappen et al., 1990). The survival of long-lived PC has been shown to involve several factors, both soluble and insoluble, that

constitute a niche for PC survival. These factors includes IL-6, CXCL12, CD44 ligands, granulocyte-macrophage colony-stimulating factor (GM-CSF), transforming growth factor-β (TGFβ) and TNFα. Besides, BM PC also require physical association with stromal cells to persist. PC may induce stromal cell production of IL-6, which then again enhances PC survival (Oracki et al., 2010).

1.2.2 Response of the stromal cells during immune response

During an immune response the size of the draining LN increases dramatically due to the massive trapping of naive lymphocytes and the proliferation of antigen-specific lymphocytes (Cyster and Schwab, 2012b) (Zhu and Fu, 2011). This implies a rapid and extensive remodeling of the various stromal cell structures that form the backbone of LN. I have previously discussed how HEV and LEC react to infection or immunization in order to regulate LN swelling. However, how the dense, rigid FRC network reacts to this rapid LN selling and its function during acute lymph node hyperplasia is only partially understood but of great importance for the successful initiation of adaptive immunity.

The existing evidence suggests an increase in the FRC network size (Katakai et al., 2004a) (Tan et al., 2012), at least in part due to FRC proliferation (Chyou et al., 2011). DC were proposed to trigger FRC proliferation directly by expressing LT⟨® (Chyou et al., 2008) (Chyou et al., 2011). RANK-ligand was also suggested as growth signal for FRC (Hess et al., 2012). It was also reported that the FRC network around HEV might be disrupted (Tzeng et al., 2010) along with a transient loss of CCL19/21 and IL-7 expression (Mueller et al., 2007) (Scandella et al., 2008). On the other hand, some functions of FRC during immune response were reported. It has been shown FRC can produce VEGF to promote endothelial cell growth during LN swelling (Chyou et al., 2008). Gp38 expression on FRC was reported to maintain VE-cadherin expression on HEV by somehow interacting with CLEC-2 on platelets. FRC were thus proposed to be essential for the overall integrity of LN vascular structures during immune response (Herzog et al., 2013). Meanwhile, FRC were also shown to prevent excessive T cell expansion during immune response by the production of iNOS and COX-2 (Siegert et al., 2011) (Lukacs-Kornek et al., 2011) (Khan et al., 2011).

1.3 The histology and physiology of intestine

The intestines consist of the small and large intestine that are responsible for digesting food, absorbing nutrients, and expelling waste. The small intestine can be further subdivided into

duodenum, jejunum, and ileum while the large intestine includes cecum, proximal colon and distal colon. The duodenum is the beginning of the small intestine and receives gastric chyme from the stomach. One main function of the duodenum is to neutralize the acids contained in the gastric chyme. It is characterized by especially long villi compared to jejunum and ileum in mice (Brennan et al., 1999). The subsequent jejunum is the longest part of the small intestine, proximally half of it, and is mainly dedicated to the digestion and absorbtion of nutrients (sugars, amino acids, fatty acids), which are finally taken up by the blood and lymphatic vessels. The ileum is the last part of the small intestine and absorbs remaining nutrients, as well as bile acids and vitamin B12 produced by commensals present in the lumen of the ileum. The main function of the large intestine is to absorb the water and salts from the remaining material which becomes the feces (Ganong, 1995) (wikipedia).

In human, the intestinal wall is composed of four concentric layers, in the following order starting from the luminal side: mucosa, submucosa, muscularis externa (the external muscular layer), and serosa. The mucosa is the innermost layer of the intestinal wall that surrounds the lumen and thus contacts directly the digested food (chyme) and the microbial flora present in the lumen. The mucosa is composed of a single layer of epithelial cells that separates the lumen from the body. The mucosa has a key role in digestion, absorption, and secretion of mucus. However, the epithelial cell layer is covered by a thick layer of mucus secreted by goblet cells which are scattered throughout the epithelium to protect it from direct contact with microbial organisms of the lumen. Right below the epithelial layer lays the lamina propria consisting of connective tissue and scattered lymphocytes and plasma cells. The submucosa consists of a dense irregular layer of connective tissue with large blood vessels, lymphatic vessels, and nerves. The muscularis externa is composed of an inner layer of circular muscle and an outer layer of longitudinal muscle to help intestinal wall movement. The serosa is the outermost connective tissue that separates the intestine from the peritoneal space (Figure 1.3) (Junqueira et al., 1995) (wikipedia).

In order to increase the surface contacting the chyme, the surface of the mucosa displays permanent foldings named circular folds (also called plicae circulares) which are large valvular flaps projecting into the lumen. In mice, circular folds are only seen in proximal colon but not in small intestine and distal colon (Abdelrahman et al., 2012). Further, all the mucosal surfaces in the small intestine develop villi and crypt structures to increase the contact surface with food content while in the large intestine only crypts exist. Intestinal villi are small, finger-like projections that protrude from the epithelial lining of the intestinal wall into the lumen while intestinal crypts are narrow but deep invaginations into the intestinal wall and often harbor glands that secret digestive enzymes, Paneth cells that secret anti-microbial peptides, and epithelial stem cells (Figure 1.3). In addition, the luminal surface of the epithelial cells display microvilli which further increase the contact surface with the luminal content to increase the

efficiency of nutrient absorption. In each villus, there are many capillaries surrounding a single lacteal (lymph capillary). The capillaries allow collecting hydrophilic nutrients including amino acid and simple sugars into the blood stream while the lacteal is to collect more hydrophobic nutrients such as triglycerides and cholesterol into the lymph fluids. The absorption of nutrients and water in the intestine largely depends on passive diffusion (Ganong, 1995) (wikipedia).
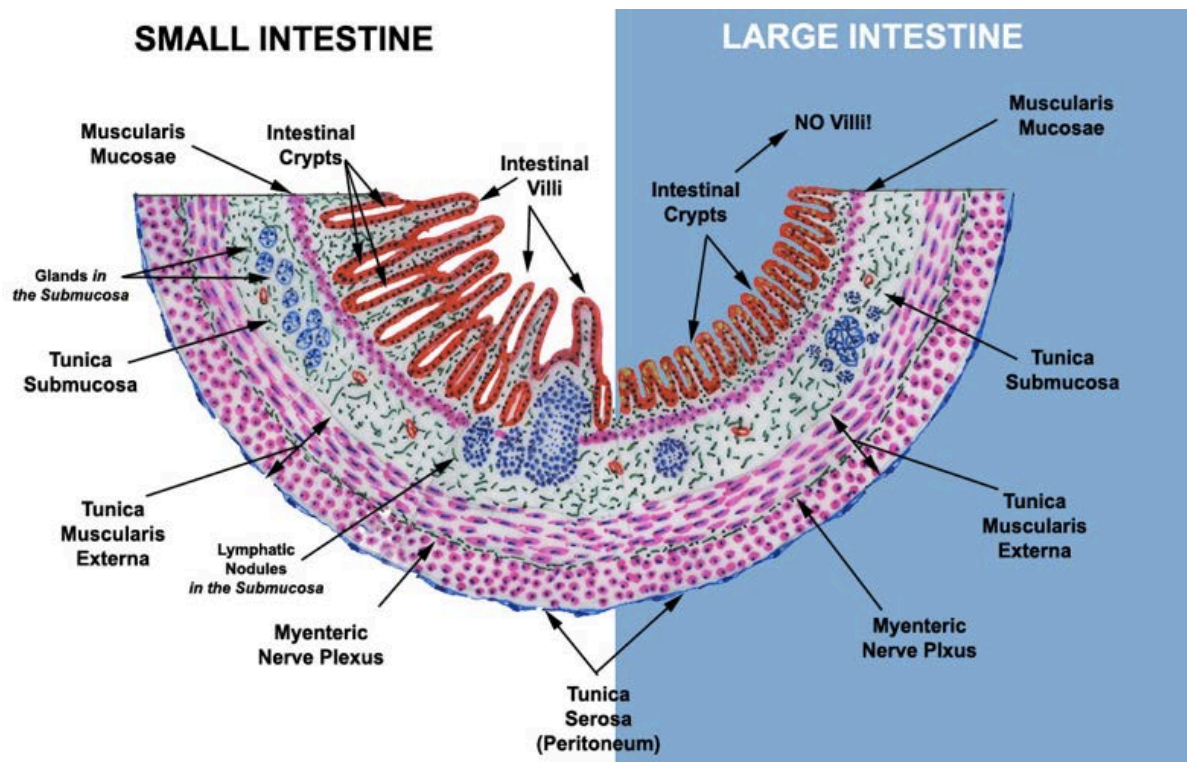
Figure 1.3 Schematic view of some of the salient features of the two major subdivisions of the intestine, and the four layers composed the intestinal wall.
(Thomas Caceci, http://www.vetmed.vt.edu/education/curriculum/vm8054/Labs/Lab19/Lab19.htm)

1.3.1 Intestinal microbiota and gut-associated lymphoid tissues (GALT)

Throughout the gastrointestinal tract the surface of the epithelium is colonized by enormous numbers of of microorganisms (including bacteria, fungi, and protozoa) that are mutualistic with the host. In a human body, around 10^{14} bacteria can be found. The composition of this microbial community is host specific, evolving throughout an individual's lifetime and susceptible to both exogenous and endogenous modifications. They are acquired from birth onward starting with the natural delivery by the mothers and later from the environment. Although humans and mice can survive without microbiota, the normal flora has been shown to be essential in providing nutrients, preventing the growth of harmful pathogens, training of the immune system and maintenance of normal host physiology (Sekirov et al., 2010).

It is not surprising that in such a microorganism-rich environment the intestine develops various gut-associated lymphoid tissues (GALT) to protect the body. These include mesenteric LN

(mLN), Peyer's patches (PP), isolated lymphoid follicles (ILF), and cryptopatches. These lymphoid tissues are the major sites for inducing immune responses to commensal or pathogenic bacteria. Besides these specialized GALT, the lamina propria and epithelium of the whole intestine are full of immune effector cells to protect the body from the intrusion by microbiota (Brandtzaeg et al., 2008). The lymphocytes which specifically reside within the epithelial barrier are named intraepithelial lymphocytes (IEL). The development and activity of these immune cells in the GALT and lamina propria are tightly regulated by the microbiota and thus contribute to various types of autoimmune disease, infectious disease, and cancer (Round and Mazmanian, 2009) (Sekirov et al., 2010).

1.3.2 Immune response in the intestine

The immune response in the gut is mainly induced in the organized GALT, including mLN, PP, and ILF. The PP and ILF are believed to be major sites where the immune system encounters the gut antigen. The epithelium above the PP or ILF are called follicle-associated epithelium (FAE) which contains microfold cells (M cells) that are specialized to transport intact antigens from the lumen of the small intestine by transcytosis to APC (mostly DC) in the subepithelial dome (SED) found right below the FAE (Mowat, 2003). The APC carrying the antigen then migrate to the T cell zone or B cell follicle to prime T and B cells. Here activated B cells will undergo immunoglobulin class switch recombination (CSR) from IgM to IgA under the control of TGFβ, IL-10, retinoic acid (RA) and cellular signals delivered by DC and T cells (Fagarasan and Honjo, 2003).

The activated T and B cells later exit the PP or ILF via lymphatic vessels that lead them to the mLN, where they may stay for a limited time for further differentiation. After leaving mLN they join again to the blood circulation via thoracic duct. Through the blood stream, these lymphocytes are programmed to home to the GALT as they express $\alpha4\beta7$ to interact with MadCAM-1 which is highly expressed on the vasculature of the mucosal surface. The expression of CCR9 on these cells allows them to be attracted by CCL25 which is highly produced by the small intestine (Kunkel and Butcher, 2003). The homed activated lymphocytes distribute into different locations in the effector sites, i.e. LP and epithelium. B-cell blasts mature into IgA-producing plasma cells and remain in the lamina propria. CD4^{+} T cells also remain in the lamina propria, while CD8^{+} T cells migrate preferentially into the epithelial layer, although ~40% of T cells in the lamina propria are CD8^{+} (Figure 1.4) (Mowat, 2003) (Eberl, 2005).

CSR to IgA of activated B cells in the gut is traditionally believed to happen inside the PP in a T cell-dependent manner as mentioned above, or in ILF in a T cell-independent manner with the

presence of IL-6 and RA produced by epithelial cells and LP DC (Sato et al., 2003) (Mora et al., 2006). However, Fagarasan et al. showed that CSR could also be observed in LP in a T cell-independent manner (Fagarasan et al., 2001) (Kinoshita et al., 2001). The CSR to IgA in LP was shown to depend on TGFβ, TSLP, APRIL, and BAFF provided by eosinophils, epithelial cells, and LP DC (Chu et al., 2014) (Tezuka et al., 2007) (Cerutti, 2008). Recent findings suggest that LP stromal cells can be the source of TGF-β1, BAFF, APRIL, IL-6, and IL-10 for promoting IgA CSR (Fagarasan et al., 2010) (Pabst, 2012).
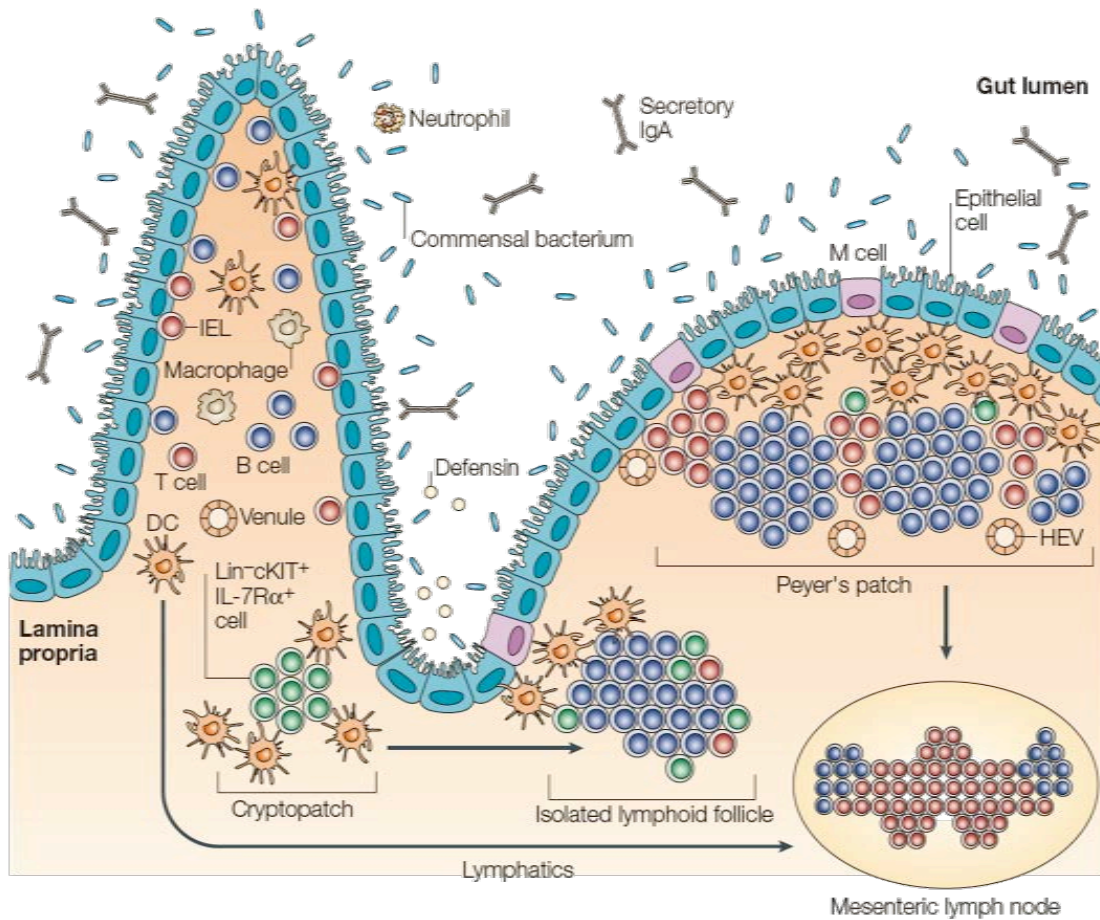
Figure 1.4 The intestinal immune system.

A single layer of epithelial cells separates the intestinal lamina propria from the gut flora. It is protected by a thick layer of mucus, bactericidal defensins, neutrophils and large amounts of antigen-specific secretory IgA. The intestinal immune system can be functionally divided into inductive sites, which include the mesenteric lymph nodes, Peyer's patches (in the small intestine), colonic patches and isolated lymphoid follicles (ILF), and into effector sites, which include the epithelium and the lamina propria. In the epithelium, intraepithelial lymphocytes (IEL) monitor epithelial damage and might recognize microbial antigens. The lamina propria contains large numbers of T cells, IgA-producing plasma cells and macrophages. It also contains many DC, which migrate to mesenteric lymph nodes through the lymph and present antigens to T cells. The follicle-associated epithelium (FAE), which covers Peyer's patches, contains Microfold (M) cells, which transport lumenal antigens to the sub-epithelial dome of Peyer's patches for sampling by DC that can also sample antigens from apoptotic epithelial cells. ILF, similar to Peyer's patches, contain B cells, DC and M cells (which are located in the adjacent FAE). HEV, high endothelial venule. (Eberl, 2005)

1.3.3 Immune tolerance in the intestine

During homeostasis, the immune cells in the gut are tolerant to food and commensal antigens. The CD4 T cells in the LP comprise T_H1, T_H2, T_H17, as well as iTreg cells. A defective T_H17

response can easily induce chronic inflammatory diseases, such as Crohn's disease (Honda and Takeda, 2009). Therefore, iTreg are important to maintain peripheral tolerance. iTreg differentiate from naïve CD4 T cells during antigen priming in the presence of TGFβ, a process which is greatly enhanced by retinoic acid (RA) (Allen et al., 2011) (Sakaguchi et al., 2008). Foxp3 is the signature transcriptional factor regulating the suppressive ability of Treg cells (Shevach, 2006).

The induction of iTreg cells in gut seems to be closely related to the DC that prime them. CD103$^+$ DC in the LP of small intestine have been shown to be the major subset to induce iTreg due to their high production of TGFβ and RA (Sun et al., 2007). CD103$^+$ DC was also shown to inhibit Th17 differentiation via TSLP expression while in turn enhancing Treg development (Spadoni et al., 2012). Besides CD103$^+$ DC, DC in the mLN that express COX-2 are shown to promote Treg differentiation by suppressing IL-4 production (Broere et al., 2009).

1.3.4 Mesenchymal cells in the intestinal lamina propria

Besides endothelial cells, there are many other types of mesenchymal cells in the small intestine reported, including fibroblasts, myofibroblasts, pericytes wrapping the vasculature, bone marrow–derived stromal stem cells, smooth muscle cells of the muscularis mucosae, and smooth muscle cells surrounding the lymphatic lacteals (Figure 1.5) (Powell et al., 2011). It is difficult to distinguish these mesenchymal cells from each other due to the lack of unique markers. Often a combination of several markers is required, such as α-SMA, desmin, vimentin, and CD90 (Table 1.2) (Pinchuk et al., 2010). Generally speaking, smooth muscle cells are highly positive in α-SMA and desmin, however, pericytes and some activated myofibroblasts are also positive for both markers (Table 1.2) (Link et al., 2007) thus making the identification of fibroblasts difficult from other cells. The ability to produce abundant extracellular matrix (ECM) can also be a good indicator for identifying fibroblasts from other mesenchymal cells. It has been shown gp38/podoplanin is expressed in the intestinal lamina propria by the non-epithelial and non-muscularis layers (Farr et al., 1992). Whether gp38 can serve as a fibroblast marker in the intestinal LP remains to be determined.

1.3.5 Intestinal fibroblast contribution to immune response

There are some studies suggesting intestinal LP fibroblasts can contribute to immune response or tolerance, most of them are done with cultured primary human colonic fibroblasts in vitro (Bega, 2012). Primary human colonic subepithelial fibroblasts were shown to up-regulate COX-

2 and iNOS expression upon LPS and/or IL-17 treatment in vitro (Zhu et al., 2012) (Zhang et al., 2005), reminiscent of FRC in the LN (Siegert et al., 2011). Myofibroblasts isolated from small intestine were also found to constitutively express iNOS mRNA and their expression can be further enhanced upon TNFα, IL-1β, or IFNγ treatment in vitro (Wu et al., 2013). Human colonic myofibroblasts were also shown to promote the expansion of Treg cells in vitro (Pinchuk et al., 2007). Besides, α-SMA^{+}CD90^{+} subepithelial myofibroblasts were proposed to be non-professional APC as they constitutively express MHCII molecules in the normal colonic mucosa and stimulate T cell proliferation in a MHCII and CD80/86 co- stimulatory molecule dependent manner in vitro (Saada et al., 2006). How these intestinal fibroblasts contribute to immune
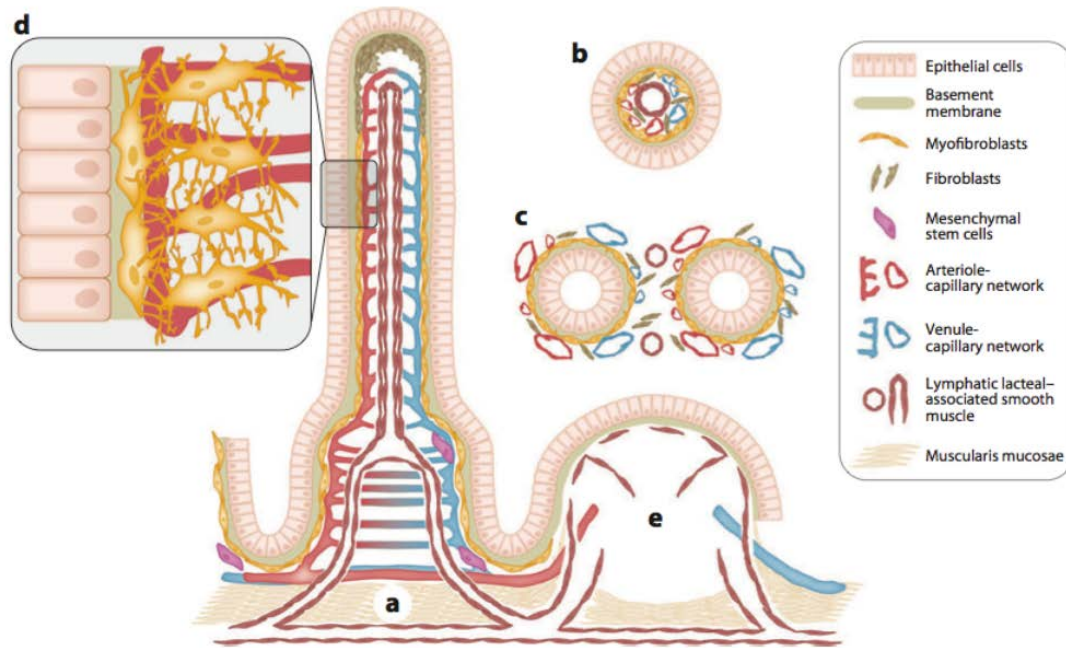
Figure 1.5 Schematic representation of the epithelium and mesenchymal elements of the small intestinal villus-crypt axis.
(a) Longitudinal representation of the villus and crypt showing the epithelium and lamina propria containing α-SMA[+] subepithelial myofibroblasts and pericytes of the capillaries, mesenchymal stem cells, and smooth muscle associated with the lymphatic lacteal and the muscularis mucosae. Fibroblasts (α-SMA[−]) are shown, especially in the upper portion of the villus. (b) Cross sections through a villus show the lymphatic lacteal with associated smooth muscle. (c) A cross section through the crypts demonstrates the lymphatic pericytes. Panels b and c also show that the subepithelial myofibroblasts are essentially pericytes in subepithelial locations of the villus. (d) A higher power depiction of the myofibroblasts and pericytes with cytoplasmic processes that surround and support the capillaries. (e) A Peyer's patch with its vascular, lymphatic, and stromal elements. (Powell et al., 2011)

Table 1.2 Mesenchymal cell markers.

Cell type	Myofibroblasts	Fibroblasts	Pericytes	Stromal stem cells	Muscularis mucosae	Lymphatic lacteal-associated smooth muscle
Markers						
α-SMA	+	−	+	+	+	+
Desmin	−	−	±	−	+	+
Vimentin	+	+	+	+	−	−
CD90	+	+	+	+	±	+

Identification of the several cell populations in the small intestine. "+" positive, "-" negative and "±" low or negative expression (Bega, 2012) (Pinchuk et al., 2010)

response in vivo remains to be determined due to the technical restriction of isolating ex vivo fibroblasts from the intestine. However, a very recent paper showed the existence of a population of gp38$^+$CD31$^-$CD45$^-$EpCAM$^-$ stromal cells in the small intestine that is involved in imprinting mucosal DC via the production of RA and GM-CSF. This process is dependent in vivo on commensals (Vicente-Suarez et al., 2014).

1.4 Aim of the thesis

Overview of the project

Fibroblastic reticular (FRC) networks can be found in all secondary lymphoid organs, including the lymph node (LN). Besides serving as scaffold for cell adhesion and migration, LN FRC contribute to naïve T cell homeostasis and function by providing chemoattractants and survival factors. New evidence suggests that LN FRC can restrain strong T cell expansion by expressing immune modulators dependent on the enzymes COX-1/2 and iNOS. Gene array data and unpublished data from our lab suggest that a subset of LN FRC may also provide survival factors for plasma cells. These findings raise the question whether the LN FRC network is modified during an ongoing immune response, or whether it is present within the gut lamina propria (LP) where scattered effector T cells and large numbers of plasma cells are present. While fibroblasts have been observed in the LP, their organization and function are poorly understood.

Part I: Elucidate how the fibroblastic reticular cell network of the T zone changes in response to the rapid lymph node swelling occurring during adaptive immunity.

LN grow strongly during immune response but at the start of this project it was not well understood how the rigid FRC network adapts to this massive increase in number of T cells: are FRC stretched, disrupted, activated or do they grow in number due to FRC proliferation? In case FRC develop an expanded network, what signals trigger their proliferation during LN swelling? Is there a particular cell population serving as FRC progenitor cells? Existing literatures imply a role of DC and LT$\alpha\beta$, in inducing expansion of FRC but the detailed mechanism is still missing. Also, it remains to be clarified whether FRC in activated LN keep their function for naïve lymphocytes, namely the expression of cytokines like IL-7, CCL19 and CCL21. (described in chapter 2)

Part II: Isolation and characterization of fibroblasts in the intestinal lamina propria.

Fibroblasts of the gut LP are poorly defined at the morphological, phenotypic and functional level. It raises the question whether sites of scattered effector lymphocytes like the LP also harbour an FRC-like network that may act as scaffold and organizer cell besides having potential roles in immune tolerance. In addition, the survival niche of plasma cells in the gut LP has not been defined. To address some of these open questions, I examined whether a fibroblast cell type is responsible for organizing a reticular network similar to LN and whether they may affect immune functions. As there was neither an established isolation protocol nor good surface markers for intestinal fibroblasts, my first aim was to establish good tools to study intestinal fibroblasts, including the identification of markers suitable for fibroblast staining, the development of isolation protocols for FACS staining and cell sorting, and the characterization

of LP fibroblast cell lines. Together, these approaches should allow a better characterization of the organization, phenotype and potential functions of intestinal fibroblasts. (described in chapter 3)

2. Mechanisms of FRC expansion during immune response in draining LN (Collaboration with T. Vogt)
Results published in PNAS, 111(1):E109-18, 2014

2.1 Results

2.1.1 Lymph node hyperplasia is accompanied by rapid FRC activation and expansion.

To study the behavior of stromal cells in an acute LN swelling model and associate it with the T cell response, ovalbumin (OVA)-specific TCR-transgenic CD8$^+$ T cells (OT-1) and CD4$^+$ T cells (OT-2) were adoptively transferred into mice that were then subcutaneously immunized with OVA antigen emulsified in an oil-in-water adjuvant, Montanide ISA-25 (Mont). A pool of 6 draining LN was enzymatically digested to analyze both hematopoietic and stromal cells by flow cytometry. OVA-injection induced rapid and strong LN swelling, peaking on day 8 and declining thereafter (Figure 2.1A). While OVA-specific T cells strongly expanded, ~85% of cells found in swollen LN were naive host-derived naive (CD69$^-$ CD44$^-$) T and B lymphocytes. Continuous in vivo BrdU labeling showed that proliferation was largely limited to OVA-specific T cells and a small B cell subset. The three major CD45$^-$ non-hematopoietic stromal cells, FRC, lymphatic endothelial cells (LEC) and blood endothelial cells (BEC) were distinguished based on their CD31 and gp38 expression (Figure 2.1B), as described previously (Link et al., 2007). Analysis of their numbers revealed a gradual expansion of all three subsets starting on day 3 and reaching a 5-fold increased number on day 8-14 (Figure 2.1C), comparable to the 5-fold increase in lymphocyte number (Figure 2.1A). The stromal cell growth was at least in part due to proliferation as up to 70% of FRC, LEC and BEC incorporated BrdU within the first 8 days after immunization (Figure 2.1C, D). To examine if LN stromal expansion occurred also during infection, the protozoan parasite *Leishmania major* was inoculated in B6 mice and LN analyzed 19 days post infection. A similar expansion of FRC, LEC and BEC was visible (Figure 2.1E), demonstrating that FRC expansion is a feature common to adaptive immunity induced by immunization or infection. (Data provided by T. Vogt)

To define the sequence of early events in more detail, LN were analyzed 20 and 40 hours after OVA/Mont immunization. Trapping of naive lymphocytes started as early as 20 hours (Figure 2.2A), while first OVA-specific T cell proliferation was detected at 40 hours (Figure 2.2B). Strikingly, an increase in FRC number and proliferation was already observed at 40 hours, in contrast to LEC and BEC which both entered cell cycle only around day 3.5 (Figure 2.2C, 2.1C). Surprisingly, FRC and LEC increased their size and granularity as early as 20 hours upon immunization, with a peak at 40 hours followed by a slow decrease over several weeks (Figure 2.2D-G). FRC as well as lymphocyte numbers in activated LN remained higher than in the naïve

LN over 2 months after immunization, however, without evidence of increased turnover (Figure 2.2H-I). (Collaborated with T. Vogt)
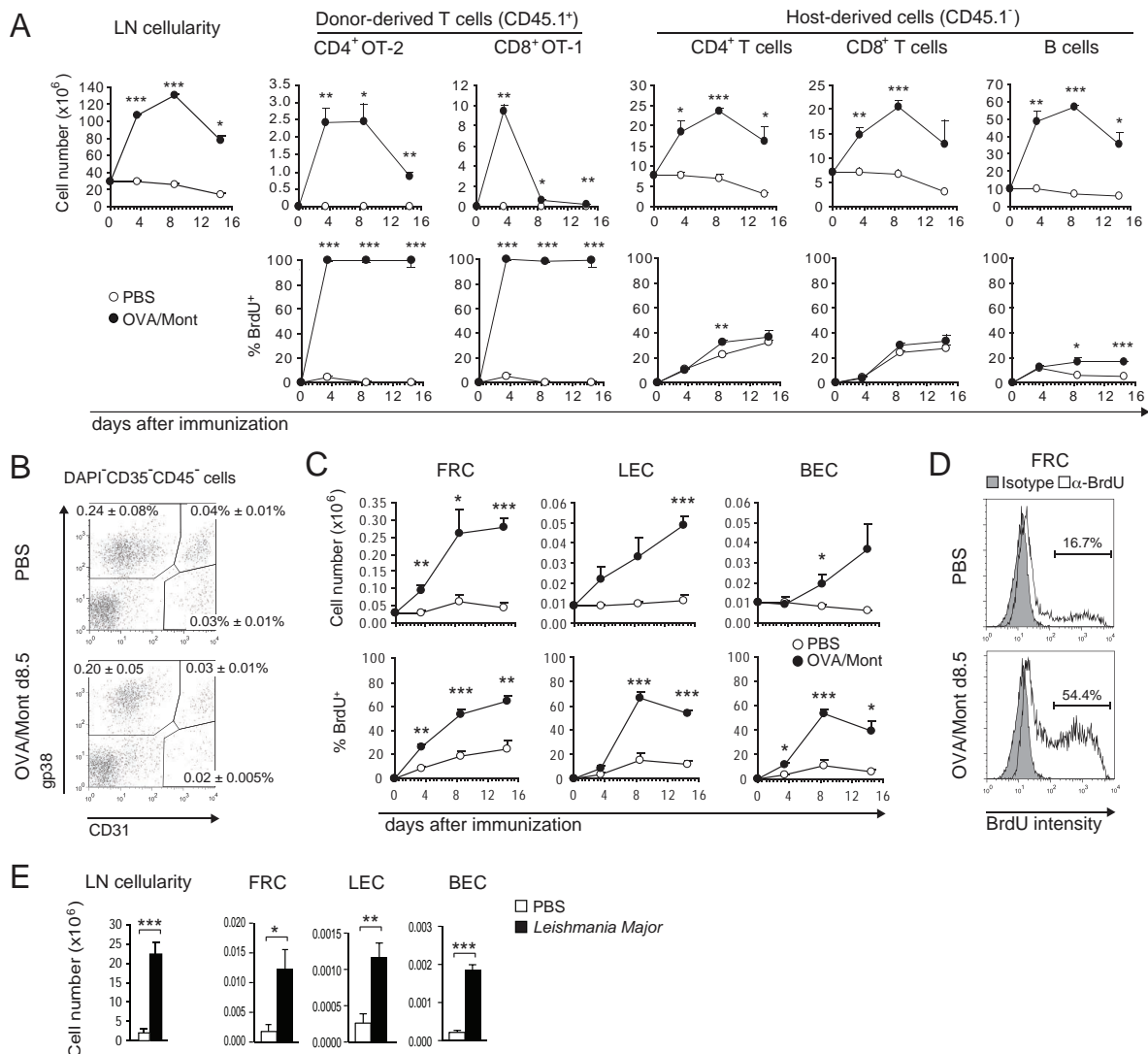
Figure 2.1 FRC and endothelial cells expand rapidly during immune response in draining peripheral lymph nodes. (Data provided by T. Vogt)

(A-D) Splenocytes from OT-1 (OVA-specific CD8+ TCR tg) and OT-2 (OVA-specific CD4+ TCR tg) C57BL/6 mice on a CD45.1$^+$ background were transferred into C57BL/6 (CD45.2$^+$) recipient mice which then received s.c. injections of OVA/Montanide (Mont) or PBS, along with BrdU administration. The six draining peripheral LN were isolated at the indicated time points after immunization, fully digested, and analyzed by flow cytometry. (A) Shown are the number (upper panel) and proliferation (BrdU incorporation; lower panel) of indicated cell populations from PBS-control (open circles) and OVA/Mont-immunized (closed circles) mice. (B) Representative dot plots of CD45$^-$CD35$^-$ pre-gated stromal cells identifying FRC (gp38$^+$CD31$^-$), LEC (gp38$^+$CD31$^+$) and BEC (gp38$^-$CD31$^+$). (C) Representative histograms showing FRC stained with an antibody to BrdU (white) or an isotype-matched control (grey area) 8.5 days after PBS or OVA/Mont injection. (D) Number (upper panel) and proliferation (lower panel) of FRC, LEC and BEC at indicated time points after OVA/Mont immunization. (E) Wild type C57BL/6 mice were infected with *Leishmania major* in both footpads. On day 19, the two draining popliteal LN were isolated and enzymatically digested and analyzed as above. Data are mean ± SD, representative for 2-3 independent experiments, with n ≥ 3 mice per group.

FRC lines have been shown to change their surface phenotype and function upon treatment with pro-inflammatory molecules (Katakai et al., 2004a) (Vega et al., 2006) (Siegert et al., 2011). Consistent with these findings, the mean fluorescence index (MFI) of gp38 but not PDGF-Rα expression increased by 200% within 40h and remained at this level until day 5.5 before declining sharply on day 8.5 (Figure 2.3A). The 50% increase in cell size can only partially explain the strong increase in gp38 surface expression,
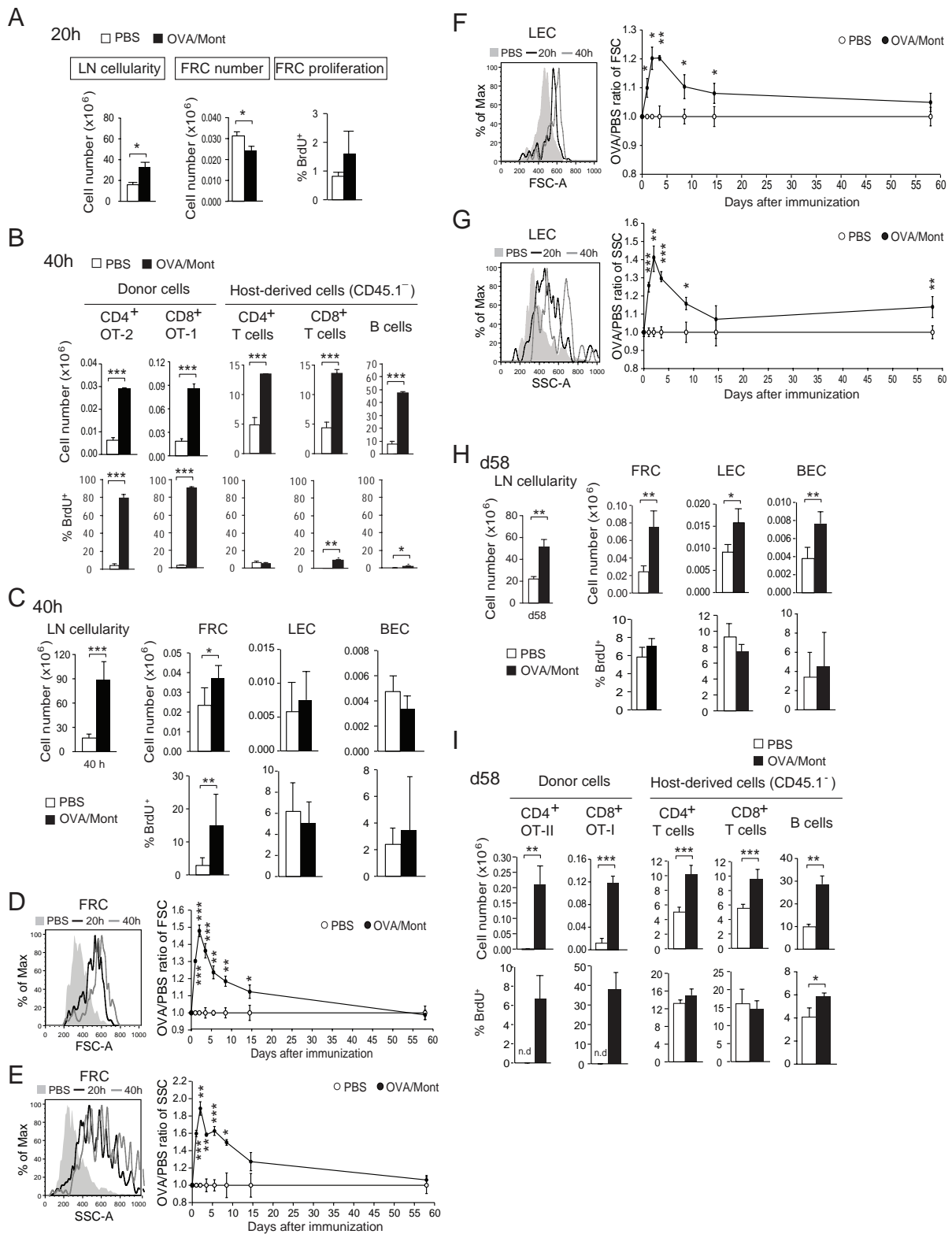
Figure 2.2 FRC increase their size within 20 hours and proliferate within 40 hours after immunization.

(Collaborated with T. Vogt)

OT-1 and OT-2 splenocytes were transferred to WT mice followed by OVA/Mont immunization. (A) LN cellularity, FRC number and proliferation are shown 20 hours after OVA/Mont immunization. (B, C) Cell numbers and proliferation of lymphocytes (B) and stromal cells (C) were assessed by flow cytometry in the draining LNs at 40 hours after immunization. (D-G) Representative histograms and kinetics for FSC (size; D, F) and SSC (granularity; E, G) of FRC (D, E) or LEC (F, G) at indicated time points after OVA/Mont immunization. The OVA/PBS ratio shows the FSC and SSC level of FRC or LEC from OVA/Mont- (closed circles) relative to PBS-injected (open circles) mice. (H-I) Cell numbers and proliferation of stromal cells (H) and lymphocytes (I) were assessed by flow cytometry in the draining LNs at 58 days after immunization. Data are mean ± SD, representative for 2-3 independent experiments, with n ≥ 3 mice per group.
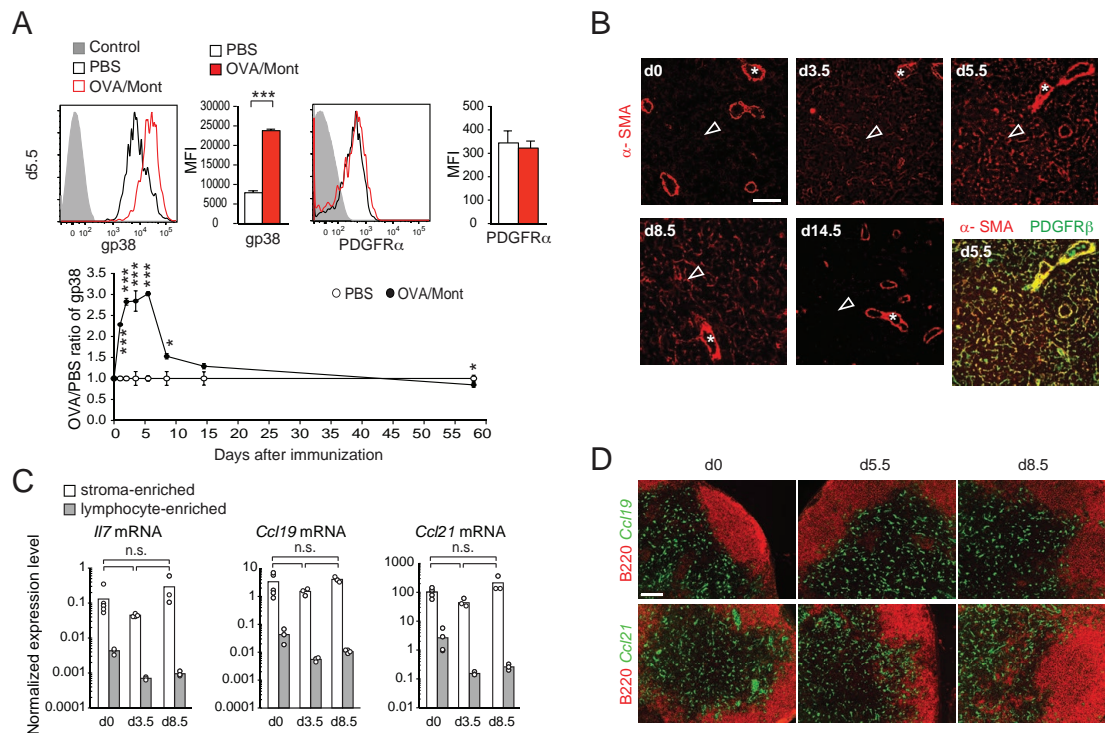
Figure 2.3 FRC from swollen lymph nodes display an activated phenotype. (Collaborated with T. Vogt and L. Scarpelino)

(A) Upper panel: representative histograms and mean fluorescence intensity (MFI) for the surface expression of gp38 and PDGFRα on FRC in the LN of PBS- (black line) or OVA/Mont-injected (red-line) mice 5.5 days after immunization. Surface protein expression on CD45^{+} cells served as negative control (grey area). Lower panel: kinetics of surface gp38 expression on FRC at indicated time points after OVA/Mont immunization (closed circles) relative to PBS control (open circles). (B) Representative images showing the expression of the myofibroblast marker, α-SMA, in LN sections taken at the indicated time points after OVA/Mont immunization, as assessed by immunofluorescence labeling. Asterisks indicate HEVs surrounded by smooth muscle cells and open arrows indicate reticular FRC, which co-stained for PDGFRβ. Labeling, exposure time and image processing were kept identical for all time points shown. (C) mRNA expression of *Il7*, *Ccl19*, and *Ccl21* were measured in stroma-enriched (white bars) and lymphocyte-enriched (grey bars) fractions from draining LN at 0, 3.5 and 8.5 days after immunization, and normalized to two housekeeping genes, as described in materials and methods. (D) Representative images of in situ hybridization analysis showing *Ccl19* and *Ccl21* transcripts (green) in lymph node sections on day 0, 5.5, and 8.5 after OVA/Mont immunization, along with B220 antibody staining (red). The slides were treated equally (ISH development, exposure time for photos, processing of images). n ≥ 3 mice per group, data in A, B and D are representative for 2-3 independent experiments. Showing mean ± SD. Scale bars represent 100 μm. n.s.: differences are statistically not significant.

particularly at d5.5 when FRC show only a 25% size increase. Increased gp38 levels were also seen in splenic FRC after viral infection (Benedict et al., 2006) (Bekiaris et al., 2008), suggesting it may serve as an activation marker of FRC. Furthermore, α-smooth muscle actin (α-SMA), a known myofibroblast marker (Tomasek et al., 2002) (Link et al., 2007), was also induced upon immunization and peaked at day 5.5 (Figure 2.3B) suggesting FRC show signs of late activation which are distinct from proliferation or gp38 up-regulation. No significant changes were observed in transcripts for *Il7*, *Ccl19* and *Ccl21*, neither by qPCR (Figure 2.3C) nor by in situ hybridization (Figure 2.3D), although a trend to lower transcript levels was observed on d5.5 (Figure 2.3C). Similarly, no marked changes were observed for CCL21 protein expression as based on histological analysis (not shown). Together, these data demonstrate that upon immunization FRC are rapidly, yet transiently, activated while maintaining expression of cytokines important for naive T cell recirculation and survival. (Collaborated with T. Vogt and L.

Scarpellino)

2.1.2 FRC network in the T zone preserves its architecture during immunization but expands into the medullary area.

Next we assessed histologically whether LN swelling leads to alterations in the integrity and organization of the LN FRC network. On day 8.5 as well as at earlier time points the organization of the FRC and matrix network in the central T zone was comparable to naïve LN, including the reticular morphology of FRC and their association with conduits (Figure 2.4A, B; not shown). These conduits remained fully functional in activated LN, with efficient lymph flow towards HEV and no evidence of fluid leakage (Figure 2.4C). 3D analysis of the central T zone indicated a comparable spacing of the FRC network in inflamed and naïve LN, fitting approximately 5-10 lymphocytes within a 2D plane (Figure 2.4D). Also comparable were the length of the total FRC network in a given volume or of individual FRC (Figure 2.4E). However, a strong increase in the volume covered by gp38$^+$ FRC networks was observed, both in the expanded T zone and medulla (Figure 2.4F). More detailed analysis of medullary cords revealed a 3D sponge-like network of laminin$^+$ fibers enwrapped by reticular cells with an FRC-like phenotype (gp38$^+$CD31$^-$ LYVE-1$^-$) that was much more pronounced in activated than naive LN (Figure 2.4G). These results demonstrate the astonishing capacity of the matrix and FRC network to adapt rapidly to the massive organ growth, while preserving some of its principal characteristics. (Data provided by T. Vogt and S. Favre)

2.1.3 Locating the BrdU$^+$ proliferating FRC in swollen LN

The kinetic of BrdU incorporation in FRC shown in Figure 1C indicates that only 60-70% of FRC have undergone proliferation at the peak of acute LN swelling while their number has increased 5-fold. If one assumes that these fibroblasts have divided at least twice it suggests that only a small subset of FRC have proliferative capacity. We therefore asked whether BrdU$^+$ FRC were found in specific zones only, like in the strongly enlarged medullary cords. However, it is very difficult to identify BrdU$^+$ FRC in the presence of abundant proliferating lymphocytes in immunized LN with immunofluorescence (IF) microscopy. In order to visualize these proliferating FRC and their distribution in the LN, mice were irradiated to deplete highly proliferating lymphocytes on day 7 after OVA/Mont immunization and then BrdU and gp38 of LN were detected by IF. In LN of lethally irradiated mice (900 rad), there were few T and B cells left and the stromal compartment seemed to be maintained. In contrast, LN of sub-lethally irradiated mice (450 rad) still showed a considerable number of lymphocytes and were therefore not
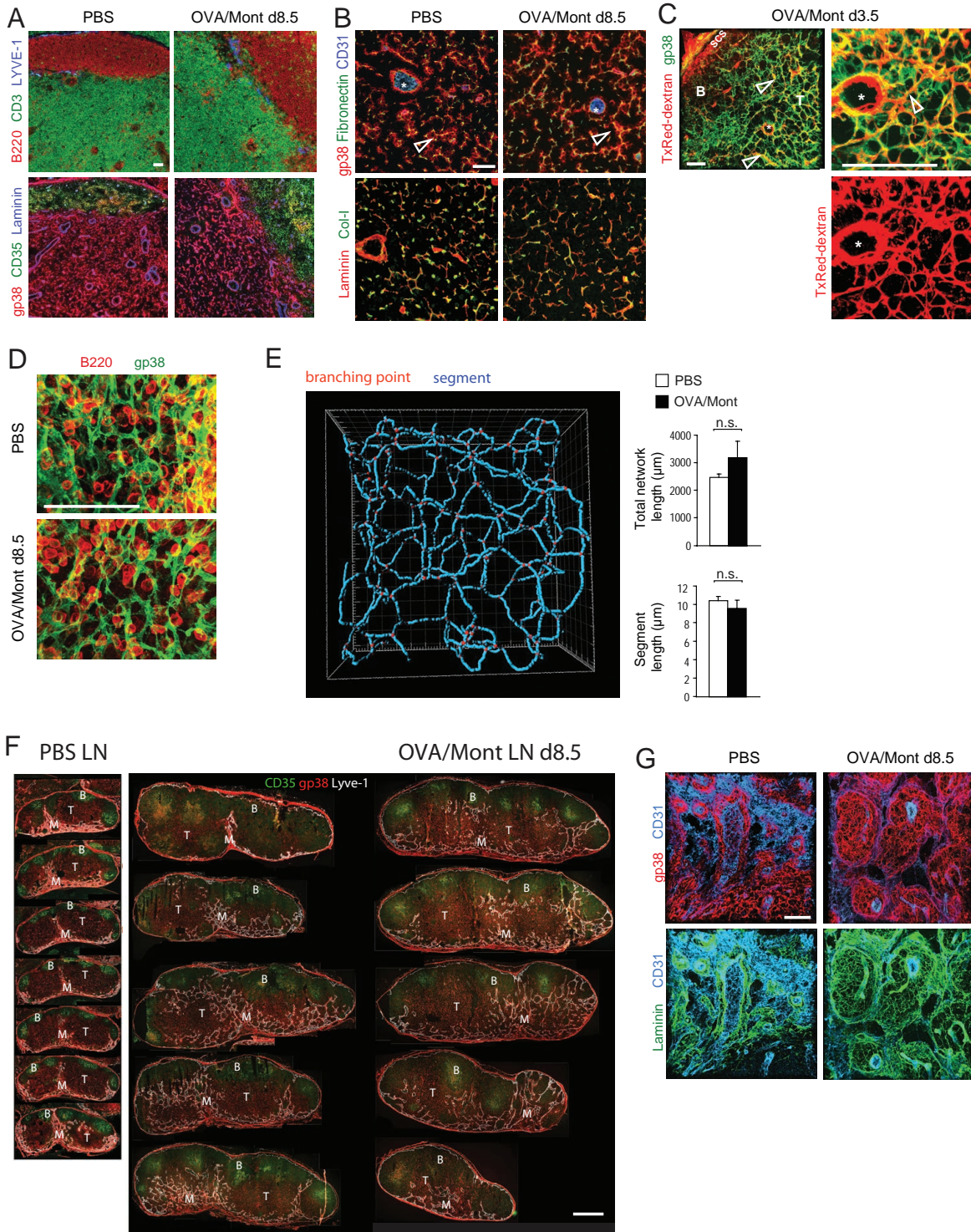
Figure 2.4 Expanding FRC network preserves its usual structure and function while extending into medullary cords. (Data provided by T. Vogt and S. Favre)

Immunofluorescence microscopy of cryostat sections (A, B, F) or 80 µm-thick vibratome sections (C-D, G) from draining LN of PBS or OVA/Mont-immunized mice were labeled with the indicated antibodies. (A) B220^{+} B cells and CD3^{+} T cells indicate B and T zones, respectively. LYVE-1 stains lymphatic vessels. Consecutive sections show FRC (gp38^{+}CD35) and FDC (gp38[+/-]CD35^{+}) networks as well as the laminin^{+} basement membranes of vessels and conduits. (B) Higher magnification of the T zone showing CD31^{+} HEV (asterisks) and reticular FRC (gp38^{+}) wrapped around fibronectin-positive conduits (open arrows); conduits are composed of collagen-I^{+} (Col-I) fibrils surrounded by a laminin[+] basement membrane. (C) Texas (Tx) Red-dextran was injected s.c. 3.5 days after OVA/Mont immunization, draining LN isolated 30 min thereafter followed by their processing for histological labeling. Open arrows highlight TxRed-dextran[+] conduits surrounded by gp38[+] FRC; asterisk shows a HEV with a perivascular space rich in TxRed-dextran. (D) Vibratome sections of the LN T zone in PBS and OVA/Mont-immunized mice demonstrating a similar density and architecture of the gp38+ FRC network in the two settings. B220^{+} B cells are shown as size comparison. (E) Filament tracer software was used to quantify the total network length and the segment length of individual FRC in images derived from gp38-labeled vibratome sections (mean ± SD), as shown in D. (F) FRC growth during immune response occurs in T zones as well as medullary cords. Serial 8 µm sections were made of entire naive or d8.5

OVA/Mont-activated lymph nodes. Every 10th section was labeled with markers for FRC (gp38^{+} Lyve1^{-}), FDC (CD35^{+}gp38^{+/-}) and lymphatic vessels (gp38^{+}Lyve1^{+}). Digital images taken of the same lymph node section were stitched together to visualize the entire LN cross-section and sequential sections of the same LN are shown in a column. FDC-rich areas indicate the B zones (B), FRC-rich regions the T zone (T) as well as the medullary cords (M) identified by a high density of lymphatic vessels. One representative example out of three investigated naïve or activated LN is depicted. Scale bar represents 500 µm and is representative for both image series. (G) 80 µm thick vibratome sections showing medullary cords displaying extensive gp38^{+} reticular FRC networks wrapping around laminin^{+} conduits and connecting with CD31^{high} HEV. The cords are demarcated by a thin layer of CD31^{int}gp38^{+} lymphatic endothelium. Data are representative for 2-3 experiments with at least 2 mice and 6 LN per mouse. Scale bars represent 100 µm except for figure F.
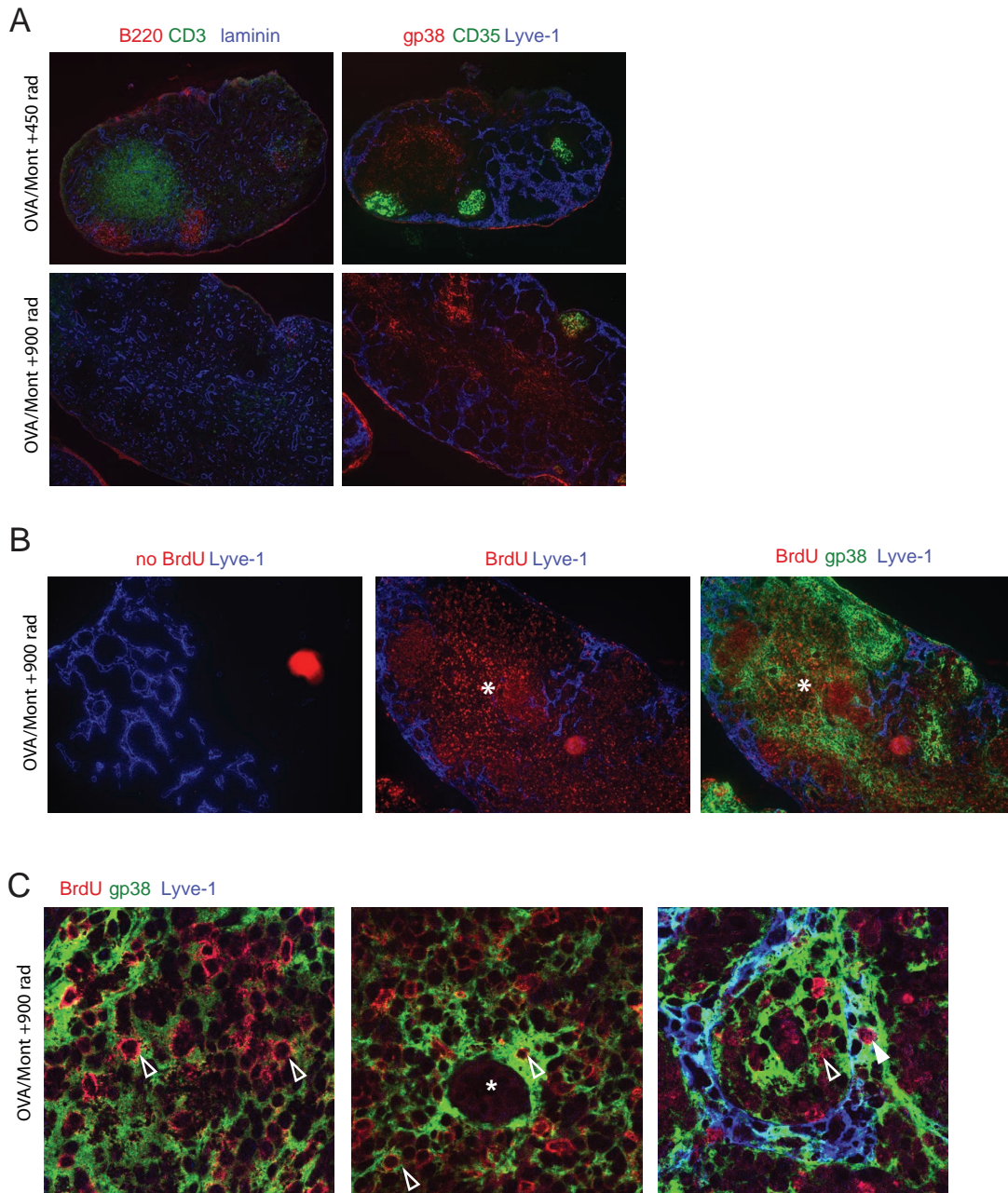
Figure 2.5 BrdU[+] FRC were found all over the T Zone and medulla.

WT mice having received OT-1 and OT-2 cells were immunized with OVA/Mont and from then onward supplied with BrdU-containing drinking water. 7 days after immunization, the immunized mice were then irradiated either with 450 rad or 900 rad, rested for 2 days before sacrifying them and preparing the tissues for immunofluorescence (IF) staining. (A) IF images of LN from mice having received 450 (upper panel) or 900 (lower panel) rad of irradiation to visualize B (B220^{+}) or T (CD3^{+}) cells and the stroma compartment (gp38+ FRC, CD35+ FDC, Lyve-1+ LEC) after irradiation. (B) Confocal images of BrdU co-staining with gp38 and Lyve-1 on LN of mice having received 900 rad of irradiation. Left: no BrdU Ab was added as negative control. Stars indicate the location of the central T zone. (C) Confocal images are shown in higher magnification to visualize BrdU+gp38+ FRC (open arrows) in the central T zone (left), around HEV (center), and in medullary cords (right). Some BrdU+ LEC are also found in medullary cords (right, closed arrow).

adequate (Figure 2.5A). In mice irradiated with 900rda, BrdU-positive cells were found throughout the whole LN but seemed to be most abundant in central T zones near the HEV (Figure 2.5B, stars). Confocal microscopy with high magnification showed BrdU$^+$gp38$^+$ cells, which are presumably proliferating FRC, can be found in the T zone (Figure 2.5C, left), around HEV (Figure 2.5C, middle), as well as inside the medullary cords (Figure 2.5C, right). In summary, there is no clear segregation of zones dominated by BrdU$^-$ versus BrdU$^+$ FRC.

2.1.4 Dendritic cells are required to initiate FRC growth during LN swelling with partial dependency on MyD88 signals.

To elucidate the sequence of events that control FRC proliferation we first examined the relative role of innate versus adaptive immunity. To this end, we injected OVA/Mont or Montanide alone into WT mice that had or had not received OT T cells. Surprisingly, injection of Montanide induced lymphocyte trapping as well as FRC proliferation (Figure 2.6A), indicating inflammatory signals are sufficient to trigger both processes in the absence of notable lymphocyte activation. While not required, adaptive immunity as induced by OVA/Mont led to a stronger lymphocyte trapping and FRC expansion than Montanide, especially when OVA-specific T cells were present (Figure 2.6A). Given that these activated lymphocytes start to be detectable only at 40h after OVA/Mont immunization, only the later FRC expansion appears to be sustained by signals present during adaptive immunity. Migratory DC are known to transmit antigen and inflammatory signals to LN and thereby start the swelling process (MartIn-Fontecha et al., 2003) (Webster et al., 2006). Indeed, mice depleted of DC showed a strongly reduced lymphocyte trapping and T cell expansion on day 3 after OVA/Mont immunization (Figure 2.6B-D) (Webster et al., 2006). Strikingly, the number and proliferation of FRC were also much reduced (Figure 2.6D), indicating a requirement for DC, consistent with a recent report (Chyou et al., 2011). Since both migratory and LN-resident DC are depleted in CD11c-DTR mice, we investigated whether transfer of migratory DC is sufficient to trigger FRC expansion. When LPS-matured bone marrow-derived DC (BMDC) with or without OVA protein were injected into WT mice, they efficiently induced LN swelling and FRC expansion (Figures 2.6E, 2.7A). Similar results were obtained with CpG-matured BMDC (Figure 2.7A). These results demonstrate that migratory DC can induce LN swelling as well as FRC expansion, with a potential contribution by adaptive immunity elicited by OVA or bovine serum proteins present in the medium. However, BMDC are not direct inducer cells for LN swelling and FRC expansion, as BMDC transfer into mice depleted of endogenous DC had hardly any effect on lymphocyte trapping and FRC expansion (Figure 2.7B), suggesting migratory DC require LN-resident DC to trigger both processes. (Collaborated with T. Vogt)

To explore whether Myd88-dependent signaling via Toll like receptor (TLR) or IL-1 cytokine family receptors (IL-1/18/33) was required in migratory DC, MyD88 knockout (KO) BMDC matured with either LPS or CpG were injected, but surprisingly they triggered a comparable
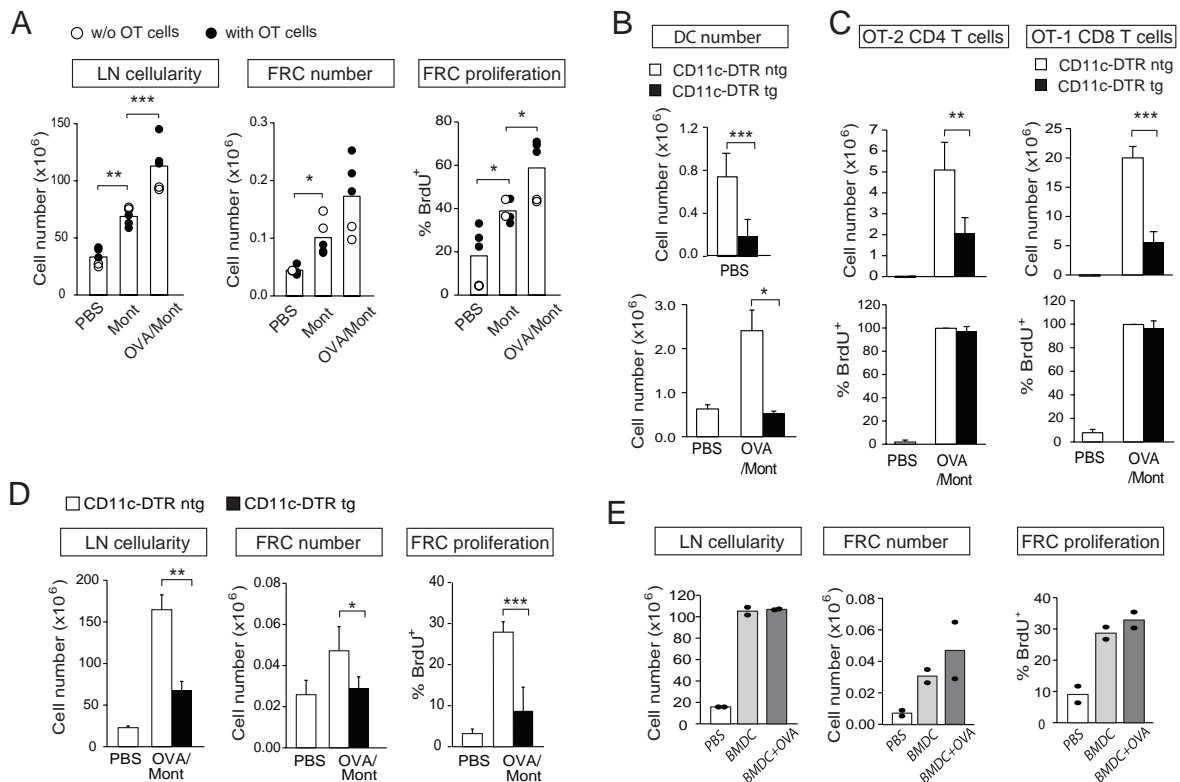
Figure 2.6 DC are required for FRC growth during immune response. (Collaborated with T. Vogt)

(A) Mice having received OT T cells (closed circle) or without (open circle) were immunized with PBS, Montanide (Mont) or OVA/Mont and draining LN analyzed 5.5 days after immunization using flow cytometry. Statistics were calculated on the pool of all data points. (B-D) CD11c- diphtheria toxin receptor (DTR) transgenic (tg) or non-transgenic (ntg) littermate mice received OT T cells, then one injection of DT one night before s.c. immunization with OVA/Mont or PBS. Draining LN were analyzed by flow cytometry on day 3 after immunization. Depletion efficiency of DC (B) and number and proliferation of OT T cells (C) were assessed. DC were identified as CD11c$^+$ MHCII$^+$ CD19$^-$ TCRβ$^-$ cells. (D) Total LN cellularity, FRC number and FRC proliferation were assessed. (E) Wild type (WT) mice having received OT T cells were immunized s.c. with 1x10^6 BMDC activated by 0.1 µg/ml LPS. The BMDC were either pulsed with OVA antigen (BMDC+OVA) or without OVA (BMDC). Mice were sacrificed and LN were analyzed by FACS 5.5 days after immunization for total LN cellularity, FRC number and FRC proliferation. Data are mean ± SD, representative for 2-3 independent experiments, with n ≥ 2 mice per group.

FRC expansion as WT BMDC (Figure 2.7A). In contrast, when WT BMDC were injected into MyD88 KO mice, lymphocyte trapping and FRC expansion was reduced relative to WT mice (Figure 2.7C). Interestingly, MyD88 KO bone marrow chimera experiments suggested that MyD88 in both hematopoietic and non-hematopoietic compartment are involved in the induction of FRC proliferation (Figure 2.7D). Meanwhile, the reduction of FRC expansion was not observed in mice deficient in signaling via TLR2, TLR4, IL-1, IL-33 (T1-Fc) or deficient in IL-1/18 processing (caspase-1 KO) (Figure 2.7E) suggesting redundancy among these pathways or alternative pathways. Similarly, cytokines induced downstream of TLR signals, including the STAT-1-dependent IFNαβ and IFNγ, showed no limiting role in this process, nor did the other TLR adaptor molecule, TRIF (Figure 2.7E). Together, the data indicate that endogenous cells, possibly DC or FRC, may respond to TLR or IL-1R signaling via MyD88 to detect danger signals,

eventually leading to FRC proliferation. (Collaborated with T. Vogt)
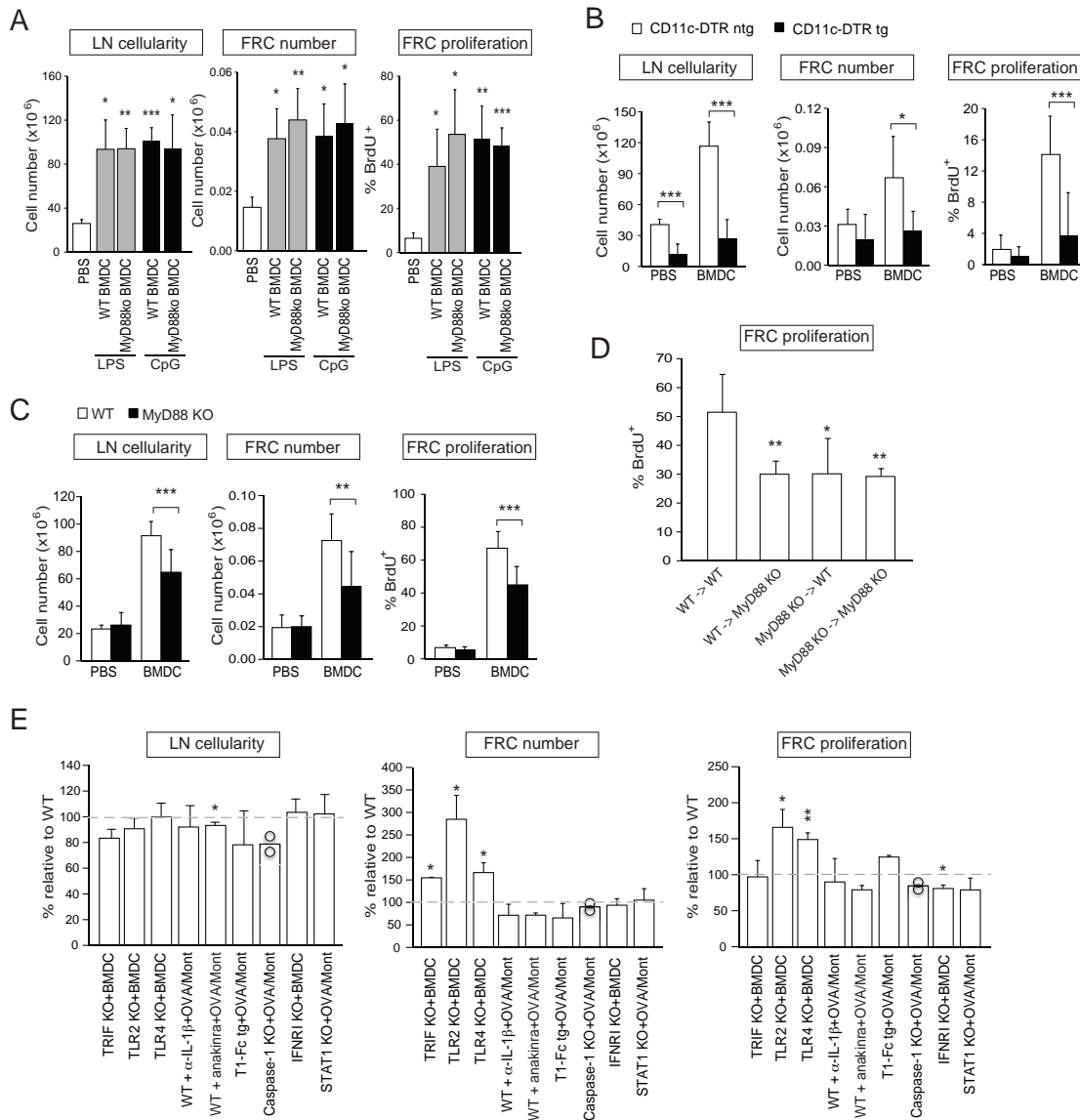
Figure 2.7 DC and MyD88-dependent signals regulate FRC growth during immune response. (Collaborated with T. Vogt)

Mice were immunized s.c. and draining LN analyzed for total LN cellularity, FRC number and proliferation by flow cytometry. (A) WT mice were immunized s.c. with WT or MyD88 KO BMDC activated either with LPS or CpG without loading of OVA antigen and analyzed on day 5.5 days after immunization. (B) CD11c-DTR transgenic (tg) or non-transgenic (ntg) littermate mice were treated with a single dose of DT and then immunized s.c. with PBS or WT BMDC activated with CpG without OVA antigen. LN were analyzed 3 days after immunization. (C) WT or MyD88 KO mice were immunized with WT BMDC activated with CpG without loading of OVA antigen and LN analyzed on day 5. (D) Lethally irradiated, WT or MyD88 KO bone marrow-reconstituted WT and MyD88 KO recipients were immunized with CpG-activated WT BMDC and LN 5.5 days later. T test was calculated relative to the WT -> WT group. (E) Role of various signaling pathways related to MyD88 in FRC expansion on day 5 of the immune response to s.c. injection of BMDC or ova/mont. Investigated were the indicated knockout, transgenic (T1-Fc), or inhibitor-treated (α-IL-1β and anakinra as soluble IL-1 receptor) mice and compared to WT control mice. Data are mean ± SD, either compiled from several experiments or representative of at least 2 experiments with n≥ 2 mice per experiment.

2.1.5 Naive lymphocyte accumulation is required and sufficient to trigger FRC growth.

As we had noted that the increase in FRC numbers closely followed the increase in hypothesis that inflammatory DC trigger FRC growth indirectly by inducing naive lymphocyte trapping. In support of this hypothesis, immunization of lymphocyte-deficient RAG2 KO mice with activated

BMDC did not trigger FRC growth (Figure 2.8B), despite the presence of endogenous DC. To further test this model, we induced lymphocyte trapping in the absence of inflammatory signals by injecting WT mice with IL-7 / α-IL7 complexes that induce abundant homeostatic T cell
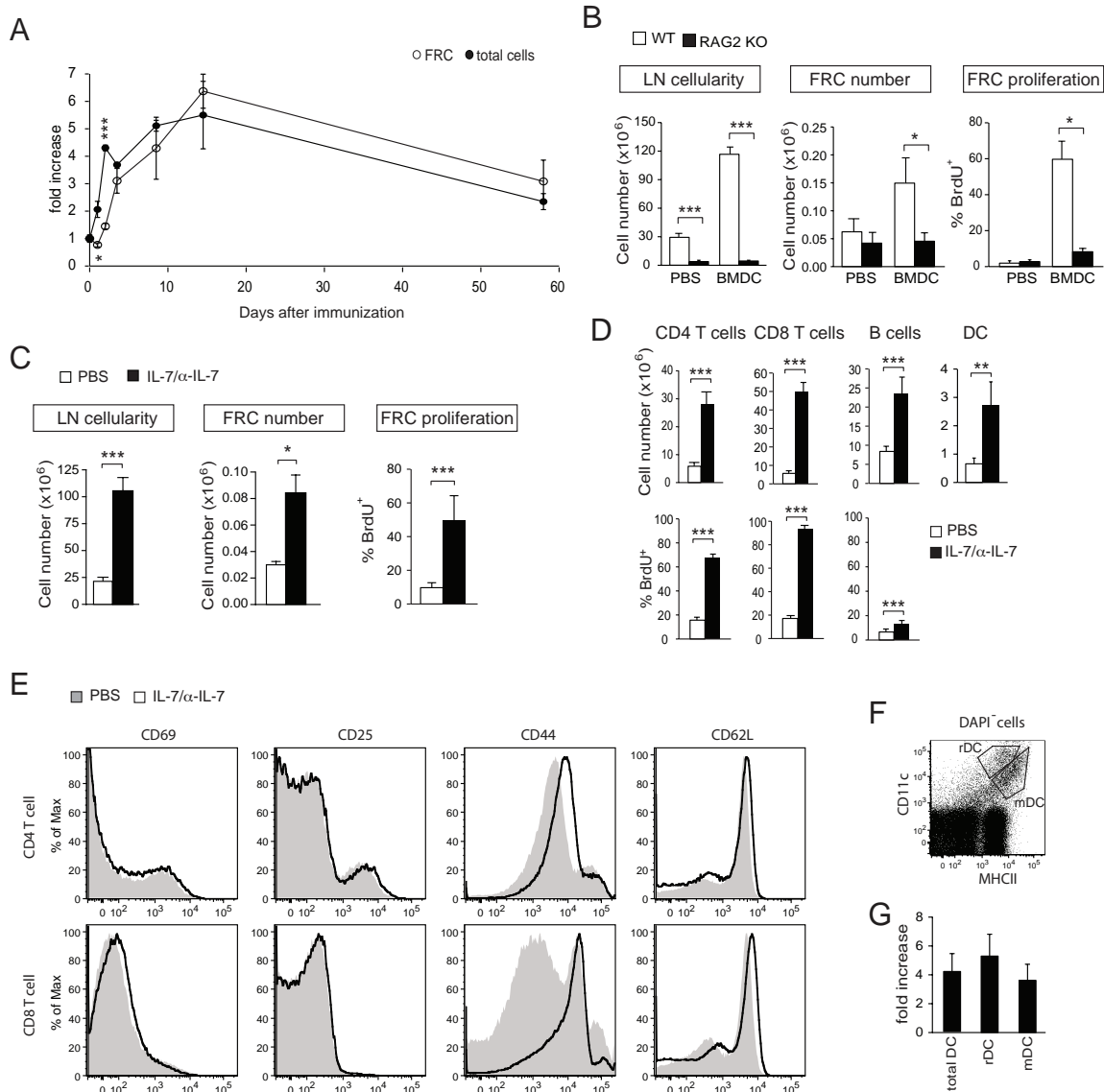
Figure 2.8 The increase in FRC numbers follows closely the one of total lymphocytes during LN swelling

(Collaborated with T. Vogt)

Flow cytometric analysis of the six draining LN after immunization. (A) Mice having received OT cells were immunized with OVA/Mont and the number of FRC and total cells were analyzed at the indicated time points. The fold increase was calculated by dividing cell numbers from OVA-immunized LN to that from naïve LN. (B) WT or T/B-cell-deficient (RAG2 KO) mice were immunized s.c. with PBS or WT BMDC activated with CpG without OVA antigen and sacrificed on day 5.5. (C, D) WT mice received i.p. injections of 200 μl of IL-7 / α-IL-7 immune complexes or PBS on day 0, 1, 2, and 3 and analyzed on day 5.5. Cell numbers and proliferation of FRC (C), lymphocytes and dendritic cells (D) are shown. (E) Representative histogram showing the surface expression of activation markers of CD4+ (upper row) and CD8+ T cells (lower row) after IL-7 / α-IL-7 immune complexes treatment. (F, G) Representative dot plot showing the gating of the two major DC subsets, resident DC (rDC) and migratory DC (mDC) (F) and the fold increase of DC numbers in IL-7 / α-IL-7 versus PBS injected mice (G). Data are mean ± SD, either compiled from several experiments or representative of at least 2 experiments with n≥ 3 mice per experiment.

proliferation (Boyman et al., 2008). Within 5 days the number of total LN cells and T cells increased several fold (Figure 2.8C-D) in the absence of significant T cell activation (Figure 2.8E). An increase in B cells as well as resident and migratory DC was also noted (Figure 2.8D,F and G). Importantly, strong FRC expansion was also observed in this setting (Figure 2.8C) indicating that an increase in naive lymphocytes due to LN trapping may be sufficient to drive FRC proliferation with no need for inflammatory signals or adaptive immunity. (Collaborated with T. Vogt)

2.1.6 Lymphotoxin-$\alpha\beta$/LIGHT signals drive the later FRC growth phase.

To further examine which molecular signals delivered by lymphocytes or DC trigger FRC expansion, we tested inflammatory and growth factor signals known to regulate stromal cell activation and proliferation (Noss and Brenner, 2008) (Zhu and Fu, 2011). Deficiency in the
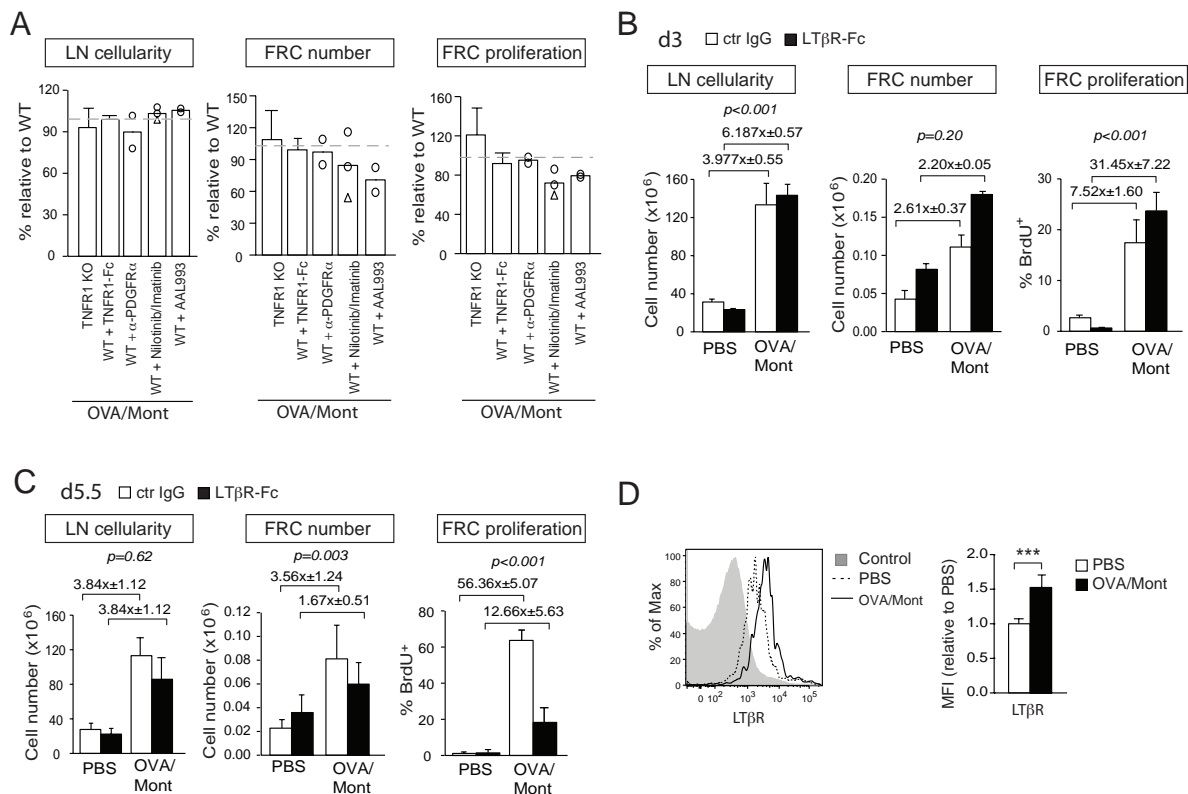
Figure 2.9 Role of LTβR and various mesenchymal cell growth factors in FRC expansion during immune response (Collaborated with T. Vogt)

Flow cytometric analysis of six draining LN after immunization. (A) Knockout mice or WT mice treated with inhibitors (TNFR1-Fc, anti-PDGFRα; Nilotinib and Imatinib as pharmacological inhibitors of PDGFR signaling, and AAL993 as pharmacological inhibitor of VEGFR signalling) were analyzed. Nilotinib (open circles) and Imatinib (open triangles) were pooled together. Shown are percentages indicating the total LN cellularity, FRC number and proliferation of knockout or inhibitor-treated mice relative to WT control mice 5.5 days after immunization. n = 1-3, showing mean ± SD. (B, C) Mice having received OT T cells were injected with LTβR-Fc or control (ctrl) IgG and then immunized with OVA/Mont or PBS followed by the flow cytometric analysis of six draining LN 3 days (B) or day 5.5 (C) after immunization. (D) Representative histogram (left) and mean fluorescence intensity (MFI; right) for the surface expression of LTbR on FRC in LN of PBS- (black line) or OVA/Mont-injected (dashed line) mice. Surface protein expression on CD45^{+} cells served as negative control (grey area).

pathays of TNFα, LTα3, PDGF or VEGF signaling did not strongly affect FRC expansion (Figure 2.9A). Notably, however, LTβR-Fc treatment which blocks LTαβ and LIGHT led to a marked reduction in the fold increase of FRC numbers and proliferation despite normal LN swelling on day 5.5 but not day 3 (Figure 2.9B,C), pointing to a role for LTαβ or LIGHT only in the later phase of FRC expansion. Consistent with this finding, FRC were found to express
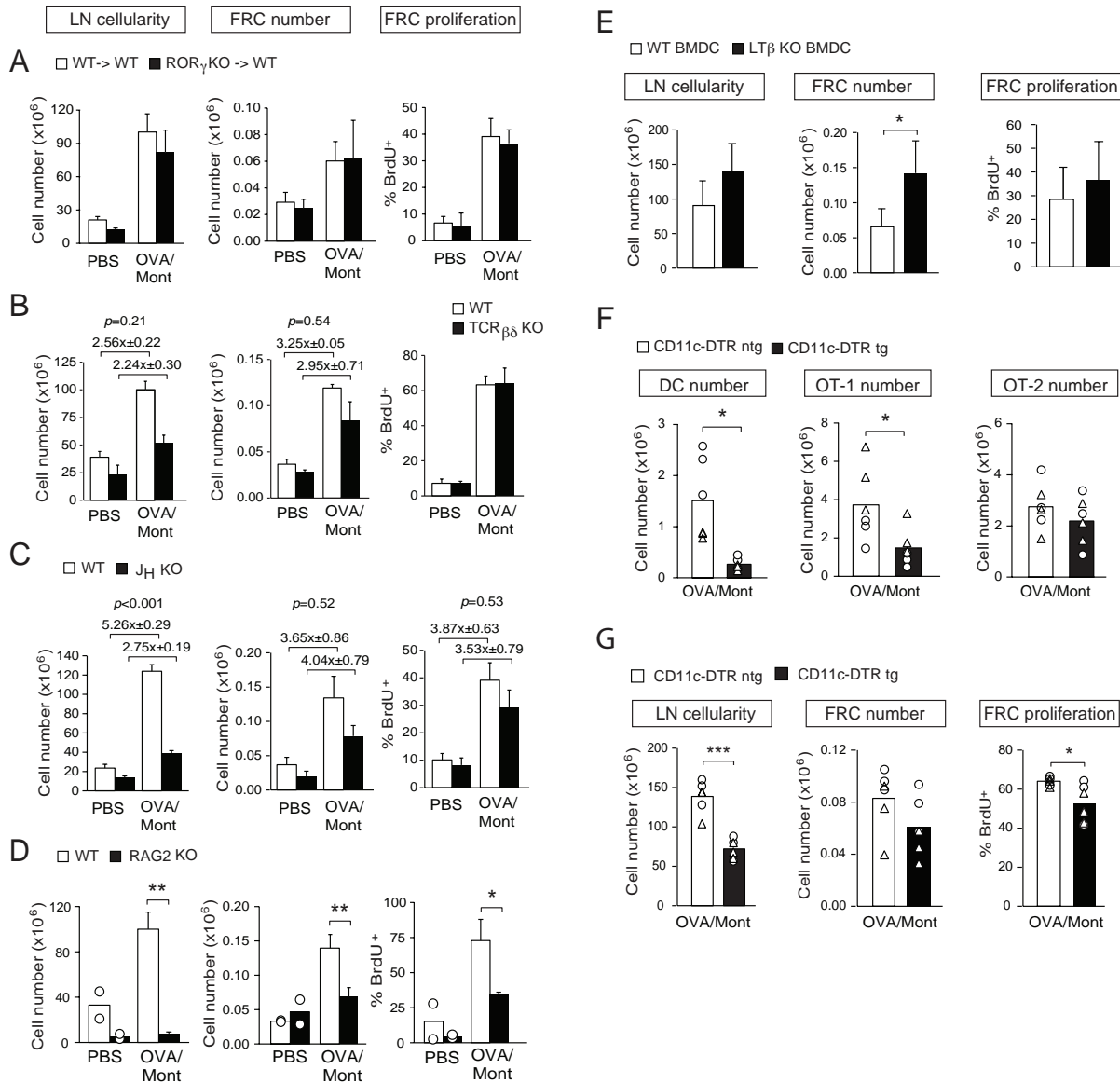
Figure 2.10 Roles of various hematopoietic cell types in providing LTβR signaling for FRC expansion during immune response (Collaborated with T. Vogt)

Flow cytometric analysis of six draining LN after immunization for total LN cellularity, FRC number and proliferation (A-E, G) or DC numbers and OT T cell numbers (F). (A-E) Mice having received OT T cells (A, C) or not (B, D, E) were immunized with OVA/Mont (A-D) or BMDC (E) and analyzed on day 5.5 after immunization. The following mice were analyzed: (A) Bone marrow chimeric WT mice having received either bone marrow from WT or RORγ KO mice (LTi-deficient); (B) WT versus TCRβδ KO (T cell deficient) mice; (C) WT versus J$_H$ KO (B cell deficient) mice; (D) WT versus T/B-cell-deficient (RAG2 KO) mice. (E) WT mice were immunized s.c. with WT or LTβ KO BMDC activated with LPS but without loading of OVA antigen. (F-G) OT T cells were adoptively transferred into CD11c-DTR transgenic (tg) or non-transgenic (ntg) littermate mice which were then immunized s.c. with OVA/Mont and received a single dose of DT 3 days after immunization. Data are pooled from 2 independent experiments that are represented by circles and triangles. The displayed figures are either representative of or compiled from at least two experiments. n ≥ 3; showing mean ± SD.

increased levels of surface LTβR on day 5.5 after immunization (Figure 2.9D). (Collaborated

with T. Vogt)

Several hematopoietic sources of LTαβ/LIGHT have been described which could be responsible for stimulating the second growth phase of LTβR-expressing FRC, including lymphoid tissue inducer (LTi) cells, lymphocytes and DC (Schneider et al., 2004) (Moussion and Girard, 2011). Lack of LTi cells in RORγ KO bone-marrow chimera mice did not alter FRC expansion upon OVA/Mont immunization (Figure 2.10A). Surprisingly, mice deficient in either T (TCRβδ KO) or B (J$_H$ KO) cells showed also normal FRC proliferation (Figure 2.10B,C). This is in stark contrast to RAG2 KO mice that failed to show FRC expansion upon immunization with OVA/Mont (Figure 2.10D), reminiscent of our observations upon BMDC transfer (Figure 2.8B). To test a role of LTαβ/LIGHT on DC two approaches were taken. LTβ-deficient BMDC injected into WT mice induced a normal FRC expansion (Figure 2.10E).

Similarly, DC depletion starting on day 3 of the response, when T cell expansion has become largely DC independent (Prlic et al., 2006) (Figure 2.10F), did not alter markedly FRC numbers and proliferation (Figure 2.10G). Both experiments exclude DC as the critical source of LTαβ/LIGHT. Together, our findings point to a key role of T and B lymphocytes in providing signals for the early and late FRC growth phase, including possibly LTαβ/LIGHT and mechanical stress signals. (Collaborated with T. Vogt)

2.1.7 T/B cells, DC, and Macrophages can promote the proliferation/ survival of a FRC line in vitro.

Next I examined whether FRC proliferation or survival can be enhanced by the presence of lymphocytes or DC. To that end I used a FRC cell line, called pLN2 and established from naive peripheral LN (Siegert et al., 2011), and co-cultured it with BMDC, dendritic cells, ex vivo lymphocytes, or peritoneal macrophages. After two days of co-culture, the number of pLN2 co-cultured with various hematopoietic cells was significantly higher than when pLN2 were cultured alone (Figure 2.11A, B), suggesting these hematopoietic cells are supporting FRC proliferation or survival, consistent with the findings obtained in vivo (Figures 2.7 and 2.10, Peduto 2009). Co-culture of MyD88 KO- or LTβ KO- BMDC with pLN2 also promoted FRC proliferation/survival to a similar extent as WT BMDC (Figure 2.11B). Together with our in vivo data, these data suggest that neither MyD88 nor LTβ are essential in activated migratory DC to induce FRC proliferation (Figure 2.7A). Although I have not formally tested it, it seems plausible that LTβ signals are provided by naive lymphocytes (Figure 2.10).
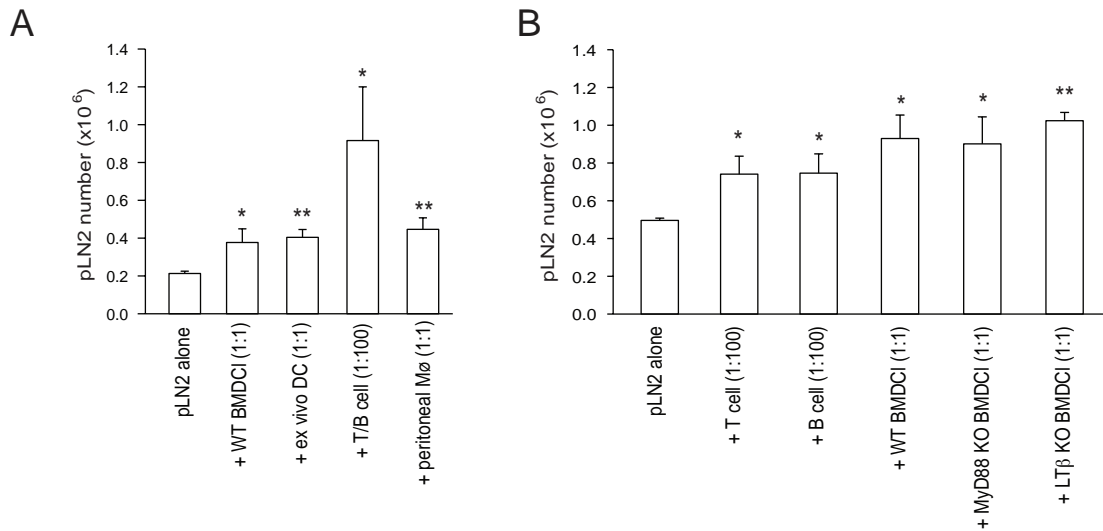
Figure 2.11 Co-culture of various hematopoietic cells enhance FRC line growth in vitro

(A, B) The FRC cell line, pLN2, was co-cultured with various hematopoietic cells. Number of pLN2 were measured after 2-3 days of co-culture using flow cytometry. The ratios indicated in the x-axis labels are number of the indicated cell type versus pLN2. The statistics were calculated in relation to 'pLN2 alone'. n ≥ 3; showing mean ± SD, The displayed figures are representative of at least two experiments.

2.2 Discussion

In this study we provide a comprehensive analysis of FRC number, phenotype and function, and correlate it with the antigen-specific T cell response over time. Rather than being disrupted or functionally altered, we show that FRC increase in size and number to cover a much larger volume while maintaining their vital functions. Within less than one day FRC become activated in a process dependent on naive lymphocyte trapping induced by DC. In a later phase activated lymphocytes further enhance this FRC expansion, presumably in a LTαβ/LIGHT-dependent but DC-independent manner.

FRC get activated at the onset of LN swelling and T cell priming, with first signs of activation after 20 hours. It suggests that FRC can sense either the increase in lymph flow, inflammatory cytokines or local DC early in the response. Alternatively, they may sense mechanical stress or other signals like hypoxia due to the large number of recently trapped naive lymphocytes. FRC proliferation initiated 40h after immunization, with 50-70% of FRC having incorporated BrdU at the peak of LN swelling, comparable to previous findings with CFA immunizations (Chyou et al., 2011) (Tan et al., 2012). Therefore, the strong expansion of the FRC network is largely due to local cell proliferation.

To visualize these proliferating FRC during LN swelling, we stained BrdU on lymphocyte-depleted swollen LN. Although the preliminary data suggest BrdU[+] FRC seems to be allover the T zone and medulla instead of showing patches of BrdU^{+} cells in certain regions, this might due

to the relatively late time point of analysis (9 days after immunization) when 60-80% of FRC are BrdU[+]. A recent paper published by Castagnaro et al. showed that subsets of splenic mesenchymal cells derived from the Nkx2-5[+]Islet1^{+} lineage could be the local precursor responsible to regenerate FRC networks after viral infection (Castagnaro et al., 2013). They also suggest the idea that resident precursor cells may exist in SLO. Our observations do not exclude a contribution by circulating fibroblasts or trans-differentiation from other cell types, that may either directly differentiate into FRC or serves as a progenitor cells (Benezech et al., 2012) (Reilkoff et al., 2011) (Gil-Ortega et al., 2013). Given that we did not see any striking morphological alteration of the existing FRC network, the expansion must go along with enhanced matrix synthesis in the new areas, as the conduit network appears to remain functional throughout the growing T zone (Gretz et al., 2000).

In contrast to previous reports investigating mostly the spleen (Mueller et al., 2007) (Scandella et al., 2008), we observed only a moderate and very transient decrease in relative transcript levels of *Il7*, *Ccl19 and Ccl21* during immune response suggesting most FRC in the LN T zone maintain not only their structural but also functional characteristics. The precise function of medullary FRC, though, remains to be established as they co-localize with plasma cells rather than T cells. Medullary FRC also localize next to LEC, suggesting they may promote lymphatic vessel growth by providing VEGF. Consistent with earlier reports (Angeli et al., 2006) (Liao and Ruddle, 2006) (Chyou et al., 2008) we observed a strong increase in both LEC and BEC numbers and proliferation during LN swelling. Therefore, LN hyperplasia is associated not only with an increase in lymphocyte numbers but also with an equivalent increase in all three major stromal cell populations that provide the organ infrastructure and organization, both for naive and activated lymphocytes. Therefore we postulate that the generation of a protective adaptive immune response strongly depends on the efficient expansion of the FRC network that provides the niches for the rapid selection, expansion and differentiation of antigen-specific lymphocytes.

How is FRC proliferation triggered during LN swelling? We observed a strong dependence of FRC expansion on migratory and resident DC, although at present we cannot formally exclude a role for subcapsular sinus macrophages which are also depleted upon injection of DT into CD11c-DTR mice (Probst et al., 2005). Comparable findings were reported by Lu and colleagues using CD11c-DTR and CCR7 KO mice (Chyou et al., 2011). They concluded that migratory DC transmit signals to CCR7-negative resident DC which then directly trigger FRC growth. We obtained several lines of evidence supporting an alternative model, in which lymphocyte numbers control FRC expansion with only an indirect role for DC: First, FRC numbers followed closely the number of total lymphocytes during LN swelling but showed no clear correlation with activated T cell numbers. Second, 3 days after DC depletion we observed a 40-70% decrease in lymphocyte numbers which correlated with the reduction in FRC numbers. This observation is consistent with reports showing that resident DC regulate naive lymphocyte

recirculation and LN cellularity by modifying HEV (Girard et al., 2012). Third, we and others (Chyou et al., 2011) saw FRC expansion in immunized WT but not RAG2 KO mice, indicating that activated DC are ineffective in promoting FRC growth in the absence of lymphocytes. Forth, DC depletion after successful T cell priming did not interfere with FRC expansion. Fifth, homeostatic T cell expansion induced by IL-7/α-IL-7 immune complexes was sufficient to trigger FRC growth by inducing LN swelling without the help of activated migratory DC or inflammatory signals. In conclusion, we propose a model in which migratory DC transmit a signal to resident DC that then trigger HEV/LEC changes leading to naive lymphocyte trapping which is critical for mediating FRC expansion (Figure 2.12). Only in a later phase activated lymphocytes appear to further boost FRC expansion.
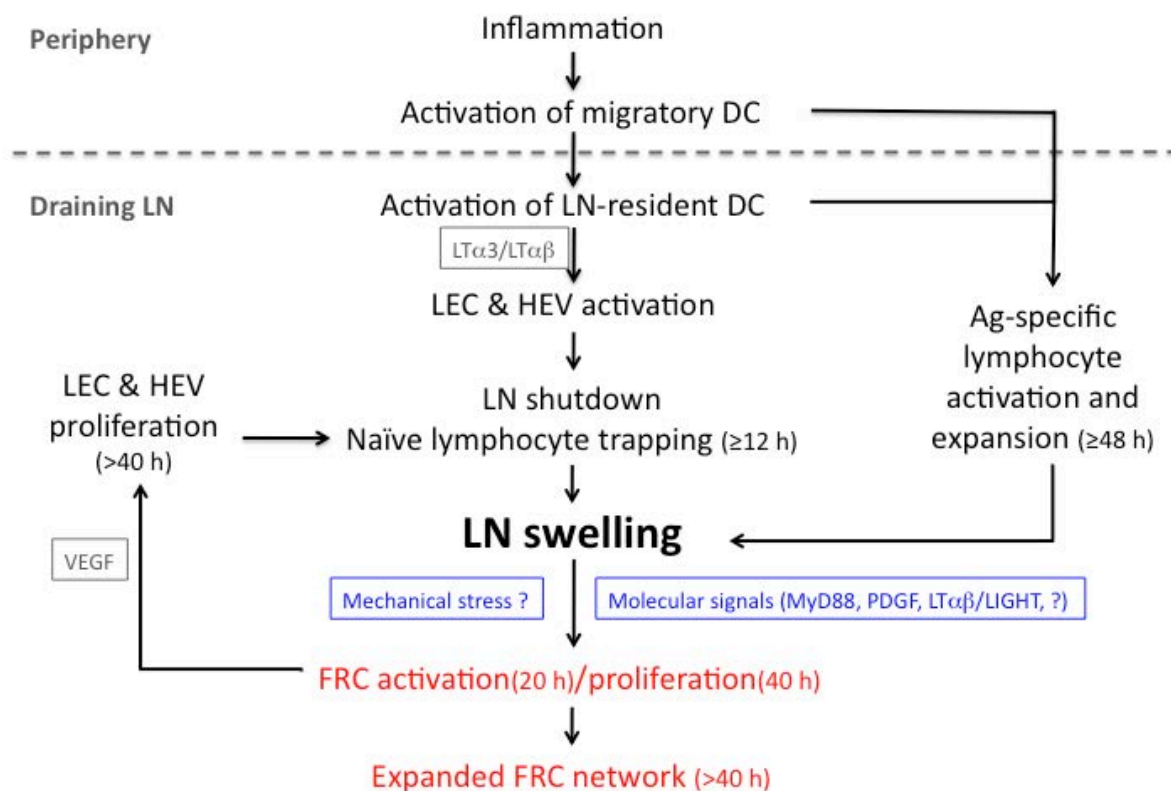
Figure 2.12 Proposed model describing the events leading to the expansion remodeling of the LN FRC network during immune response.

Inflammatory signals trigger the activation of local DC which then migrate to the next draining lymph node to alert LN-resident (endogenous) DC. Activated DC are known to trigger the activation and later the proliferation of both LEC and HEV, presumably by LTα3/LTαβ signals (Girard et al., 2012; Webster et al., 2006), thereby inducing within 12h increased immigration of naive lymphocytes and decreased emigration, collectively termed lymphocyte trapping. This early LN swelling, possibly along with lymph-based inflammatory signals, triggers FRC activation (at 20 h) and later FRC proliferation (at 40 h) independently of the adaptive immune response, either due to mechanical stress signals and/or molecular signals that may include MyD88 and PDGF. Soon thereafter the cognate lymphocytes get activated by antigen-presenting DC, expand and differentiate within the T zone microenvironment. This adaptive immune response leads to increased LTαβ/LIGHT expression by lymphocytes reinforcing FRC growth eventually leading to a strongly enlarged FRC network extending into the medullary cords. VEGF released by FRC (Chyou et al., 2011) may act like a positive feedback loop acting on HEV and possibly medullary LEC, leading to further trapping of naive lymphocytes and further FRC growth. In summary, FRC are highly reactive and adapt their numbers rapidly to the number of lymphocytes thereby preserving and extending the functional scaffold of the T zone.

The second positive regulator of FRC expansion we identified is LTβR, as LTβR-Fc partially

inhibited FRC expansion by blocking the two ligands LTαβ and LIGHT. As LIGHT also binds to HVEM, a role for this alternative receptor cannot be formally ruled out. Given that this pathway shows little effects on stromal cell biology, we favor a model involving the LTαβ-LTβR pathway (Ware, 2008).

In vitro co-culture of the FRC cell line pLN2 with various hematopoietic cells suggests DC, T, B cells, and macrophages can all promote pLN2 growth. In vivo, naive lymphocytes and NK cells express low levels of LTαβ which are strongly up-regulated during activation (Schneider et al., 2004). Recirculating LTαβ$^+$VEGF$^+$ B cells are known to contribute to stromal cell growth (Ngo et al., 2001) (Angeli et al., 2006) but surprisingly B lymphocytes were not required in our experimental setting, nor were T lymphocytes. Migratory DC were proposed to express LTαβ and VEGF and thereby could regulate the growth of HEV and LEC once they have homed into the T zone, both in homeostasis and immune response (Girard et al., 2012). LTαβ$^+$ DC also stimulate HEV-proximal FRC to express more CCL21 and VEGF which may then indirectly increase lymphocyte recirculation and vessel growth (Wendland et al., 2011) (Tzeng et al., 2010) (Ngo et al., 1999). Here we show that LN FRC numbers in homeostasis depend on both DC and B cells, but without a limiting role for LTβR ligands. In contrast, upon immunization we observed a requirement for DC in combination with either T or B lymphocytes for FRC proliferation to occur, leading us to propose that DC trigger this process via naive lymphocyte trapping. As LTβR-Fc inhibited only the later phase of FRC expansion, a role for LTαβ expression by DC or LTi cells appears less likely and may be rather due to activated lymphocytes expressing high levels of LTαβ and LIGHT in this later phase of the response (Schneider et al., 2004). Similarly, HEV expansion during LCMV infection is dependent on activated LTαβ$^+$ B cells (Kumar et al., 2010). Interestingly, non-cognate B cells provide LTβR signals to remodel the medullary cords during immune response (Abe et al., 2012). Therefore, the later LTαβ/LIGHT-dependent growth phase of FRC may occur predominantly in that zone with contributions by naive B cells.

Besides chemical signals there may be also physical signals triggering FRC expansion. Fibroblasts are known to be mechanosensitive (Tomasek et al., 2002). Given that FRC form a network throughout the T zone it is conceivable that early in the response FRC sense the physical pressure of trapped lymphocytes (Link et al., 2007). In addition, FRC may detect the increase in lymph flow within conduits which accompanies skin inflammation (Roozendaal et al., 2008). Indeed, FRC lines can respond to fluid flow with increased proliferation and CCL21 expression (Tomei et al., 2009). The incoming lymph could allow within minutes the transport of pro-inflammatory mediators from inflammatory sites to LN T zones (Roozendaal et al., 2008) possibly explaining the observed FRC activation after 20 hours and the partial MyD88 dependence of this process. Consistent with LN FRC being early sensors of infection, 12 hours after LPS injection in vivo LN FRC showed marked transcriptional changes (Malhotra et al.,

2012). Similarly, FRC lines responded rapidly to pro-inflammatory cytokines such as IL-1, IFNαβ, IFNγ and TNFα in vitro (Katakai et al., 2004b) (Siegert et al., 2011). In vivo, a recent paper also showed that the VEGF production of FRC could be enhanced by IL-1β produced by CD11c^{+} DC or monocytes (Benahmed et al., 2014). While FRC size, granularity and gp38 expression were up-regulated within hours after immunization intracellular α-SMA expression peaked 2-4 days later suggesting different stages in FRC activation and possibly function.

In conclusion, our data demonstrate that FRC are early sensors of inflammation and rapidly adapt structurally and functionally to accommodate more lymphocytes in inflamed LN. It seems likely that several cells and signals collaborate to regulate FRC numbers in the T zone and medulla and thereby the number of lymphocyte niches, as summarized in our model (Figure 2.12). Whether the opposite process of LN shrinking is regulated by the absence of those positive signals or by specialized anti-inflammatory factors remains an exciting open question of high clinical relevance.

3. Isolation and characterization of stromal cells in the intestinal lamina propria (Collaboration with S. Siegert)

3.1 Results

3.1.1 Identification of a reticular fibroblast network in the intestinal lamina propria

In secondary lymphoid organs fibroblast populations organize hematopoietic cells into different microenvironments by providing a scaffold for adhesion and migration, besides actively recruiting hematopoietic cells by means of chemokine production. Currently it is unclear how hematopoietic cells that are scattered throughout the intestinal lamina propria (LP) are organized, and whether there is an underlying fibroblast network comparable to secondary lymphoid organs. Still today, fibroblasts are often identified as 'lineage-negative' or desmin/α-SMA$^+$ populations as there is still a lack of specific surface markers to characterize these cells. On the other hand it is well accepted that fibroblasts do serve as major ECM-producing cells in the body and collagen production may be used as primary fibroblast marker. To identify fibroblasts potentially present within the lamina propria, we used a Collagen-Iα1-GFP transgenic mouse model in which the collagen-Iα1-expressing cells express a cytoplasmic GFP reporter. On the other hand, gp38 has been used as a surface marker in the LN and spleen to identify specific subsets of fibroblasts with immune functions. To test if gp38 is also expressed by some fibroblasts in the LP we first co-stained gp38 on sections of different parts of the intestine from Col-GFP mice. Histological analysis showed that there is an abundance and high density of both GFP$^+$ and gp38$^+$ cells in the LP of all gut parts investigated. Many gp38$^+$ cells appear to co-localize with GFP$^+$ cells throughout the intestinal LP (Figure 3.1A, open arrows). LEC that form collecting lymphatic vessels and central lacteals found within the villi express Lyve-1 and gp38 but are low for CD31, while blood vessels could be identified by high CD31 expression and lack of Lyve-1 and gp38 staining (Figure 3.1B, closed arrows, photo courtesy of S. Siegert). To examine more carefully the fibroblast network along with the lacteal found within each villus of the small intestine, confocal images were taken at high magnification to show that GFP$^+$ cells are not co-localizing with Lyve-1$^+$gp38$^+$ LEC in the central lacteal (Figure 3.1B, closed arrows, photo courtesy of S. Siegert) but correspond to reticular Lyve-1$^-$ cells expressing gp38 at the cell membrane and localizing both next to lacteals, throughout the LP of the villi, including along the basement membrane below the epithelial barrier thereby forming a continuous 3-dimensional cell network (Figure 3.1B, open arrows). Therefore, these data strongly suggest that there are many gp38$^+$ ECM-producing fibroblasts in the intestinal LP which form a scaffold potentially involved in the organization of local hematopoietic cells.
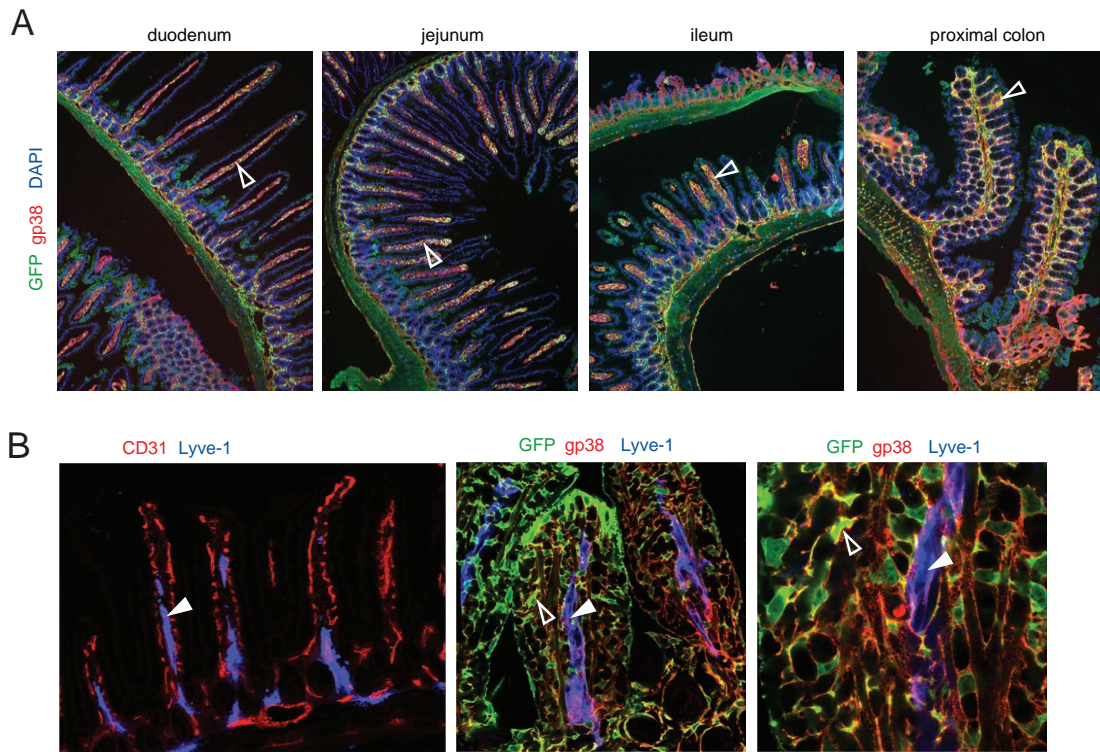
Figure 3.1 Histological identification of FRC-like fibroblasts and vessels in the intestinal lamina propria.

Microscopic analysis of murine gut tissues stained for stromal cell markers. (A) Sections of small and large intestine of Collagen-Iα1-GFP mice were stained with gp38 and DAPI and analyzed by fluorescence microscopy. Open arrows indicate villi of the LP where numerous gp38^{+} and Col-GFP^{+} cells can be observed. (B, images provided by S. Siegert) Left: Representative images showing blood vessels (CD31^{+}) and central lacteals (CD31^{+}Lyve-1^{+}, closed arrows) inside the LP of the villi in the small intestine of WT mice. Middle and right: confocal images showing the surface expression of gp38 on Col-GFP^{+} cells in the LP (open arrows) of the small intestine.

3.1.2 Isolation of stromal cells from intestine and phenotypic characterization by FACS

In order to study these gp38[+] fibroblasts (FB) localized in the LP in more detail we first established an isolation protocol for stromal cells to analyze them by flow cytometry. To reach this aim my colleagues (H. Bega, S. Siegert, J. Bernier-Latmani) and I started out with a protocol for LP lymphocyte isolation (provided by N. Harris, EPFL) and started to modify many parameters to improve the isolation efficiency for stromal cells. In most tested procedures the following aspects were done the following way (see materials and methods for more details): The intestine was excised from CO2-euthanized mice and the attached mesenteries and Payer's patches were removed. The intestine was opened longitudinally and the intestinal content was flushed out. To detach the epithelium tissues were incubated in an EDTA-containing solution. After washing out EDTA and epithelial cells with PBS the remaining intact tissues were cut into small pieces and digested with an enzyme solution. After digestion, the suspension was meshed through a filter and cells were centrifuged.

Different conditions tested:

1. EDTA concentration during epithelium detachment: 1 – 10 mM
2. EDTA incubation time during epithelium detachment: 10 – 40 min
3. Mechanical force to get rid of epithelial cells: stirring or shaking while EDTA incubation, or scratch out most epithelium after incubation.
4. Avoid air or bubble contact or not
5. Type of digestion enzymes used: collagenase 4, 8, D, and blendzyme 1, 3; enzyme concentrations used
6. Mechanical force during enzymatic digestion: stirring, shaking, or pipetting.

Before I explain the outcome of these different trials, I wish to explain first how we assessed the outcomes by flow cytometric analysis. Figure 3.2A depicts a representative analysis of a cell suspension from small intestine showing the gating strategy used to identify stromal cell subsets. First, the gating for the FSC and SSC of the cells was performed based on the size of lymphocytes to exclude red blood cells (RBC) and dead cells or apoptotic bodies that are smaller than lymphocytes. Only cells bigger than lymphocytes were considered as healthy or living cells, especially for stromal cells that should be bigger than lymphocytes. The gated cells were then stained with dead cell exclusion dye, like DAPI, 7AAD (depicted in Fig. 2A) or Aqua, to exclude dead cells. As a further way to exclude RBC besides their small cell size, we gated on Ter-119- FSC$^{int/high}$ cells. The living non-RBC cells were then subjected to EpCAM and CD45 labeling, which identify most epithelial and hematopoietic cells, respectively. Non-epithelial, non-hematopoietic cells were then further characterized for CD31 and gp38 expression, as previously shown for LN stromal cells. Also in the intestine, four different stromal cell populations could be distinguished based on CD31 and gp38 expression which based on our histological analysis should correspond to LEC (gp38$^+$CD31$^+$), BEC (gp38$^-$CD31$^+$), gp38$^+$ FRC-like stromal cells (gp38$^+$FB), and poorly characterized double negative cells (DN).

During the first few trials on small and large intestine, we found that the survival rate of the cells differs a lot depending on the origin of cells, and depending on the speed of preparation and analysis. Cells isolated from the colon showed a general survival rate of 60 – 90% (Figure 3.2B, upper panel) whereas the survival rate of total cells from small intestine was very poor (14.5%). However, most identified hematopoietic and stromal cell types in the small intestine had a survival rate of 50 – 80% (Figure 3.2B, lower panel), raising the question which type of cells died during the isolation process. To find out what these DAPI$^+$ cells are in the sample of small intestine, we analyzed them with their surface markers and found that these DAPI$^+$ cells express low to intermediate level of most of the markers stained (Figure 3.2C upper panel), probably due to their higher autofluorescence in these channels or their stickiness for antibodies. On one hand this makes the identification of cell types among these DAPI$^+$ cells very difficult as they do not have a clear positive and negative population – the staining patterns are smeared – which is
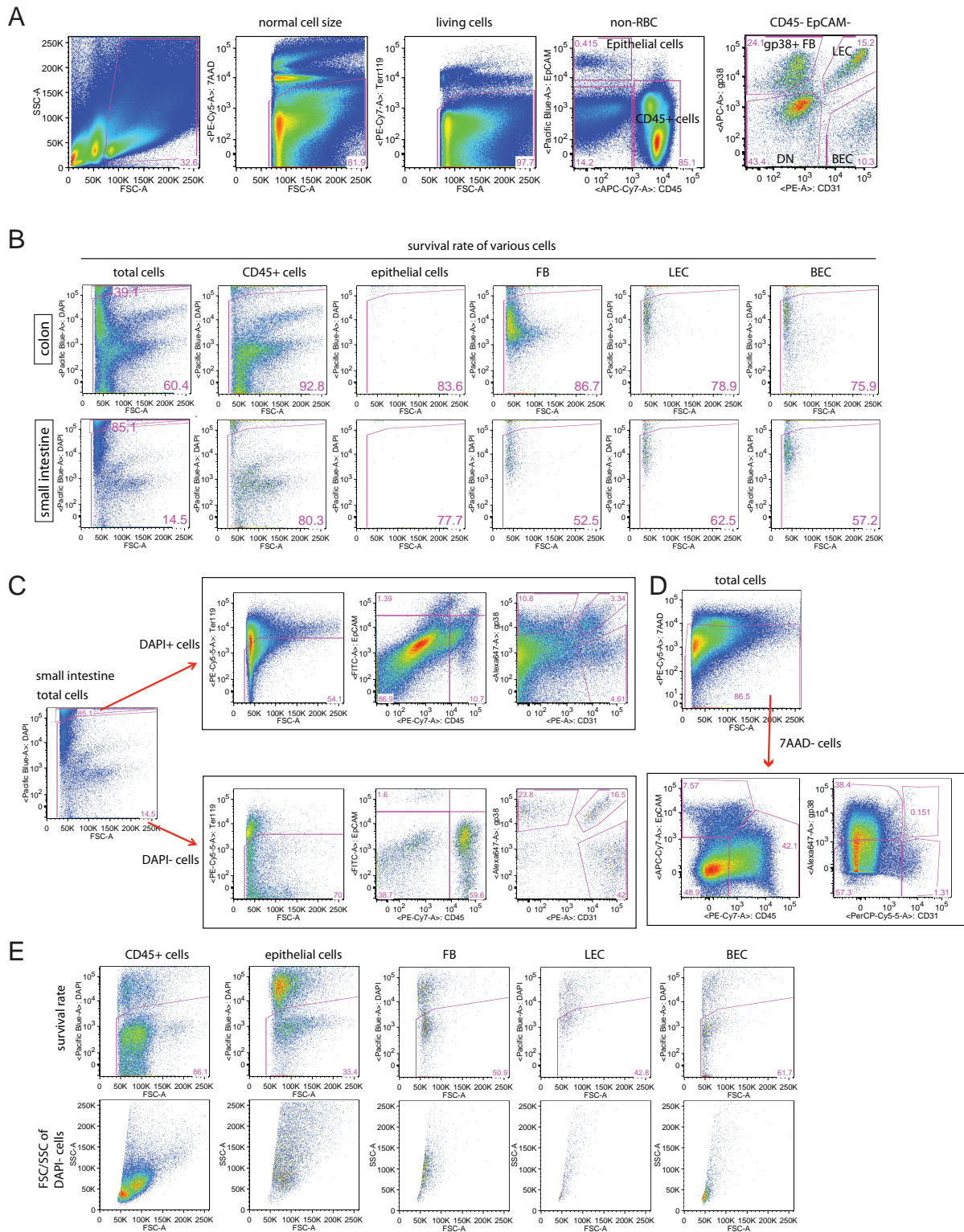
Figure 3.2 Flow cytometric identification and analysis of fibroblasts and vascular cells isolated from the intestinal lamina propria.

Small and large intestines were isolated, fully digested, labeled with various markers and analyzed by flow cytometry. (A) Representative dot plots showing the gating strategy of intestinal cell suspensions: size of nucleated cells, intact membrane integrity as a readout for living cells (7AAD-) and absence of the . red blood cell (RBC) marker Ter-119, EpCAM is specifically expressed by epithelial cells and CD45^{+} by hematopoietic cells. Non-hematopoietic, non-epithelial cells were further divided into gp38^{+} fibroblasts (gp38^{+} FB), gp38^{+}CD31^{+} lymphatic endothelial cells (LEC), CD31^{+} blood endothelial cells (BEC), and double negative cells (DN). (B) Survival rate of various cell types from colon and small intestines using a preliminary isolation protocol, using 1.5 mg/ml collagenase 8 for 2 times of 20 minutes incubation plus pipetting. 'Total cells' represents all cells which are equal or bigger than lymphocytes. Different cells are gated based on their surface marker expression and then subjected to DAPI staining. (C) Comparison of various surface markers expressed on DAPI[+] (dead cells, upper panel) and DAPI[-] (living cells, lower panel) cells of the small intestine. (D, data provided by S. Siegert) Representative dot plots of cells from the small

very different from DAPI⁻ cells (Figure 3.2C, lower panel) that show a clear separation. On the other hand since most live cells possess at least one marker that is expressed at levels above those observed for DAPI⁺ cells they are mostly DAPI⁻ and can be still analyzed in a meaningful way. In general, fast preparation and analysis of the intestinal cells allowed to get the highest yield of live stromal cells, but there were considerable variations from one experimental day to another.

Another issue we encountered was that even dyes used for dead cell exclusion worked sometimes inefficiently. As shown in figure 2D (upper plot) the majority of cells showed low to intermediate staining levels for 7AAD and were sometimes not clearly separated from 7AAD⁺ cells, resulting in a poor separation of the different cell populations (Figure 3.2D, lower panel) (data provided by S. Siegert). This situation cannot be improved by using higher concentration of 7AAD or shift to DAPI (unpublished data). As a further readout of cell viability we checked the cell size (FSC) and granularity (SSC) of DAPI⁻ stromal cells which could be clearly separated into different stromal cell subsets (FB, LEC, BEC). Surprisingly, they are smaller and more granular than most lymphocytes (Figure 3.2E). This raised the concern that these 'events' may in fact represent fragments of stromal cells that have lost their nucleus. Another possibility is that the dead cell exclusion dye alone is sometimes not sufficient enough to identify live cells. Thus, these technical issues had to be addressed first before evaluating the performance of different isolation protocols.

To improve the identification of truly live cells, I applied another viability dye besides 7AAD, namely calcein-AM. Calcein-AM is an acetomethoxy derivate of calcein that is cell permeable. After entering living cells, esterases inside living cells can cleave the acetomethoxy group from calcein that is not membrane permeable and will be trapped inside the cells (Figure 3.3).
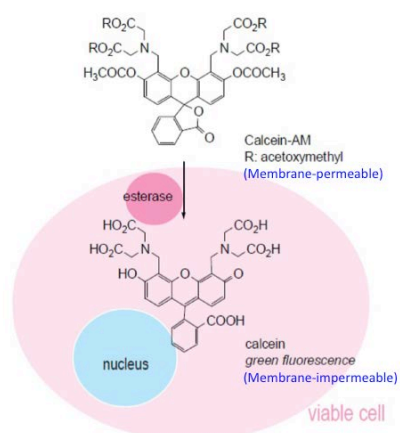
Figure 3.3 Chemical structure and application of calcein-AM for labeling living cells.

Calcein-AM is a membrane permeable dye. After entering cells, the active cytoplasmic esterase cuts off the AM group, dequenching the fluorescent calcein molecule that is now no more membrane-permeable and thus trapped in the living cells. Dead cells lack active esterase and thus fail to cleave calcein-AM.

As dead cells lack active esterase, they won't be labeled by this dye. So in contrast to 7AAD, calcein-AM stains living cells only. To test these reagents I first used cells from digested LN as these cells show reproducibly higher viability than those from the intestine. The combination of calcein-AM and 7AAD allowed the clear separation of living (calcein-AM$^+$ 7AAD$^-$) and dead (calcein-AM$^-$7AAD$^+$) LN cells, for both non-hematopoietic and hematopoietic cell subsets (Figure 3.4A). Similarly, when applying the same staining to gp38+ FB isolated from the ileum, 30% of cells were clearly dead (calcein-AM$^-$7AAD$^+$) and a comparable fraction was clearly alive (calcein-AM$^+$7AAD$^-$). Comparison of the FSC-SSC profile of these two populations showed that living cells are much bigger than dead cells (Figure 3.4B), which is consistent with the literature. However, there also a considerable fraction (37.9% in Figure 3.4B, upper right) of calcein-AM$^-$ and 7AAD$^-$ cells which were not prominent in LN isolates. These cells showed an intermediate cell size, suggesting that they are probably in the process of dying (Figure 3.4B) and would be missed by a simple 7AAD staining. Therefore, the addition of calcein-AM as a second dead cell discrimination component is useful to investigate the performance of different isolation conditions for intestinal cells.

Among all the different factors tested, it seemed that the type and concentration of digestion enzyme used and the duration of the incubation are very critical parameters for achieving a good recovery and viability of stromal cells from small intestine. For example, when digestions using 3 mg/ml of collagenase 4 and 8 were compared, I obtained more truly living cells with digestions using collagenase 4 rather than 8, for both stromal cells (Figure 3.4C) and hematopoietic cells (Figure 3.4D). In addition, the level of calcein-AM staining in living cells was higher for collagenase 4 digested tissues, making the identification of live cells more reliable. This experiment also suggests that a digestion of 20 min along with repetitive pipetting during the time of incubation is optimal when considering both stromal cell recovery and survival. However, pipetting may also harm some hematopoietic cells as calcein-AM staining is reduced (Figure 3.4C, D). In conclusion, we have decided to use for the followup work a 20 min, 3 mg/ml of collagenase 4 digestion along with some gentle pipetting described in materials and methods. This protocol allows for the isolation of various stromal cell types with more than 50% of the cells being 7AAD$^-$ and around 20 – 70% being calcein-AM$^+$7AAD$^-$ (Figure 3.4E). In addition, many CD45$^+$ cells types can be isolated with the same protocol, including $\alpha\beta$ T cells, $\gamma\delta$ T cells, IgA$^+$ plasma cells, granulocytes (Gø), F4/80$^+$ macrophages (Mø), and various subsets of DC (Figure 3.4F).

3.1.3 Phenotypic characterization of intestinal stromal cells by FACS

To confirm that the isolated CD45$^-$CD31$^-$gp38$^+$ cells are indeed fibroblasts and not lymphatic

endothelial cells which also express gp38 a reporter mouse strain for lymphatic endothelial cells, namely Prox-1-mOrange2, was used (provided by T. Petrova, Dep. of Oncology, UNIL). Within this mouse strain, the lymphatic endothelial cell specific promoter Prox1 drives expression of the
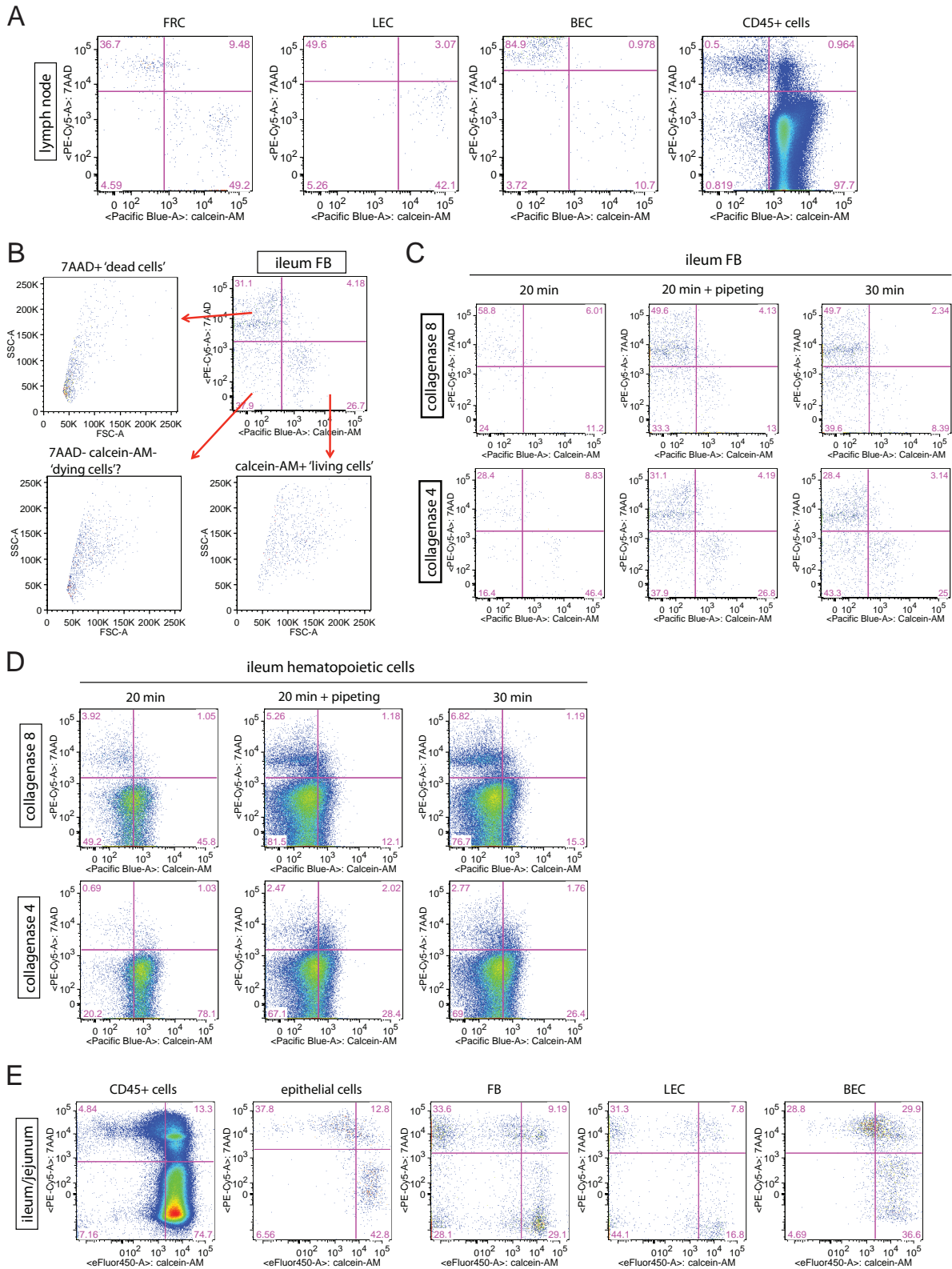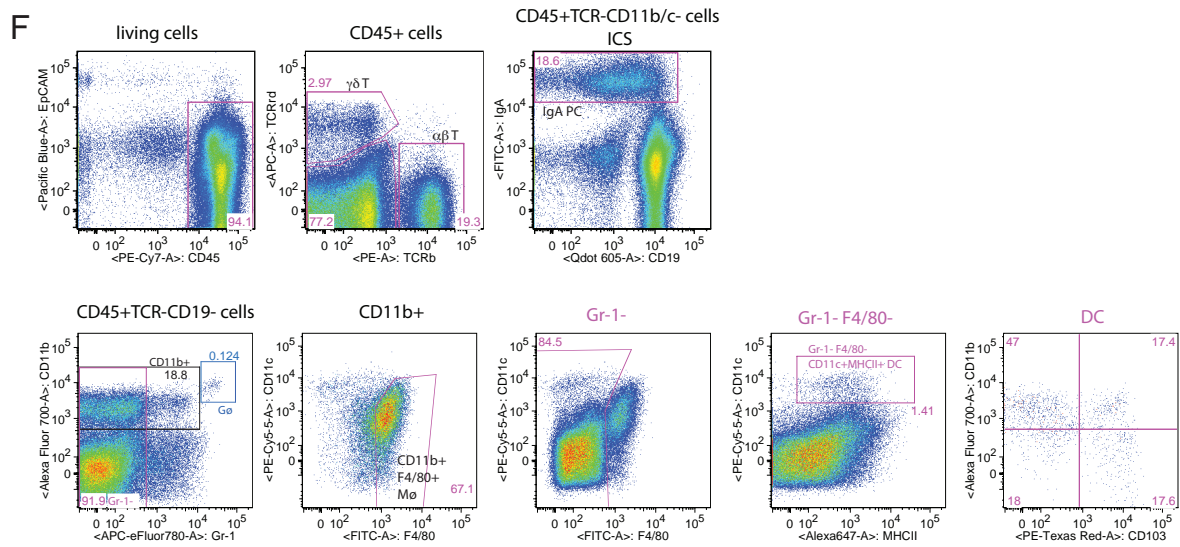
Figure 3.4 Flow cytometric determination of cell survival through the use of calcein-AM or 7AAD labeling versus cell size or granularity.

A-D and F were done with a preliminary protocol established by me while E was done with a protocol established by S Siegert and J Bernier-Latmani. (A) Representative dot plots showing calcein-AM and 7AAD labeling of the indicated lymph node cell populations to clearly distinguish dead (7AAD$^+$ calcein-AM$^-$) from live cells (7AAD$^-$ calcein-AM$^+$). (B) Fibroblasts (FB) from ileum that are 7AAD$^+$, calcein-AM$^+$ or double negative, were further analyzed for their FSC (cell size) and SSC (granularity) profile. (C, D) Comparison of cell survival of FB (C) or hematopoietic cells (D) isolated from ileum after digestion with either collagenase 4 or 8 and by varying the digestion time. Cell survival was analyzed using calcein-AM and 7AAD. (E) Survival rate of various cell types from ileum/jejunum pool with a digestion protocol established by S Siegert and J Bernier-Latmani described in materials and methods. (F) Various types of hematopoietic cells identified with the preliminary protocol, including γδ T and αβ T cells (upper middle), IgA producing PC (upper right, with intracellular staining, ICS), granulocytes (Gø, lower far left), CD11b$^+$F4/80$^+$ macrophages (Mø, lower central left), and Gr-1$^-$F4/80$^-$CD11c$^+$MHCII$^+$ DC that can be further subsets by their expression of CD11b or CD103 (lower central right and right).

fluorochrome mOrange2, thus allowing the validation of our FB versus LEC gating. Around 90% of the CD31$^+$gp38$^+$ LEC were found to express mOrange2 in the small intestine, with hardly any mOrange2 observed in the other stromal cell types investigated (Figure 3.5A upper panel). Similar data were obtained for LN stroma (Figure 3.5A lower panel). In the LN, it has been shown that most FRC express PDGFRα with minimal staining in other stromal cell types (Figure 3.5A, lower panel). Stromal cells of the small intestine showed a similar phenotype with PDGFRα being only on FRC while a subset of gp38$^+$CD31$^-$ lacked this marker (Figure 3.5A, lower panel). These data confirmed that, like in the LN, the CD31$^+$gp38$^+$ cells identified in the intestine are indeed LEC with CD31$^-$gp38$^+$ cells being of a different, presumably mesenchymal lineage. Next, isolates from small intestine and LN of collagen-Iα1-GFP reporter mice were used to validate the fibroblast identity of CD31$^-$gp38$^+$ cells. Indeed, over 80% of these cells in both intestine and LN express GFP, but there is more heterogeneity in the expression level within the intestine than the LN. Approximately 60% of LEC from both sites also express lower levels of GFP (Figure 3.5B). These data suggest that the CD31$^-$gp38$^+$ stromal cells are the main producers of collagen-I and comparable to FRC found inside LN.

To further characterize the different stromal cell subsets within the intestine, we stained for common stromal cell markers. Around 60 – 90% of FB in both small and large intestine highly

express PDGFRα (Figure 3.6A and Figure 3.5A) with 25% in the small intestine expressing CD34 (Figure 3.6B). Using histological analysis we found that these CD34$^+$ FB may be mainly arranged around the crypts (Figure 3.6C, open arrows) but not in the villi. As expected, CD34 is also expressed by BEC, as shown by both FACS and IF (Figure 3.6B and 3.6C, closed arrows).
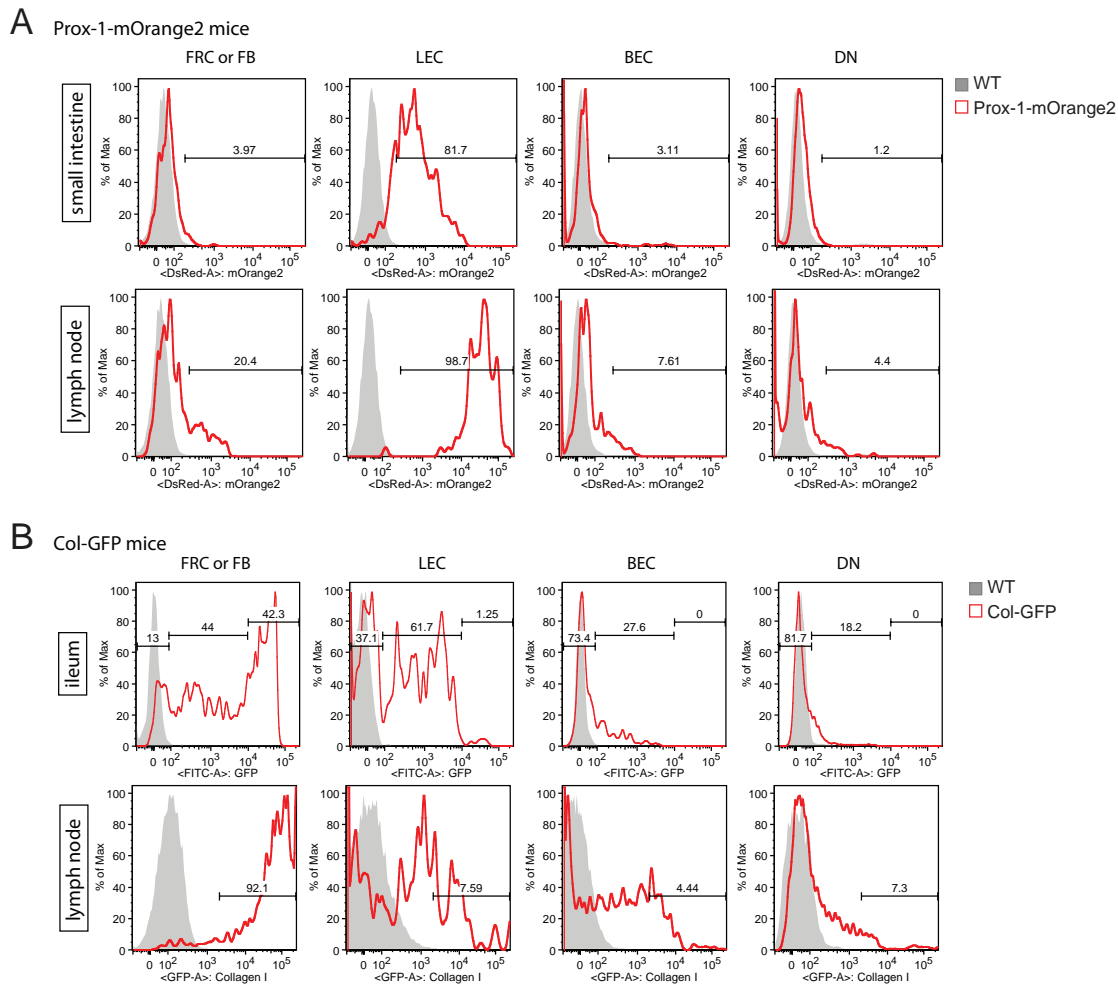
Figure 3.5 Validation of intestinal stromal cell identification procedure using cell lineage reporter mice.

Stromal cells were isolated from small intestine (upper panels) or LN (lower panels) of either Prox-1-mOrange2 (A) or Collagen-Iα1-GFP (B) reporter mice and analyzed by flow cytometry. (A) Validation of LEC staining using the LEC reporter mice Prox-1-mOrange2. Representative histograms showing mOrange2 expression in the indicated cell populations from WT (grey area) or Prox-1-mOrange2 reporter (red line) mice. (B) Validation of FB staining using the fibroblast reporter mice Collagen-Iα1-GFP. Representative histograms showing GFP expression of stromal cells from WT (grey area) or Col-GFP reporter (red line) mice.

Next we investigated the expression level of desmin and α-SMA on intestinal stromal cells. In former publications it has been shown by histology that desmin is expressed on dermal fibroblast and LN FRC (Kalluri and Zeisberg, 2006) (Link et al., 2007) whereas α-SMA is mainly expressed in myofibroblasts, including in human LP (Powell et al., 2011). To that end we performed intracellular staining for these two markers followed by flow cytometric analysis. Our FACS results depicted in Figure 3.6D indicate that in both small and large intestine, 20 – 30% of the CD31$^-$gp38$^+$ FB are α-SMA positive, suggesting that there may be a subset of myofibroblasts. Interestingly, most α-SMA^{high}desmin^{high} cells were observed in the DN population (CD31$^-$gp38$^-$), raising the possibility that the majority of the DN cells could be muscle
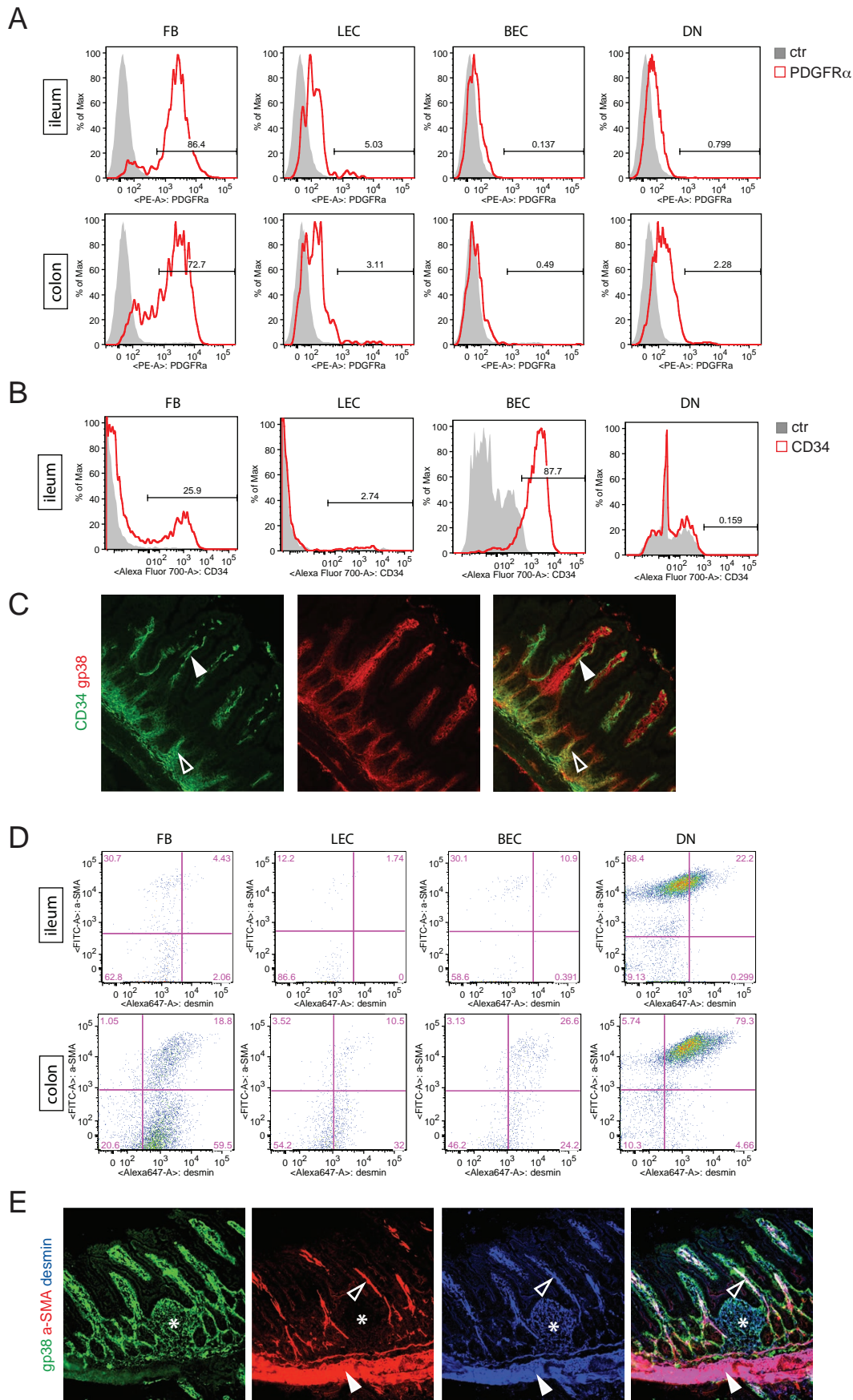
Figure 3.6 Further phenotypic characterization of intestinal stromal cells

The indicated stromal cell populations from ileum or colon were further characterized by antibody labeling and analyzed either flow cytometry on cell suspensions (A, B, D) or immunofluorescence microscopy of thin cryosections (C, E). (A) Histograms of surface PDGFRα (red line) expression on isolated stromal cells from ileum (upper panel) and proximal colon (lower panel). PDGFRα expression on CD45^{+} cells was taken as negative control (grey area). (B) Histograms of CD34 expression in the indicated stromal cells of the ileum (red line) versus no antibody control (grey

area). (C, provided by S. Siegert) Ileum sections stained for gp38 and CD34 protein. Open arrows indicate CD34$^+$gp38$^+$ cryptic FB and closed arrows indicate CD34$^+$ blood vessel cells. (D) Intracellular staining for α-SMA and desmin in the indicated stromal cells isolated from ileum (upper panel) and proximal colon (lower panel). (E, provided by S. Siegert) Ileum sections stained for gp38, α-SMA, and desmin. Closed arrows indicate α-SMA$^+$desmin$^+$gp38$^-$ muscle cells and open arrows indicate α-SMA$^+$desmin$^+$gp38$^+$ central lacteal and rare triple-positive FB. There are also α-SMA$^+$desmin$^-$gp38$^+$ and α-SMA$^-$desmin$^+$gp38$^+$ FB detectable in the LP. The gp38$^+$ fibroblasts in isolated lymphoid follicles (ILF, stars) seem to be α-SMA$^-$desmin$^+$.

cells either isolated from muscularis mucosae (Figure 3.6E, closed arrows) or the lacteal-associated smooth muscle (Figure 3.6E, open arrows). Given that there was not a perfect concordance of flow cytometric and histology data, more work is needed to firmly establish these notions. Of note, similar to the LN, gp38$^+$ FB in the isolated lymphoid follicles (ILF) of the small intestine are α-SMA$^-$desmin$^+$ (Figure 3.6E, stars).

In summary the data show that around 80% of the gp38$^+$ FB we isolate from the small intestine express PDGFRα, around 25% of them are CD34$^+$ - most probably cryptic FB - and around 30% are α-SMA$^+$ myofibroblasts that are possibly around the lacteal. Further we propose that the majority of DN cells isolated are probably muscle cells. All together these data demonstrate that FB in the intestine are very heterogeneous in their protein expression profile and location suggesting also diverse functions for each subset.

3.1.4 Elucidating possible functions of intestinal gp38$^+$ fibroblasts

To elucidate the possible functions of intestinal gp38$^+$ FB, we first determined if they express the chemokine CCL19 as do the gp38$^+$ LN FRC to mediate the recruitment and survival of T cells. CCL19-cre X ROSA-EYFP mice were used as CCL19 reporter mice and their LN and intestine analyzed by histology for EYFP expression along with staining for α-SMA and DAPI. In these mice all cells having expressed at one point CCL19 are genetically tagged to express EYFP, in a process called cell fate mapping. As reported before, there are many EYFP$^+$ cells throughout the T zone of LN (Chai et al., 2013), however no EYFP$^+$ cells are found in the LP of both the small and large intestine (Figure 3.7A) with the exception of reticular cells found in the isolated lymphoid follicles (ILF) indicating their role in recruiting naïve lymphocytes to the ILF (Figure 3.7A, arrows). Based on these data we suggest that the FB in the LP have other functions than recruiting naïve lymphocytes to the LP, consistent with the presence of effector rather than naive lymphocytes in these sites.

Our preliminary evidence suggests that effector T cells, DC, macrophages and IgA$^+$ plasma cells localize within the FB network of the small intestine suggesting these FB may help to regulate the survival or activity of these hematopoietic cells (unpublished data). LN FRC have been shown to attenuate the proliferation of primed T cells via iNOS and COX expression
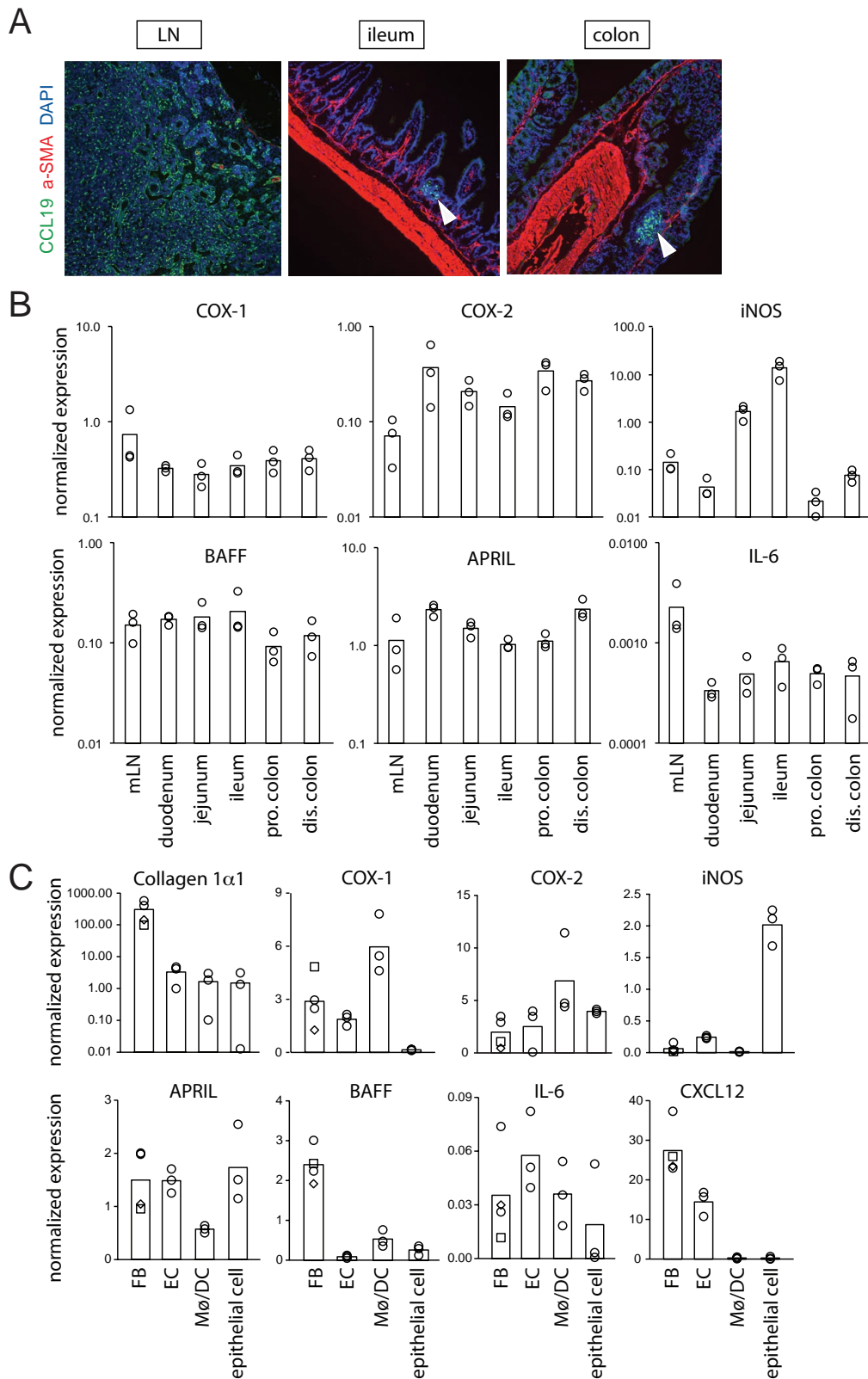
Figure 3.7 Gene expression analysis on different gut parts and in various sorted intestinal stromal cells.

(A) IF images of LN, ileum and colon from CCL19-cre X ROSA-EYFP mice showing EYFP (green) co-stained with α-SMA (red) and DAPI (blue). Closed arrow indicates an isolated lymphoid follicle (ILF). (B) mLN and tissues from different parts of the intestine were analyzed by qRT-PCR for mRNA expression of the indicated genes (normalized with two housekeeping genes). Pro. Colon: proximal colon; dis. colon: distal colon. (C) gp38^{+}CD31^{-}FB, CD31^{+}EC (including BEC and LEC), CD11b/c^{+} macrophages(Mø) or DC, and EpCAM^{+} epithelial cells were sorted from the small intestine and analyzed by qRT-PCR for mRNA expression of the indicated genes (normalized with two housekeeping genes). Bars: average values. FB: gp38^{+} fibroblasts; diamond: CD34^{+} FB; square: CD34^{-} FB; EC: endothelial cells.

(Siegert et al., 2011), and to modulate their homing profile (Hammerschmidt et al., 2008). Given

that the gut environment is constantly exposed to gut commensals and food, potent mechanisms must be in place to dampen immune responses to non-harmful antigens. In addition, the LP is the site where most plasma cells (PC) reside, most notably of the IgA isotype. As there is preliminary evidence for LN FRC expressing PC survival genes, including BAFF, April and IL-6 (Malhotra et al., 2012), intestinal fibroblasts may have a similar role in the maintenance of IgA[+] PC. Therefore, transcripts for some candidate genes were measured by qRT-PCR, initially on whole tissue lysates from distinct parts of the intestine to identify the regions of highest interest. Compared to the mLN, the gut tissues produce two fold less COX-1 but instead 2-3 folds more COX-2 regardless of the different location in the gut. The relative level of expression for both COX enzymes is comparable suggesting both enzymes may be involved in immune regulation allover the gut. Interestingly, iNOS expression varies up to 600 fold depending on their location in the gut. In general, iNOS expression is highest in the lower part of the small intestine, possibly correlating with the higher bacterial load in the ileum and jejunum than in duodenum (Figure 3.7B, upper panel). The levels of BAFF and APRIL mRNA in the gut are similar to the level of the mLN. In contrast, the relative expression of IL-6 (~0.0005) in the various gut parts is much lower than the ones of APRIL (~1.5) and BAFF (~0.15) in the gut, and is five fold less than in the mLN (Figure 3.7B, lower panel). These data suggest BAFF and APRIL are more likely to act as PC survival factors for PC in the LP than IL-6.

Based on this gross analysis of gene expression we decided to focus on the ileum as this site combines high commensal load, high numbers of IgA[+] PC and prominent expression of immune regulatory and PC survival genes. To analyze the cell types that produce the different factors, including the FB, the lower part of the small intestine was digested and various cell populations sorted by flow cytometry: gp38^{+} fibroblasts (FB), CD31^{+} endothelial cells (EC, including LEC and BEC), CD11b^{+} or CD11c^{+} macrophages plus DC (Mø/DC), and EpCAM^{+} epithelial cells. Using qRT-PCR first the purity of FB was checked by analyzing collagen-Iα1 transcripts. Consistent with the FACS data of Col-GFP reporter mice, gp38[+] FB produce ~300 folds more collagen-I than all other cell type investigated, indicating also that the sorted cell populations were of high purity. COX-1 mRNA was found mainly in Mø/DC; 2 fold more than in FB and 40 fold more than in epithelial cells while COX-2 mRNA level were similar among different cells. In contrast, epithelial cells seems to be the major source of iNOS as they express 10 times more than EC and 200 fold more than Mø/DC with minimal amounts being detected in FB (Figure 3.7C, upper panel). APRIL and IL-6 are produced fairly equally in most of the cell types tested. BAFF is mainly produced by FB as is CXCL12 (Figure 3.7C, lower panel). These data suggest that FB could be more important in supporting survival and recruitment of PC than other cell types present in the small intestine.

3.1.5 mRNA expression in primary cell lines established from intestinal digests

The study of intestinal FB function would be facilitated by the availability of intestinal FB cell lines. As such lines had been established previously in the lab by culturing the digested cell suspension or whole tissue from either small or large intestine (done by H. Bega and S. Siegert), their transcript expression level was investigated for six out of the eight investigated genes and compared to the sorted ex vivo cells (Figure 3.8). While the expression of IL-6, COX-1/ 2, and CXCL12 in cell lines is comparable to sorted intestinal FB, expression of APRIL and BAFF are largely lost in the cultured cell lines, similar to the LN FRC line pLN2. Besides, the expression level of different genes varies among individual cell lines but appears to be independent of their anatomical origin of small versus large intestine (Figure 3.8).
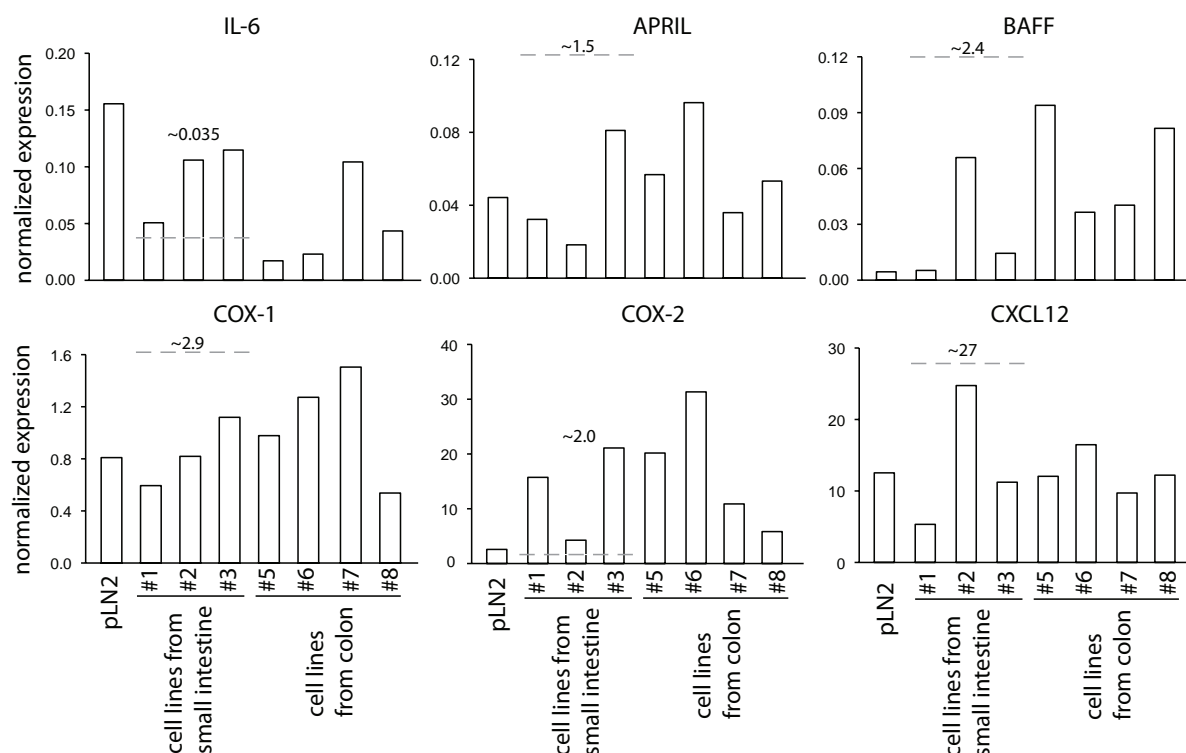
Figure 3.8 Gene expression analysis in stromal cell lines established from small and large intestine.

Primary stromal cell lines established by outgrowth of adherent cells from suspensions of total small intestine (3 lines) or total colon (4 lines) were analyzed by qRT-PCR for mRNA expression of the indicated genes (normalized with two housekeeping genes). As comparison a FRC cell line generated previously from LN (pLN2) was included in this analysis. The dashed lines and numbers indicate the mRNA level measured in ex vivo FB sorted from small intestine (as shown in Figure 3.7C).

3.2 Discussion

The gut LP is a lymphoid tissue where immune cells are found in a scattered arrangement. Whether a fibroblast network exists in these sites similar to the lymphoid organs was not known at the start of this study. Also unclear was the potential function of such fibroblasts. In this part

of the thesis, we established markers useful for the study of fibroblasts and used them to show that fibroblasts are very abundant inside the LP and organize in a network-like fashion throughout the LP of all gut parts, thereby localizing next to most immune cells. In order to allow a more extensive phenotypic and functional analysis we have developed a protocol for isolating stromal cells from intestinal LP, both from the small and large intestine. Similar to the LN FRC, most of the LP FB also express gp38, PDGFRα, and collagen-I. However their function appears to be very different, as they don't produce much CCL19 and IL-7. Instead they express more BAFF, APRIL, and CXCL12 compared to LN TRC and other intestinal cells, suggesting a role in regulating IgA[+] PC survival or development in the small intestine.

Compared to LN, the digestion of intestinal tissue proofed to be very tricky as LP stromal cells are shielded off by epithelial and smooth muscle layers. In addition, especially for the small intestine, there is an abundance of mucus, food content, bacteria, anti-microbial peptides, and digestion enzymes in the gut lumen and possibly the tissue that might interfere with the digestion process and may cause cell death during the digestion or staining process. Indeed, the performance of digestion varies dramatically among individual experiments. Furthermore, the abundant stromal and myeloid cells show high autofluorescence in most of the channels used for flow cytometry, especially after they have died, making FACS compensation and analysis very difficult. Finally, since there are highly heterogeneous cell populations in the intestine, the distribution of cell size and granularity varies dramatically which make duplet exclusion or even cell counting difficult. To overcome these difficulties, a lot of efforts were made to avoid misjudgement, including the combined use of dead cell exclusion dye (7AAD) and viable cell dye (calcein-AM). By using 7AAD and calcein-AM, I could show that collagenase 8 which is widely used currently is quite harmful for both hematopoietic and stromal cells in 20 minutes digestion when compared to collagenase 4. Interestingly, a recent paper published also uses collagenase 4 in a 20 min digestion protocol to isolate successfully intestinal fibroblasts (Vicente-Suarez et al., 2014).

By using Col-GFP transgenic mice as a bona-fide fibroblast reporter, we verified gp38 is a good marker for most of the intestinal fibroblasts, although it seems some of the intestinal FB are low in gp38 and some gp38^{+} cells are low for GFP, both by FACS and by IF. The recent paper describing LP FB in mouse small intestine also using gp38 as FB marker (Vicente-Suarez et al., 2014). Similar to the LN FRC, most of the intestinal FB are positive for PDGFRα. Besides, the intestinal FB around the crypt are positive for CD34. In conclusion, gp38 is a reasonable fibroblast marker for the gut but there may be considerable heterogeneity in the fibroblast population. What the differences are in function between LN FRC, CD34^{+} and CD34^{-} intestinal FB remains to be explored.

In contrast to findings on human gut fibroblasts, it seems the subepithelial myofibroblasts are absent or less differentiated in mouse small intestine by IF as α-SMA signals were virtually absent below the epithelial barrier (Powell et al., 2011). One possibility is that the α-SMA signal is quite low in these myofibroblasts compared to smooth muscle cells and thus needs longer exposure time to visualize it. However, with FACS, there seems to be 20-30% of intestinal FB which are positive for α-SMA, but the IF suggest these gp38$^+\alpha$-SMA$^+$ cells may mostly localize close to the lacteals instead of the epithelium. But since these experiments didn't include costaining with Lyve-1 or CD31, it is not possible to conclude whether these cells are actually LEC, smooth muscle cells associated with the lacteal, or myofibroblasts localizing close to the lymphatics. Higher resolution IF microscopy will be needed to confirm it, including costains of α-SMA with Lyve-1, CD31, gp38 or Col-GFP.

In contrast to LN FRC, intestinal FB don't express high levels of CCL19, CCL21 and IL-7 transcripts (unpublished data) which raises the question what function they may have for the neighboring immune, vascular and epithelial cells. Most fibroblasts were found to associate with various matrix proteins (not shown) suggesting they may be the source of it. Consistent with it, I found high levels of collagen-Iα1 transcripts in sorted FB but not other cell types. In the following we screened for cytokines and enzymes potentially expressed by intestinal FB, by focusing initially on transcripts previously found in various fibroblast types (Malhotra et al., 2012). LN FRC were shown to produce iNOS and COX-2 which both have a role in dampening CD8 T cells proliferation (Siegert et al., 2011) (Lukacs-Kornek et al., 2011) (Khan et al., 2011). Indeed, LP FB also produce COX-1 and COX-2 at a level comparable to macrophages and DC. In contrast, iNOS in the intestine is mainly produced by epithelial cells with iNOS expression levels following the amount of microflora in the lumen, with iNOS playing a role in the defense against infections (Mirza et al., 2011).

In contrast to the LN where medullary FRC are shown to support PC survival by producing IL-6 (manuscript in preparation), BAFF and APRIL are much more abundant and might be more important in supporting PC survival and function in the small intestine. However, the LP FB cell lines seems to lose their BAFF/APRIL expression after culturing, ex vivo LP FB cell sorted might be tested to co-culture with PC for supporting their survival. Further more, conditional knockout mice can be generated by using PDGFRα-cre X BAFF/APRIL$^{flox/flox}$ to study their contribution on PC function. On the other hand, the recent paper showing LP FB can produce retinoic acid (RA) to imprint mucosal DC for gut tropism (Vicente-Suarez et al., 2014). Interestingly, RA also can promote IgA plasma cell CSR (Fagarasan et al., 2010). Thus LP FB can also contribute to T-independent IgA CSR by producing RA. To test this hypothesis, IgA CSR of B cells after stimulating with LPS in the presence of TGFβ can be measured when co-culturing with LP FB, and see if adding RALDH inhibitor, DEAB, can inhibit this phenomenon.

In conclusion, we are able to isolate the LP FB from intestine and characterize them by FACS and qPCR. Current data suggest the LP FB could be important in regulating PC function in the small intestine. To study this possibility, LP FB cell lines that maintain BAFF and APRIL expression or conditional knockout mice will be needed to address this question. The contribution of RA produced by LP FB to PC functions remains to be clarified.

4. General discussion and perspectives

In chapter 2, we describe how the FRC network expands along with LN swelling and the extent of FRC expansion correlates nicely with LN cellularity. The signals that trigger FRC expansion involve LTβR signaling probably provided by B and T lymphocytes, reminiscent of LTi cell and LTo cell interaction during LN development. The functions of different subsets of FRC seem to be tightly related to the lymphocytes they contact. TRC express abundant CCL19/21 and IL-7 which are important for naïve T cell homeostasis while FRC observed in the medullary zone (MedFRC) were recently shown by Hsin-Ying Huang in our lab (unpublished) to express high levels of IL-6, APRIL, and BAFF to sustain plasma cell survival in the medullary zone. These findings suggest that effector lymphocytes may also depend on the FRC network for their development and function. Especially resident cells like the medullary plasma cells may rely on a specific FRC niche for their retention and survival. It is not clear yet to what extent activated T cells use this network for their proliferation, differentiation and migration. How the differentiation and finally the function of different FRC subsets are being determined remains a promising area for future research. Is it programmed in the progenitor cells that reside in the different area of the LN or is there a common progenitor cell and the function of different FRC is induced by the lymphocytes and innate immune cells they encountered? What are the signals required? These questions ask for a careful analysis of LN FRC heterogeneity in development, homeostasis and immunity.

In chapter 3 we have described a dense FRC-like network expressing collagen-I within the gut LP where mostly effector lymphocytes and myeloid cells localize. Indeed, a careful scanning electron-microscopic study of the rat jejunum from 1985 has already revealed a typical fibroblastic reticular structure in the villi different from those surrounding the crypts (Takahashi-Iwanaga and Fujita, 1985). Together with the limited human studies I am tempted to suggest that human LP contain a similar FRC network which has been conserved in evolution of vertebrates that have an adaptive immune system. In future, studies should be undertaken to validate additional fibroblast markers that work on human gut tissue. Given that several fibroblast markers have been established for human LN (Link et al., 2011), they should be tested on LP tissue. In addition, cell sorting and cell line experiments could provide insight into the function of FP in human gut. Whether a conduit system exists in the LP fibroblastic reticular structure comparable to LN and spleen is still unclear and merits also further investigation, such as by using small fluorescent molecules that may resist acids and degrading enzymes if given orally.

The finding of a LP FB network raised the possibility that effector lymphocytes, including IgA^{+} plasma cells, may rely on a similar cell as scaffold, organizer and regulator. The finding that these LP express abundant transcripts for the PC survival factors APRIL and BAFF are

suggestive, and reminiscent of MedFRC in activated LN. More direct experiments using cocultures and conditional deletion of these factors in LP FB are needed to further support this hypothesis.

LP FB also produce COX-1 and COX-2 that may contribute to immune tolerance to commensals. In future it should be of interest to see whether COX and possibly iNOS are induced in FP upon colitis induction or pathogen insult, and whether their deletion has any impact on the disease course. To this end, good genetic tools need to be established to delete genes selectively within LP FB versus other cell types. Preliminary evidence by our lab suggests that Collagen-I-Cre or – CreERT2 mice may be a useful tool with some deletion in other cell types as well. Alternatively, coculture experiments using ex vivo cells or cell lines could be used.

Of note, Vicente-Suarez et al. recently showed in germfree mice that adding microbiota induces RALDH expression preferentially among stromal cells within gut LP. The stromal cell phenotype (CD31$^-$Epcam$^-$Pdpn$^+$) and distribution throughout the villi suggests these are the same FB I described in my thesis. Interestingly, they identified FB as being the major cell type showing a constitutive expression of enzymes metabolizing vitamin A. These findings indicate that the environment, including nutrients, have a direct impact on the function of local FB. In addition, the observed the frequent co-localization of FB with CD11c$^+$CD103$^+$DC, and conditioning of these DC by the FB induced RA production in a GM-CSF dependent manner. These data represent the first published evidence for gut FB having an impact on immune cells other than providing extracellular matrix proteins (Vicente-Suarez et al., 2014). They are fully consistent with our preliminary evidence of immunomodulatory cytokines being expressed in LP FB. In future it should be interesting to delete RALDH enzymes from FB in vivo to test their effects on DCs and the balance of Treg-Th17 cells which is RA-dependent.

A phenotypical and functional comparison of LN FRC and LP FB are shown in Table 4.1.

Table 4.1 Comparison of lymph node FRC and lamina propria FB

	Phenotype	Subsets	mRNA expression	Functions
LN FRC	gp38$^+$ PDGFRα^+ Col1α1-GFP ^{high} α-SMA$^+$ (after activation)	MRC TRC MedFRC	IL-7, CCL19, CCL21, COX-2, BAFF, APRIL, IL-6, CXCL12, iNOS (after activation)	Conduit; naïve T cell survival and attraction; attenuation of T cell expansion; PC survival
LP FB	gp38$^+$ PDGFRα^+ Col1α1-GFP ^{high}	CD34$^+$ crypt FB CD34$^-$ villi FB α-SMA$^{+/-}$ FB	COX-1/2, BAFF, APRIL, CXCL12 RALDH	T cell tolerance? PC survival?

Little is currently known on the heterogeneity of gut FB. While crypt and villi FB showed different phenotypes (CD34), preliminary data showed no obvious difference in the expression of mRNA examined except for COX-1 (Figure 3.7). Whether the expression of CD34 on the cryptic FB correlates with the difference in the network structure or other functions remains to be elucidated. In contrast to LN, where clear compartments are visible, the LP consists of scattered cells that show only limited organization into specialized zones. However, there is some evidence that DC are more often concentrated in the tips of villi, while IgA[+] PC are found preferentially in the middle. The base of the villi, adjacent to epithelial stem cells, may represent yet another area where gp38[+] FB form a network. A promising area of future research is to further characterize the function and heterogeneity of LP FB, by comparing their transcriptome to that of activated LN FRC subsets or skin fibroblasts. Such an approach would allow to identify tissue- and region-specific specialization in function of FRC. Similar to LN, the cells and signals leading to FB differentiation need to be established. An interesting candidate is represented by LTβ which is an important cytokine for LN FRC development (Chai et al., 2013).

The function of gp38 on LN FRC has been investigated and showed their contribution to HEV integrity and DC motility via interaction with CLEC-2 on platelets (Herzog et al., 2013) and DC (Acton et al., 2012), respectively. The functions of gp38 on LP FB are not yet known. The transcription of gp38 can be upregulated on synoviocytes or keratinocytes by several pro-inflammatory cytokines as well as TGFβ (Astarita et al., 2012). Indeed, expression of gp38 on activated LN FRC and LP FB are higher than naïve LN FRC (data not shown). Activation of gp38 results in cytoskeletal rearrangements which may increase the cells to move and invade tissues (Astarita et al., 2012) thus forming a more flexible network that can adapt to physical stretch or space demands in a quick way, like in LN swelling or peristalsis of intestine, and facilitate the infiltration and residence of immune cells. Given that floxed Pdpn/gp38 mice have been reported, it would be of interest to delete it on gut FB and investigate its impact on FB in gut homeostasis or disease.

Gp38[+] (myo)fibroblasts are often found in chronic inflammatory sites, including cancer and autoimmune diseases (Peduto et al., 2009) (Pula et al., 2013) (Ekwall et al., 2011). These stromal cells may actually serve as the organizer cells for the newly formed lymphoid aggregates by producing chemokines and survival factors (Peduto et al., 2009). In addition, gp38 is highly expressed in the invasion front of the tumors (Pula et al., 2013). The manipulation of these fibroblasts may be the potential target to control chronic inflammation and cancer progression. Peduto et al. showed that myeloid cells play a role in regulating gp38^{+} stromal cells during the ontogeny of tertiary lymphoid tissue, with no role observed for MyD88, LTβ, and lymphocytes (Peduto et al., 2009), in contrast to our finding in the activated LN. This highlights the complexity of fibroblasts biology in various tissues and microenvironments.

In summary, FRC and FRC-like cells in LN and intestine, respectively, form dense reticular networks that are in direct contact with immune cells, including naïve lymphocytes, effector lymphocytes and dendritic cells. These specialized fibroblasts have the potential to provide both physical and chemical support to the function of immune cells, and therefore regulate immune response or tolerance. Similar gp38[+] fibroblasts can be found in many inflammatory sites and were proposed to be involved in pathogenesis by supporting the local adaptive immune response (Peduto et al., 2009) (Link et al., 2011). A better understanding of the mechanisms of FRC development, expansion and functional specialization in LN and disease sites is likely to provide valuable clues to the identification of therapeutic molecules which may target the fibroblastic niche cells and thereby indirectly the adaptive immune response.

5. Materials and Methods

5.1 Mice

C57BL/6 mice were from Janvier. OT-1 and OT-2 mice were from Jackson Laboratory and bred onto a CD45.1$^+$ C57BL/6 background. RAG2 KO, Caspase-1 KO and CD11c-DTR/GFP transgenic mice were from Jackson. MyD88 KO (Adachi et al., 1998), TRIF KO mice (Yamamoto et al., 2003), TLR2 KO mice (Takeuchi et al., 1999), and TLR4 KO mice (Hoshino et al., 1999) were kindly provided by S. Akira (Osaka); T1-Fc mice (Senn et al., 2000) by D. Pinschewer (Geneva), RORγ KO (Sun et al., 2000) by D. Littman (New York); LTβ KO mice (Koni et al., 1997) by M. Heikenwälder; and IFNαR1 KO (Muller et al., 1994) by H. Acha-Orbea (Lausanne). STAT1 KO and J$_H$ KO mice were from Taconic; TCR$\beta\delta$ KO and TNF-R1 KO were from Jackson.

5.2 Mouse treatments

10^6 OT-1 and 10^6 OT-2 splenocytes were injected i.v. 24 h before immunization. OVA protein (Sigma) was dissolved in PBS and then mixed with Montanide ISA 25 (Seppic) in a 3:1 ratio by vortexing. Mice received six s.c. injections (50 µg OVA each) in areas drained by axial, brachial and inguinal lymph nodes. Alternatively, bone-marrow derived dendritic cells (BMDC) were generated as described previously (Vogt et al., 2009) and activated with 0.1 µg/ml LPS (Sigma) or 5 µg/ml CpG (ODN1668, Trilink) for 16 h prior to injection. BMDCs were labeled using 2 µM CFSE (Invitrogen), resuspended in PBS and 10^6 BMDC were injected were injected each site s.c. as described above. For BrdU administration, mice were injected with 100 µl of 10 mg/ml BrdU in PBS and then kept on BrdU-containing drinking water (0.8 mg/ml). For IL-7 / α-IL-7 immune complex injection, anti-human IL-7 antibodies (M25, 50 µg/ml) were mixed with mouse IL-7 (10 µg/ml) by the same volume and delivered i.p. each mouse 200 µl on day 0, 1, 2, and 3. To deplete DC, diphtheria toxin (DT, Sigma) dissolved in PBS was injected once i.p. at 4 ng/g body weight 16 hours before immunization. For *Leishmania major* infection, 3×10^6 stationary LV39 *L. major* promastigotes were injected s.c. into the hind limb footpads. For LT$\alpha\beta$/LIGHT blocking, 200 µg of mLTβR-Fc or control human IgG1 antibody (Biogen) were injected one day before immunization and then 100 µg every two days intraperitoneally. For PDGFRα blocking in vivo, 200 µg of anti-PDGFRα (APA5, hybridoma kindly provided by S.-I. Nishikawa) and control IgG2a antibody (2A3, BioXCell) were injected intraperitoneally one day before immunization, and then 100 µg every two days. For IL-1β blocking, 200 µg of neutralizing antibody (Novartis Pharmaceuticals) were injected intraperitoneally one day before and one day after immunization. For Anakinra (soluble IL-1R; Kineret), WT mice were injected intraperitoneally 200 µg Anakinra every 12 hours. Imatinib (Novartis) was dissolved in water and injected i.p. 50 µg/g everyday. Nilotinib (Manley et al., 2010) and AAL993 (Manley et al., 2002) (both

from Novartis) were dissolved in N-methylpyrrolidinone (NMP) and diluted 1/10 in PEG300 to give mice every day p.o. 150 mg/kg or 100 mg/kg, respectively. For bone-marrow chimera mice, CD45.1$^+$ or .2$^+$ recipients were lethally γ-irradiated (2x 450 rad in 3 h interval) and then injected i.v. with 10^7 total BM cells from CD45.1$^+$ WT mice, MyD88 KO or RORγτ KO mice. Chimeras were analyzed 8 weeks after reconstitution. All animal experiments were authorized by the Swiss Federal Veterinary Office.

5.3 Isolation of LN stromal cells

Peripheral LN (axillary, brachial, inguinal) or mesenteric LN were dissected from CO2-euthanized mice and then opened with 26-gauge needles. For FRC isolation, LNs were digested in 1.5 ml of RPMI-1640 (Invitrogen) containing collagenase 4 (3 mg/ml, Worthington), DNase I (40 µg/ml, Roche) and 2% (v/v) Fetal Bovine Serum (FBS; PAA) at 37 °C for 30 min with gentle stirring. The suspension was then gently pipetted to break up remaining aggregates until no visible fragments remained. Viable cells were counted using trypan blue staining prior to antibody labeling.

5.4 Isolation of gut lamina propria stromal cells

14 cm of lower small intestine (containing ileum and part of the jejunum) was excised from CO2-euthanized mice and the attached mesenteries and Payer's patches were removed. The intestine was opened longitudinally and the intestinal content was flushed out. To detach the epithelium tissues were incubated in 30 ml of PBS containing 10 mM EDTA, 2% FBS, 1 mM sodium pyruvate (Sigma-Aldrich), and 20 mM HEPES at 37 °C with stirring. 30 min after incubation, epithelium was detached by vigorously shacking. The supernatant was discard and the remaining tissue was washed with excess PBS for 3 times. The remaining intact tissues were then cut into small pieces and digested with 3 mg/ml of collagenase 4 (Worthington) in 10 ml DMEM containing 10% FBS (Sigma-Aldrich), 50 µg/ml DNase (Roche), and 2 mM CaCl$_2$ (Sigma-Aldrich) at 37 °C with stirring. 20 min after digestion, the suspension was gently pipetted for a few times. The suspension, and quite often some undigested pieces were then meshed through a filter and cells were centrifuged.

5.5 Cell staining, flow cytometry and FACS sorting

Cells are blocked with 2% normal mouse serum (Sigma) for 20 min on ice and then stained with antibodies in PBS containing 2% FBS, 2 mM EDTA and 0.1% (w/v) NaN3 for 30 min on ice. Biotin-conjugated primary antibodies were detected with streptavidin. Dead cells were excluded using 7-AAD or DAPI (Invitrogen). BrdU (Sigma) administration to mice as well as surface-staining (using doubled antibody concentrations) and fixation of cells were as described before (Link et al., 2007), except that cells were incubated with 70 Kunitz U/ml DNase I (Roche) for 45 min at 37°C and with FITC-conjugated anti-BrdU mAb or an isotype-matched control mAb (Becton Dickinson) for 60 min at room temperature. For calcein-AM

staining, cells are incubated with 2 µM calcein-AM (eBioscience) in 100 µl of PBS containing 2% FBS for 30 min in room temperature prevented from light. Data were acquired on a LSRII (Becton Dickinson) and analyzed with FlowJo software (TreeStar). FACS cell sorting is performed on Aria II (Becton Dickinson) and cells are sorted into RLT buffer (Qiagen) directly for RNA isolation. Antibodies used for flow cytometry are listed in Table 5.1.

5.6 Immunofluorescence (IF) staining and imaging

Cryostat sections (8-10 µm) of Tissue-Tek OCT (Sakura)-embedded LN or intestine were collected on Superfrost/Plus glass slides (Fisher Scientific) then air dried overnight, fixed in ice-cold acetone for 10 min and rehydrated in PBS. Sections were quenched using 0.3% H_2O_2 in PBS, blocked using 0.1% BSA and 1-4% animal serum in PBS followed by a streptavidin-biotin blocking kit (Vector Laboratories), as described before (Link et al., 2007). Stainings were performed for 60 min at room temperature using antibodies listed in Table 5.2. For gp38, the staining was revealed using HRP-conjugated secondary reagents followed by Tyramide Signal Amplification (Molecular Probes Kit #22) according to the manufacturer's instructions, but using a borate buffer (0.1 M in PBS, pH 8.5) for tyramide dilution. Images were acquired on Leica DM5500 microscope with a Leica DFC320 camera or on a DM IRE2 microscope with laser scanning confocal head TCS SP2 AOBS (Leica). To visualize functional conduits, 20 µl of TexasRed-labeled 10 kDa dextran (Invitrogen) was injected subcutaneously at 5 mg/ml into the footpad and mice sacrificed after 30 min. LN were then removed and fixed in 4% PFA at 4°C for 2 h, then saturated in 30% sucrose for 3 h at 4°C before embedding in Tissue-Tek OCT (Sakura) and freezing in an ethanol dry ice bath.

5.7 Visualizing the conduit system by IF

To visualize functional conduits, 20 µl of TexasRed-labeled 10 kDa dextran (Invitrogen) was injected subcutaneously at 5 mg/ml into the footpad and mice sacrificed after 30 min. LN were then removed and fixed in 4% PFA at 4°C for 2 h, then saturated in 30% sucrose for 3 h at 4°C before embedding in Tissue-Tek OCT (Sakura) and freezing in an ethanol dry ice bath. The sections were then stained with the IF procedure described above.

5.8 Visualizing BrdU[+] FRC by IF

Mice received OT1 and OT2 cells are immunized with OVA/Mont and supplied with BrdU administration. Seven days later, mice were irradiated with sub-lethal (450 rad) or lethal dose (2x450 rad) and two days later the mice were sacrificed and LN were embedded. For visualizing BrdU by IF, sections were fixed with 1% PFA, following by the antigen retrieval which is done by boiling the slides in citrate buffer (10 mM citric acid and 10 mM trisodium citrate) at 85 °C for 20 min. The sections were then stained with normal IF procedure described above.

5.9 Isolation of ex vivo hematopoietic cells and cell culture

pLN2 cells were generated by S. Siegert (Siegert et al., 2011). For isolating ex vivo T, B, and DC, spleens were meshed through 40 μm strainer, and the cell suspension were panned with CD19-coated plate. The attached cells are B cells. The rest of cells are subjected to dynabeads (Dynabeads FlowComp Flexi, Invitrogen) conjugated with anti-CD11c antibody (N418) to purify DC according to the user manual. The flowthrough after DC purification were taken as T cell. For isolating peritoneal macrophages, 5 ml PBS containing 10% FBS was injected to the peritoneal cavity with 26G needle and the mouse was shacked to detach the peritoneal Mø. The PBS that contained Mø was then collected with pipette. The cells were cultured at 37°C with 4.5% CO2 in RPMI medium containing 10% FBS, (PAA), 10mM HEPES (Sigma), 50IU/ml penicillin, 50 μg/ml streptomycin (Sigma).

5.10 Vibratome sections

Isolated LN were fixed overnight at 4°C in freshly prepared 1% PFA in PBS, washed, embedded in 4% low-gelling agarose (Sigma) in PBS and 100-200 μm sections cut using a vibratome (Microm HM 650V). Sections were blocked with 1% BSA for 1 h and stained for at least 3-12 h with the antibodies listed in Table 5.2. Subsequently sections were washed extensively in PBS and embedded using Elvanol (Mowiol, Calbiochem). Images were taken with a Zeiss Axio Imager upright microscope. 3D-image reconstructions were made with Imaris software and segment length was assessed using the FilamentTracer plugin (both from Bitplane).

5.11 RNA isolation and quantitative RT-PCR analysis

For fractionated LN samples, LN were mashed through a 40 μm filter using a plunger, with the filtered cells being the soluble fraction and the remaining white matter being the non-soluble fraction. For whole tissue lysate from different part of intestines, around 0.5 cm of the tissue are cut from each part of the intestine for RNA isolation. RNA of tissue and cell lines were extracted using TRIzol reagent (Invitrogen). RNA of sorted cells is extracted with RNeasy Micro Kit (Qiagen). First-strand cDNA synthesis (Superscript II; Invitrogen) was performed according to the manufacturer's instructions using random nonamer primers (Microsynth). cDNA was purified with the NucleoSpin Extract II Kit (Macherey-Nagel) and individual transcripts assessed by quantitative PCR using the Light Cycler-FastStart DNAMaster SYBR Green I kit (Roche Diagnostics) on a Light Cycler 2.0 machine (Roche Diagnostics). Efficiency-corrected gene expression of target genes was normalized with the geometric mean of expression of two housekeeping genes, hypoxanthine guanine phosphoribosyl transferase (*hprt1*) and TATA-binding protein (*tbp*). Primer sequences (Microsynth) were listed in Table 5.3.

5.12 In situ hybridization

The *Ccl19*, *Ccl21*, and *Il7* 'riboprobe' were cloned and used as described previously (Link et al., 2007). In brief: Frozen sections (8 µm in thickness) were fixed in 4% (wt/vol) paraformaldehyde, washed in PBS, incubated with prehybridization solution followed by an overnight incubation at 60 °C with sense or antisense digoxigenin-labeled 'riboprobes'. After several washes, sections were incubated with sheep anti-digoxigenin antibody followed by alkaline phosphatase–coupled donkey anti-sheep antibody. The color reaction was achieved using nitro blue tetrazolium (Bio-Rad) and 5-bromo-4-chloro-3-indolylphosphate (Sigma), followed by antibody staining for B220 and laminin. Hybridization signals were imaged using transmission microscopy and false-colored in green.

5.13 Statistical analysis

Statistical significance was determined using an unpaired two-tailed Student's t-test for unequal variances. P values are indicated as * for $p < 0.05$, ** for $p < 0.01$, *** for $p < 0.001$, and n.s. for ¨statistically not significant¨.

5.14 Reagents

Table 5.1 Antibodies used for flow cytometric analysis

Target	Species	Clone	Conjugate	Vendor
α-SMA	Mouse	1A4	FITC	Sigma
BrdU	Mouse	3D4	FITC	BD Pharmingen
CD4	Rat	GK1.5	PE	BioLegend
CD4	Rat	RM4-5	eFluor 450	eBioscience
CD8α	Rat	53-6.7	PE-Cy7	BioLegend
CD11b	Rat	M1/70	Alexa 700	eBioscience
CD11c	Arm. Hamster	N418	PE	eBioscience
CD11c	Arm. Hamster	N418	PE-Cy5	BioLegend
CD11c	Arm. Hamster	N418	PE-Cy5.5	BioLegend
CD19	Rat	ID3	BV605	BD Horizon
CD19	Rat	6D5	PE-Cy5.5	BioLegend
CD25	Rat	PC61	PE	eBioscience
CD31	Rat	390	PE	BioLegend
CD34	Rat	RAM34	Alexa 700	eBioscience
CD35	Rat	eBlo8D9	PE-Cy7	eBioscience
CD44	Rat	IM7	Biotin	eBioscience
CD45	Rat	30-F11	PE-Cy7	eBioscience
CD45	Rat	30-F11	PE-Cy7	BioLegend
CD45.1	Mouse	A20.1	Alexa647	Hybridoma, ATCC
CD45R (B220)	Rat	RA3-6B2	PE-Texas Red	BD Pharmigen
CD62L	Rat	MEL-14	FITC	Biolegend
CD69	Arm. Hamster	H1.2F3	FITC	eBioscience
CD103	Rat	M290	Biotin	Hybridoma, ATCC
CD140a (PDGFRα)	Rat	APA5	Biotin	eBioscience
CD140a (PDGFRα)	Rat	APA5	PE	BioLegend
CD326 (EpCAM)	Rat	G8.8	eFluor 450	eBioscience
CD326 (EpCAM)	Rat	G8.8	FITC	Hybridoma, ATCC
Desmin	Rabbit		None	Progen
F4/80	Rat	F4/80	FITC	Hybridoma, ATCC
gp38	Syrian Hamster	8.1.1	Alexa 647	Hybridoma, Developmental Studies Hybridoma Bank
Gr-1	Rat	RB6-8c5	APC- eFluor 780	eBioscience
IgA	Rat	11-44-2	FITC	Southern Biotech
LTβR	Rat	3C8	Biotin	eBioscience
MHCII	Rat	M5/114.15.2	Alexa 647	Hybridoma, ATCC
Streptavidin			APC	Biolegend
Streptavidin			PE-Texas Red	Invitrogen
TCRβ	Arm. Hamster	H57-597	APC-eFluor 780	eBioscience
TCRβ	Arm. Hamster	H57-597	PE	eBioscience
TCRγδ	Arm. Hamster	GL-3	APC	BioLegend
Ter119	Rat	Ter-119	BV605	BioLegend
Ter119	Rat	Ter-119	PE-Cy5.5	eBioscience
Ter119	Rat	Ter-119	PE-Cy7	BioLegend
VCAM-1	Rat	M/K2.7	Biotin	Hybridoma

All hybridomas from ATCC were obtained from American Type Culture Collection, Manassas, USA and purified and conjugated using standard protocols.

Table 5.2 Antibodies used for in situ hybridization or immunofluorescence staining of vibratome- or cryostat-sections

Target	Species	Clone	Conjugate	Vendor
α-SMA	Mouse	1A4	Cy3	Sigma
B220	Rat	RA3-6B2	None	Hybridoma
CD3ε	Armenian hamster	145-2C11	None	Hybridoma
CD31	Rat	GC-51	None	Hybridoma
CD34	Rat	RAM34	None	eBioscience
CD35 (CR1)	Rat	8C12	None	Hybridoma
Collagen-I	Goat	#1200-01S	None	Southern Biotech (Birmingham, USA)
Desmin	Rabbit		None	Progen
Digoxigenin	Sheep		None	Roche
Fibronectin	Rabbit		None	Sigma
Goat IgG	Donkey		Alexa 488	Molecular probes
GFP	Rabbit		None	Invitrogen
gp38	Syrian hamster	8.1.1	None	Developmental Studies Hybridoma Bank
Hamster IgG	Goat		Alexa 488	Molecular probes
Laminin	Rabbit	046K4766	None	Sigma
LYVE-1	Rabbit	#103-PA50	None	RELIATech (Wolfenbüttel, Germany)
Rabbit IgG	Donkey		Cy3	Jackson ImmunoResearch Laboratories
Rabbit IgG	Donkey		Alexa 488	Molecular probes
Rabbit IgG	Donkey		Alexa 647	Molecular probes
Rat IgG	Chicken		Alexa 647	Molecular probes
Rat IgG	Donkey		Alexa 488	Molecular probes
Rat IgG	Donkey		Cy3	Jackson ImmunoResearch Laboratories
Sheep IgG	Donkey		Alkaline phosphate	Jackson ImmunoResearch Laboratories
Syrian hamster IgG	Goat		Cy3	Jackson ImmunoResearch Laboratories

Table 5.3 Primers used for quantitative RT-PCR

Target	Forward	Reverse
April	GGTGGTATCTCGGGAAGGAC	CCCCTTGATGTAAATGAAAGACA
Baff	AGACGCGCTTTCCAGGGACC	TAGTCGGCGTGTCGCTGTCTG
Ccl19	CTGCCTCAGATTATCTGCCAT	GTCTTCCGCATCATTAGCAC
Ccl21	ATCCCGGCAATCCTGTTCTC	GGTTCTGCACCCAGCCTTC
Collagen-Iα1	GCTCCTCTTAGGGGCCACT	CCACGTCTCACCATTGGGG
Cox-1	CCAGAGTCATGAGTCGAAGGAAG	CCTGGTTCTGGCACGGATAG
Cox-2	TGGTGCCTGGTCTGATGATG	GTGGTAACCGCTCAGGTGTTG
Cxcl12	TGCATCAGTGACGGTAAACCA	TTCTTCAGCCGTGCAACAATC
Hprt1	GTTGGATATGCCCTTGAC	AGGACTAGAACACCTGCT
Il6	ATGGATGCTACCAAACTGGAT	TGAAGGACTCTGGCTTTGTCT
Il7	GTGCCACATTAAAGACAAAGAAG	GTTCATTATTCGGGCAATTACTATC
Inos	GTTCTCAGCCCAACAATACAAGA	GTGGACGGGTCGATGTCAC
Tbp	CCTTCACCAATGACTCCTATGAC	CAAGTTTACAGCCAAGATTCAC

6. References

Abdelrahman, M.A., Marston, G., Hull, M.A., Markham, A.F., Jones, P.F., Evans, J.A., and Coletta, P.L. (2012). High-Frequency Ultrasound for in Vivo Measurement of Colon Wall Thickness in Mice. Ultrasound Med Biol *38*, 432-442.

Abe, J., Ueha, S., Yoneyama, H., Shono, Y., Kurachi, M., Goto, A., Fukayama, M., Tomura, M., Kakimi, K., and Matsushima, K. (2012). B cells regulate antibody responses through the medullary remodeling of inflamed lymph nodes. International Immunology *24*, 17-27.

Acton, S.E., Astarita, J.L., Malhotra, D., Lukacs-Kornek, V., Franz, B., Hess, P.R., Jakus, Z., Kuligowski, M., Fletcher, A.L., Elpek, K.G.*, et al.* (2012). Podoplanin-Rich Stromal Networks Induce Dendritic Cell Motility via Activation of the C-type Lectin Receptor CLEC-2. Immunity *37*, 276-289.

Adachi, O., Kawai, T., Takeda, K., Matsumoto, M., Tsutsui, H., Sakagami, M., Nakanishi, K., and Akira, S. (1998). Targeted disruption of the MyD88 gene results in loss of IL-1- and IL-18-mediated function. Immunity *9*, 143-150.

Aguzzi, A., Kranich, J., and Krautler, N.J. (2014). Follicular dendritic cells: origin, phenotype, and function in health and disease. Trends Immunol *35*, 105-113.

Allen, S., Turner, S.J., Bourges, D., Gleeson, P.A., and van Driel, I.R. (2011). Shaping the T-cell repertoire in the periphery. Immunol Cell Biol *89*, 60-69.

Anderson, A.O., and Anderson, N.D. (1975). Studies on the structure and permeability of the microvasculature in normal rat lymph nodes. Am J Pathol *80*, 387-418.

Angeli, V., Ginhoux, F., Llodra, J., Quemeneur, L., Frenette, P.S., Skobe, M., Jessberger, R., Merad, M., and Randolph, G.J. (2006). B cell-driven lymphangiogenesis in inflamed lymph nodes enhances dendritic cell mobilization (vol 24, pg 203, 2006). Immunity *25*, 689-689.

Asperti-Boursin, F., Real, E., Bismuth, G., Trautmann, A., and Donnadieu, E. (2007). CCR7 ligands control basal T cell motility within lymph node slices in a phosphoinositide 3-kinase independent manner. Journal of Experimental Medicine *204*, 1167-1179.

Astarita, J.L., Acton, S.E., and Turley, S.J. (2012). Podoplanin: emerging functions in development, the immune system, and cancer. Front Immunol *3*, 283.

Bajenoff, M., Egen, J.G., Koo, L.Y., Laugier, J.P., Brau, F., Glaichenhaus, N., and Germain, R.N. (2006). Stromal cell networks regulate lymphocyte entry, migration, and territoriality in lymph nodes. Immunity *25*, 989-1001.

Bajenoff, M., and Germain, R.N. (2009). B-cell follicle development remodels the conduit system and allows soluble antigen delivery to follicular dendritic cells. Blood *114*, 4989-4997.

Batista, F.D., and Harwood, N.E. (2009). The who, how and where of antigen presentation to B cells. Nature Reviews Immunology *9*, 15-27.

Bekiaris, V., Timoshenko, O., Hou, T.Z., Toellner, K., Shakib, S., Gaspal, F., McConnell, F.M., Parnell, S.M., Withers, D., Buckley, C.D.*, et al.* (2008). Ly49H+ NK cells migrate to and protect splenic white pulp stroma from murine cytomegalovirus infection. J Immunol *180*, 6768-6776.

Benahmed, F., Chyou, S., Dasoveanu, D., Chen, J., Kumar, V., Iwakura, Y., and Lu, T.T. (2014). Multiple CD11c+ cells collaboratively express IL-1beta to modulate stromal vascular endothelial growth factor and lymph node vascular-stromal growth. J Immunol *192*, 4153-4163.

Benedict, C.A., De Trez, C., Schneider, K., Ha, S., Patterson, G., and Ware, C.F. (2006). Specific remodeling of splenic architecture by cytomegalovirus. PLoS Pathog *2*, e16.

Benezech, C., Mader, E., Desanti, G., Khan, M., Nakamura, K., White, A., Ware, C.F., Anderson, G., and Caamano, J.H. (2012). Lymphotoxin-beta Receptor Signaling through NF-kappaB2-RelB Pathway Reprograms Adipocyte Precursors as Lymph Node Stromal Cells. Immunity *37*, 721-734.

Boyman, O., Ramsey, C., Kim, D.M., Sprent, J., and Surh, C.D. (2008). IL-7/Anti-IL-7 mAb complexes restore T cell development and induce homeostatic T cell expansion without lymphopenia. Journal of Immunology *180*, 7265-7275.

Brandtzaeg, P., Kiyono, H., Pabst, R., and Russell, M.W. (2008). Terminology: nomenclature of mucosa-associated lymphoid tissue. Mucosal Immunol *1*, 31-37.

Brennan, P.C., McCullough, J.S., and Carr, K.E. (1999). Variations in cell and structure populations along the length of murine small intestine. Cells Tissues Organs *164*, 221-226.

Broere, F., du Pre, M.F., van Berkel, L.A., Garssen, J., Schmid-Weber, C.B., Lambrecht, B.N., Hendriks, R.W., Nieuwenhuis, E.E.S., Kraal, G., and Samsom, J.N. (2009). Cyclooxygenase-2 in mucosal DC mediates induction of regulatory T cells in the intestine through suppression of IL-4. Mucosal Immunol *2*, 254-264.

Castagnaro, L., Lenti, E., Maruzzelli, S., Spinardi, L., Migliori, E., Farinello, D., Sitia, G., Harrelson, Z., Evans, S.M., Guidotti, L.G.*, et al.* (2013). Nkx2-5(+)Islet1(+) Mesenchymal Precursors Generate Distinct Spleen Stromal Cell Subsets and Participate in Restoring Stromal Network Integrity. Immunity *38*, 782-791.

Cerutti, A. (2008). The regulation of IgA class switching. Nature Reviews Immunology *8*, 421-434.

Chai, Q., Onder, L., Scandella, E., Gil-Cruz, C., Perez-Shibayama, C., Cupovic, J., Danuser, R., Sparwasser, T., Luther, S.A., Thiel, V.*, et al.* (2013). Maturation of Lymph Node Fibroblastic Reticular Cells from Myofibroblastic Precursors Is Critical for Antiviral Immunity. Immunity *38*, 1013-1024.

Chen, Q., Fisher, D.T., Clancy, K.A., Gauguet, J.M., Wang, W.C., Unger, E., Rose-John, S., von Andrian, U.H., Baumann, H., and Evans, S.S. (2006). Fever-range thermal stress promotes lymphocyte trafficking across high endothelial venules via an interleukin 6 trans-signaling mechanism. Nat Immunol *7*, 1299-1308.

Chu, V.T., Beller, A., Rausch, S., Strandmark, J., Zanker, M., Arbach, O., Kruglov, A., and Berek, C. (2014). Eosinophils Promote Generation and Maintenance of Immunoglobulin-A-Expressing Plasma Cells and Contribute to Gut Immune Homeostasis. Immunity *40*, 582-593.

Chyou, S., Benahmed, F., Chen, J.F., Kumar, V., Tian, S., Lipp, M., and Lu, T.T. (2011). Coordinated Regulation of Lymph Node Vascular-Stromal Growth First by CD11c(+) Cells and Then by T and B Cells. Journal of Immunology *187*, 5558-5567.

Chyou, S., Ekland, E.H., Carpenter, A.C., Tzeng, T.C.J., Tian, S., Michaud, M., Madri, J.A., and Lu, T.T. (2008). Fibroblast-type reticular stromal cells regulate the lymph node vasculature. Journal of Immunology *181*, 3887-3896.

Cohen, J.N., Guidi, C.J., Tewalt, E.F., Qiao, H., Rouhani, S.J., Ruddell, A., Farr, A.G., Tung, K.S., and Engelhard, V.H. (2010). Lymph node-resident lymphatic endothelial cells mediate peripheral tolerance via Aire-independent direct antigen presentation. Journal of Experimental Medicine *207*, 681-688.

Cyster, J.G. (2005). Chemokines, sphingosine-1-phosphate, and cell migration in secondary lymphoid organs. Annual Review of Immunology *23*, 127-159.

Cyster, J.G., and Schwab, S.R. (2012a). Sphingosine-1-Phosphate and Lymphocyte Egress from Lymphoid Organs. Annual Review of Immunology, Vol 30 *30*, 69-94.

Cyster, J.G., and Schwab, S.R. (2012b). Sphingosine-1-phosphate and lymphocyte egress from lymphoid organs. Annu Rev Immunol *30*, 69-94.

Eberl, G. (2005). Inducible lymphoid tissues in the adult gut: recapitulation of a fetal developmental pathway? Nat Rev Immunol *5*, 413-420.

Ekwall, A.K.H., Eisler, T., Anderberg, C., Jin, C.S., Karlsson, N., Brisslert, M., and Bokarewa, M.I. (2011). The tumour-associated glycoprotein podoplanin is expressed in fibroblast-like synoviocytes of the hyperplastic synovial lining layer in rheumatoid arthritis. Arthritis Res Ther *13*.

Endres, R., Alimzhanov, M.B., Plitz, T., Futterer, A., Kosco-Vilbois, M.H., Nedospasov, S.A., Rajewsky, K., and Pfeffer, K. (1999). Mature follicular dendritic cell networks depend on expression of lymphotoxin beta receptor by radioresistant stromal cells and of lymphotoxin beta and tumor necrosis factor by B cells. J Exp Med *189*, 159-168.

Fagarasan, S., and Honjo, T. (2003). Intestinal IgA synthesis: Regulation of front-line body defences. Nature Reviews Immunology *3*, 63-72.

Fagarasan, S., Kawamoto, S., Kanagawa, O., and Suzuki, K. (2010). Adaptive Immune Regulation in the Gut: T Cell-Dependent and T Cell-Independent IgA Synthesis. Annual Review of Immunology, Vol 28 *28*, 243-273.

Fagarasan, S., Kinoshita, K., Muramatsu, M., Ikuta, K., and Honjo, T. (2001). In situ class switching and differentiation to IgA-producing cells in the gut lamina propria. Nature *413*, 639-643.

Farr, A., Nelson, A., and Hosier, S. (1992). Characterization of an Antigenic Determinant Preferentially Expressed by Type-I Epithelial-Cells in the Murine Thymus. J Histochem Cytochem *40*, 651-664.

Flanagan, K., Moroziewicz, D., Kwak, H., Horig, H., and Kaufman, H.L. (2004). The lymphoid chemokine CCL21 costimulates naive T cell expansion and Th1 polarization of non-regulatory CD4+ T cells. Cell Immunol *231*, 75-84.

Fletcher, A.L., Lukacs-Kornek, V., Reynoso, E.D., Pinner, S.E., Bellemare-Pelletier, A., Curry, M.S., Collier, A.R., Boyd, R.L., and Turley, S.J. (2010). Lymph node fibroblastic reticular cells directly present peripheral tissue antigen under steady-state and inflammatory conditions. J Exp Med *207*, 689-697.

Friedman, R.S., Jacobelli, J., and Krummel, M.F. (2006). Surface-bound chemokines capture and prime T cells for synapse formation. Nat Immunol *7*, 1101-1108.

Fu, Y.X., Huang, G., Wang, Y., and Chaplin, D.D. (1998). B lymphocytes induce the formation of follicular dendritic cell clusters in a lymphotoxin alpha-dependent fashion. J Exp Med *187*, 1009-1018.

Gil-Ortega, M., Garidou, L., Barreau, C., Maumus, M., Breasson, L., Tavernier, G., Garcia-Prieto, C.F., Bouloumie, A., Casteilla, L., and Sengenes, C. (2013). Native Adipose Stromal Cells Egress from Adipose Tissue In Vivo: Evidence During Lymph Node Activation. Stem Cells *31*, 1309-1320.

Girard, J.P., Moussion, C., and Forster, R. (2012). HEVs, lymphatics and homeostatic immune cell trafficking in lymph nodes. Nat Rev Immunol *12*, 762-773.

Goldrath, A.W., Bogatzki, L.Y., and Bevan, M.J. (2000). Naive T cells transiently acquire a memory-like phenotype during homeostasis-driven proliferation. Journal of Experimental Medicine *192*, 557-564.

Gonzalez, M., Mackay, F., Browning, J.L., Kosco-Vilbois, M.H., and Noelle, R.J. (1998). The sequential role of lymphotoxin and B cells in the development of splenic follicles. J Exp Med *187*, 997-1007.

Gretz, J.E., Anderson, A.O., and Shaw, S. (1997). Cords, channels, corridors and conduits: critical architectural elements facilitating cell interactions in the lymph node cortex. Immunol Rev *156*, 11-24.

Gretz, J.E., Norbury, C.C., Anderson, A.O., Proudfoot, A.E.I., and Shaw, S. (2000). Lymph-borne chemokines and other low molecular weight molecules reach high endothelial venules via specialized conduits while a functional barrier limits access to the lymphocyte microenvironments in lymph node cortex. Journal of Experimental Medicine *192*, 1425-1439.

Hall, J.G., and Morris, B. (1965). The immediate effect of antigens on the cell output of a lymph node. Br J Exp Pathol *46*, 450-454.

Hammerschmidt, S.I., Ahrendt, M., Bode, U., Wahl, B., Kremmer, E., Forster, R., and Pabst, O. (2008). Stromal mesenteric lymph node cells are essential for the generation of gut-homing T cells in vivo. Journal of Experimental Medicine *205*, 2483-2490.

Hanayama, R., Tanaka, M., Miwa, K., Shinohara, A., Iwamatsu, A., and Nagata, S. (2002). Identification of a factor that links apoptotic cells to phagocytes. Nature *417*, 182-187.

Hanayama, R., Tanaka, M., Miyasaka, K., Aozasa, K., Koike, M., Uchiyama, Y., and Nagata, S. (2004). Autoimmune disease and impaired uptake of apoptotic cells in MFG-E8-deficient mice. Science *304*, 1147-1150.

Hay, J.B., and Hobbs, B.B. (1977). The flow of blood to lymph nodes and its relation to lymphocyte traffic and the immune response. J Exp Med *145*, 31-44.

Henrickson, S.E., and von Andrian, U.H. (2007). Single-cell dynamics of T-cell priming. Curr Opin Immunol *19*, 249-258.

Herzog, B.H., Fu, J.X., Wilson, S.J., Hess, P.R., Sen, A., McDaniel, J.M., Pan, Y.F., Sheng, M.J., Yago, T., Silasi-Mansat, R.*, et al.* (2013). Podoplanin maintains high endothelial venule integrity by interacting with platelet CLEC-2. Nature *502*, 105-+.

Hess, E., Duheron, V., Decossas, M., Lezot, F., Berdal, A., Chea, S., Golub, R., Bosisio, M.R., Bridal, S.L., Choi, Y.*, et al.* (2012). RANKL Induces Organized Lymph Node Growth by Stromal Cell Proliferation. Journal of Immunology *188*, 1245-1254.

Honda, K., and Takeda, K. (2009). Regulatory mechanisms of immune responses to intestinal bacteria. Mucosal Immunol *2*, 187-196.

Hoshino, K., Takeuchi, O., Kawai, T., Sanjo, H., Ogawa, T., Takeda, Y., Takeda, K., and Akira, S. (1999). Cutting edge: Toll-like receptor 4 (TLR4)-deficient mice are hyporesponsive to lipopolysaccharide: evidence for TLR4 as the Lps gene product. Journal of Immunology *162*, 3749-3752.

Jarjour, M., Jorquera, A., Mondor, I., Wienert, S., Narang, P., Coles, M.C., Klauschen, F., and Bajenoff, M. (2014). Fate mapping reveals origin and dynamics of lymph node follicular dendritic cells. Journal of Experimental Medicine *211*, 1109-1122.

Jawdat, D.M., Rowden, G., and Marshall, J.S. (2006). Mast cells have a pivotal role in TNF-independent lymph node hypertrophy and the mobilization of Langerhans cells in response to bacterial peptidoglycan. Journal of Immunology *177*, 1755-1762.

Junt, T., Moseman, E.A., Iannacone, M., Massberg, S., Lang, P.A., Boes, M., Fink, K., Henrickson, S.E., Shayakhmetov, D.M., Di Paolo, N.C.*, et al.* (2007). Subcapsular sinus macrophages in lymph nodes clear lymph-borne viruses and present them to antiviral B cells. Nature *450*, 110-+.

Junt, T., Scandella, E., and Ludewig, B. (2008). Form follows function: lymphoid tissue microarchitecture in antimicrobial immune defence. Nat Rev Immunol *8*, 764-775.

Kaldjian, E.P., Gretz, J.E., Anderson, A.O., Shi, Y., and Shaw, S. (2001). Spatial and molecular organization of lymph node T cell cortex: a labyrinthine cavity bounded by an epithelium-like monolayer of fibroblastic reticular cells anchored to basement membrane-like extracellular matrix. Int Immunol *13*, 1243-1253.

Kalluri, R., and Zeisberg, M. (2006). Fibroblasts in cancer. Nat Rev Cancer *6*, 392-401.

Katakai, T. (2012). Marginal reticular cells: a stromal subset directly descended from the lymphoid tissue organizer. Front Immunol *3*, 200.

Katakai, T., Hara, T., Lee, J.H., Gonda, H., Sugai, M., and Shimizu, A. (2004a). A novel reticular stromal structure in lymph node cortex: an immuno-platform for interactions among dendritic cells, T cells and B cells. International Immunology *16*, 1133-1142.

Katakai, T., Hara, T., Sugai, M., Gonda, H., and Shimizu, A. (2004b). Lymph node fibroblastic reticular cells construct the stromal reticulum via contact with lymphocytes. J Exp Med *200*, 783-795.

Katakai, T., Suto, H., Sugai, M., Gonda, H., Togawa, A., Suematsu, S., Ebisuno, Y., Katagiri, K., Kinashi, T., and Shimizu, A. (2008). Organizer-like reticular stromal cell layer common to adult secondary lymphoid organs. Journal of Immunology *181*, 6189-6200.

Khan, O., Headley, M., Gerard, A., Wei, W., Liu, L., and Krummel, M.F. (2011). Regulation of T cell priming by lymphoid stroma. PLoS One *6*, e26138.

Kinoshita, K., Harigai, M., Fagarasan, S., Muramatsu, M., and Honjo, T. (2001). A hallmark of active class switch recombination: Transcripts directed by I promoters on looped-out circular DNAs. P Natl Acad Sci USA *98*, 12620-12623.

Koni, P.A., Sacca, R., Lawton, P., Browning, J.L., Ruddle, N.H., and Flavell, R.A. (1997). Distinct roles in lymphoid organogenesis for lymphotoxins alpha and beta revealed in lymphotoxin beta-deficient mice. Immunity *6*, 491-500.

Kranich, J., Krautler, N.J., Heinen, E., Polymenidou, M., Bridel, C., Schildknecht, A., Huber, C., Kosco-Vilbois, M.H., Zinkernagel, R., Miele, G., and Aguzzi, A. (2008). Follicular dendritic cells control engulfment of apoptotic bodies by secreting Mfge8. Journal of Experimental Medicine *205*, 1293-1302.

Krautler, N.J., Kana, V., Kranich, J., Tian, Y., Perera, D., Lemm, D., Schwarz, P., Armulik, A., Browning, J.L., Tallquist, M.*, et al.* (2012). Follicular dendritic cells emerge from ubiquitous perivascular precursors. Cell *150*, 194-206.

Kumar, V., Scandella, E., Danuser, R., Onder, L., Nitschke, M., Fukui, Y., Halin, C., Ludewig, B., and Stein, J.V. (2010). Global lymphoid tissue remodeling during a viral infection is orchestrated by a B cell-lymphotoxin-dependent pathway. Blood *115*, 4725-4733.

Kunkel, E.J., and Butcher, E.C. (2003). Plasma-cell homing. Nat Rev Immunol *3*, 822-829.

Lee, J.W., Epardaud, M., Sun, J., Becker, J.E., Cheng, A.C., Yonekura, A.R., Heath, J.K., and Turley, S.J. (2007). Peripheral antigen display by lymph node stroma promotes T cell tolerance to intestinal self. Nat Immunol *8*, 181-190.

Liao, S., and Ruddle, N.H. (2006). Synchrony of high endothelial venules and lymphatic vessels revealed by immunization. J Immunol *177*, 3369-3379.

Link, A., Hardie, D.L., Favre, S., Britschgi, M.R., Adams, D.H., Sixt, M., Cyster, J.G., Buckley, C.D., and Luther, S.A. (2011). Association of T-zone reticular networks and conduits with ectopic lymphoid tissues in mice and humans. Am J Pathol *178*, 1662-1675.

Link, A., Vogt, T.K., Favre, S., Britschgi, M.R., Acha-Orbea, H., Hinz, B., Cyster, J.G., and Luther, S.A. (2007). Fibroblastic reticular cells in lymph nodes regulate the homeostasis of naive T cells. Nat Immunol *8*, 1255-1265.

Lo, C.G., Xu, Y., Proia, R.L., and Cyster, J.G. (2005). Cyclical modulation of sphingosine-1-phosphate receptor 1 surface expression during lymphocyte recirculation and relationship to lymphoid organ transit. Journal of Experimental Medicine *201*, 291-301.

Lukacs-Kornek, V., Malhotra, D., Fletcher, A.L., Acton, S.E., Elpek, K.G., Tayalia, P., Collier, A.R., and Turley, S.J. (2011). Regulated release of nitric oxide by nonhematopoietic stroma controls expansion of the activated T cell pool in lymph nodes. Nat Immunol *12*, 1096-U1105.

Luther, S.A., Tang, H.L., Hyman, P.L., Farr, A.G., and Cyster, J.G. (2000). Coexpression of the chemokines ELC and SLC by T zone stromal cells and deletion of the ELC gene in the plt/plt mouse. P Natl Acad Sci USA *97*, 12694-12699.

Magnusson, F.C., Liblau, R.S., Von Boehmer, H., Pittet, M.J., Lee, J.W., Turley, S.J., and Khazaie, K. (2008). Direct presentation of antigen by lymph node stromal cells protects against CD8 T-cell-mediated intestinal autoimmunity. Gastroenterology *134*, 1028-1037.

Malhotra, D., Fletcher, A.L., Astarita, J., Lukacs-Kornek, V., Tayalia, P., Gonzalez, S.F., Elpek, K.G., Chang, S.K., Knoblich, K., Hemler, M.E.*, et al.* (2012). Transcriptional profiling of stroma from inflamed and resting lymph nodes defines immunological hallmarks. Nat Immunol *13*, 499-510.

Manley, P.W., Furet, P., Bold, G., Bruggen, J., Mestan, J., Meyer, T., Schnell, C.R., Wood, J., Haberey, M., Huth, A.*, et al.* (2002). Anthranilic acid amides: a novel class of antiangiogenic VEGF receptor kinase inhibitors. J Med Chem *45*, 5687-5693.

Manley, P.W., Stiefl, N., Cowan-Jacob, S.W., Kaufman, S., Mestan, J., Wartmann, M., Wiesmann, M., Woodman, R., and Gallagher, N. (2010). Structural resemblances and comparisons of the relative pharmacological properties of imatinib and nilotinib. Bioorg Med Chem *18*, 6977-6986.

Marsland, B.J., Battig, P., Bauer, M., Ruedl, C., Lassing, U., Beerli, R.R., Dietmeier, K., Ivanova, L., Pfister, T., Vogt, L.*, et al.* (2005). CCL19 and CCL21 induce a potent proinflammatory differentiation program in licensed dendritic cells. Immunity *22*, 493-505.

MartIn-Fontecha, A., Sebastiani, S., Hopken, U.E., Uguccioni, M., Lipp, M., Lanzavecchia, A., and Sallusto, F. (2003). Regulation of dendritic cell migration to the draining lymph node: impact on T lymphocyte traffic and priming. J Exp Med *198*, 615-621.

Matloubian, M., Lo, C.G., Cinamon, G., Lesneski, M.J., Xu, Y., Brinkmann, V., Allende, M.L., Proia, R.L., and Cyster, J.G. (2004). Lymphocyte egress from thymus and peripheral lymphoid organs is dependent on S1P receptor 1. Nature *427*, 355-360.

McLachlan, J.B., Hart, J.P., Pizzo, S.V., Shelburne, C.P., Staats, H.F., Gunn, M.D., and Abraham, S.N. (2003). Mast cell-derived tumor necrosis factor induces hypertrophy of draining lymph nodes during infection. Nat Immunol *4*, 1199-1205.

Mempel, T.R., Henrickson, S.E., and Von Andrian, U.H. (2004). T-cell priming by dendritic cells in lymph nodes occurs in three distinct phases. Nature *427*, 154-159.

Mirza, H., Wu, Z.N., Kidwai, F., and Tan, K.S.W. (2011). A Metronidazole-Resistant Isolate of Blastocystis spp. Is Susceptible to Nitric Oxide and Downregulates Intestinal Epithelial Inducible Nitric Oxide Synthase by a Novel Parasite Survival Mechanism. Infect Immun *79*, 5019-5026.

Miyasaka, M., and Tanaka, T. (2004). Lymphocyte trafficking across high endothelial venules: dogmas and enigmas. Nat Rev Immunol *4*, 360-370.

Mohr, E., Serre, K., Manz, R.A., Cunningham, A.F., Khan, M., Hardie, D.L., Bird, R., and MacLennan, I.C.M. (2009). Dendritic Cells and Monocyte/Macrophages That Create the IL-6/APRIL-Rich Lymph Node Microenvironments Where Plasmablasts Mature. Journal of Immunology *182*, 2113-2123.

Moon, J.J., Chu, H.H., Pepper, M., McSorley, S.J., Jameson, S.C., Kedl, R.M., and Jenkins, M.K. (2007). Naive CD4(+) T cell frequency varies for different epitopes and predicts repertoire diversity and response magnitude. Immunity *27*, 203-213.

Mora, J.R., Iwata, M., Eksteen, B., Song, S.Y., Junt, T., Senman, B., Otipoby, K.L., Yokota, A., Takeuchi, H., Ricciardi-Castagnoli, P.*, et al.* (2006). Generation of gut-homing IgA-secreting B cells by intestinal dendritic cells. Science *314*, 1157-1160.

Moussion, C., and Girard, J.P. (2011). Dendritic cells control lymphocyte entry to lymph nodes through high endothelial venules. Nature *479*, 542-U273.

Mowat, A.M. (2003). Anatomical basis of tolerance and immunity to intestinal antigens. Nat Rev Immunol *3*, 331-341.

Mueller, S.N., and Germain, R.N. (2009). Stromal cell contributions to the homeostasis and functionality of the immune system. Nature Reviews Immunology *9*, 618-629.

Mueller, S.N., Hosiawa-Meagher, K.A., Konieczny, B.T., Sullivan, B.M., Bachmann, M.F., Locksley, R.M., Ahmed, R., and Matloubian, M. (2007). Regulation of homeostatic chemokine expression and cell trafficking during immune responses. Science *317*, 670-674.

Muller, U., Steinhoff, U., Reis, L.F., Hemmi, S., Pavlovic, J., Zinkernagel, R.M., and Aguet, M. (1994). Functional role of type I and type II interferons in antiviral defense. Science *264*, 1918-1921.

Navarro, A., Perez, R.E., Rezaiekhaligh, M., Mabry, S.M., and Ekekezie, II (2008). T1alpha/podoplanin is essential for capillary morphogenesis in lymphatic endothelial cells. Am J Physiol Lung Cell Mol Physiol *295*, L543-551.

Navarro, A., Perez, R.E., Rezaiekhaligh, M.H., Mabry, S.M., and Ekekezie, I.I. (2011). Polarized migration of lymphatic endothelial cells is critically dependent on podoplanin regulation of Cdc42. Am J Physiol-Lung C *300*, L32-L42.

Ngo, V.N., Cornall, R.J., and Cyster, J.G. (2001). Splenic T zone development is B cell dependent. Journal of Experimental Medicine *194*, 1649-1660.

Ngo, V.N., Korner, H., Gunn, M.D., Schmidt, K.N., Riminton, D.S., Cooper, M.D., Browning, J.L., Sedgwick, J.D., and Cyster, J.G. (1999). Lymphotoxin alpha/beta and tumor necrosis factor are required for stromal cell expression of homing chemokines in B and T cell areas of the spleen. J Exp Med *189*, 403-412.

Nolte, M.A., Belien, J.A.M., Schadee-Eestermans, I., Jansen, W., Unger, W.W.J., van Rooijen, N., Kraal, G., and Mebius, R.E. (2003). A conduit system distributes chemokines and small blood-borne molecules through the splenic white pulp. Journal of Experimental Medicine *198*, 505-512.

Noss, E.H., and Brenner, M.B. (2008). The role and therapeutic implications of fibroblast-like synoviocytes in inflammation and cartilage erosion in rheumatoid arthritis. Immunol Rev *223*, 252-270.

Okada, T., and Cyster, J.G. (2007). CC chemokine receptor 7 contributes to Gi-dependent T cell motility in the lymph node. J Immunol *178*, 2973-2978.

Onder, L., Narang, P., Scandella, E., Chai, Q., Iolyeva, M., Hoorweg, K., Halin, C., Richie, E., Kaye, P., Westermann, J.*, et al.* (2012). IL-7-producing stromal cells are critical for lymph node remodeling. Blood *120*, 4675-4683.

Oracki, S.A., Walker, J.A., Hibbs, M.L., Corcoran, L.M., and Tarlinton, D.M. (2010). Plasma cell development and survival. Immunol Rev *237*, 140-159.

Osada, M., Inoue, O., Ding, G., Shirai, T., Ichise, H., Hirayama, K., Takano, K., Yatomi, Y., Hirashima, M., Fujii, H.*, et al.* (2012). Platelet Activation Receptor CLEC-2 Regulates Blood/Lymphatic Vessel Separation by Inhibiting Proliferation, Migration, and Tube Formation of Lymphatic Endothelial Cells. Journal of Biological Chemistry *287*, 22241-22252.

Pabst, O. (2012). New concepts in the generation and functions of IgA. Nature Reviews Immunology *12*, 821-832.

Palframan, R.T., Jung, S., Cheng, G., Weninger, W., Luo, Y., Dorf, M., Littman, D.R., Rollins, B.J., Zweerink, H., Rot, A., and von Andrian, U.H. (2001). Inflammatory chemokine transport and presentation in HEV: a remote control mechanism for monocyte recruitment to lymph nodes in inflamed tissues. J Exp Med *194*, 1361-1373.

Peduto, L., Dulauroy, S., Lochner, M., Spath, G.F., Morales, M.A., Cumano, A., and Eberl, G. (2009). Inflammation recapitulates the ontogeny of lymphoid stromal cells. Journal of Immunology *182*, 5789-5799.

Pham, T.H.M., Baluk, P., Xu, Y., Grigorova, I., Bankovich, A.J., Pappu, R., Coughlin, S.R., McDonald, D.M., Schwab, S.R., and Cyster, J.G. (2010). Lymphatic endothelial cell sphingosine kinase activity is required for lymphocyte egress and lymphatic patterning. Journal of Experimental Medicine *207*, 17-27.

Pham, T.H.M., Okada, T., Matioubian, M., Lo, C.G., and Cyster, J.G. (2008). S1P(1) receptor signaling overrides retention mediated by G alpha(i)-coupled receptors to promote T cell egress. Immunity *28*, 122-133.

Pinchuk, I.V., Beswick, E.J., Saida, J.I., Reyes, V.E., and Powell, D.W. (2007). Human colonic myofibroblasts promote the expansion of Cd4+Cd25high Foxp3+regulatory T cells. Gastroenterology *132*, A397-A397.

Pinchuk, I.V., Mifflin, R.C., Saada, J.I., and Powell, D.W. (2010). Intestinal mesenchymal cells. Curr Gastroenterol Rep *12*, 310-318.

Powell, D.W., Pinchuk, I.V., Saada, J.I., Chen, X., and Mifflin, R.C. (2011). Mesenchymal Cells of the Intestinal Lamina Propria. Annu Rev Physiol *73*, 213-237.

Prlic, M., Hernandez-Hoyos, G., and Bevan, M.J. (2006). Duration of the initial TCR stimulus controls the magnitude but not functionality of the CD8+ T cell response. J Exp Med *203*, 2135-2143.

Probst, H.C., Tschannen, K., Odermatt, B., Schwendener, R., Zinkernagel, R.M., and Van Den Broek, M. (2005). Histological analysis of CD11c-DTR/GFP mice after in vivo depletion of dendritic cells. Clin Exp Immunol *141*, 398-404.

Pula, B., Witkiewicz, W., Dziegiel, P., and Podhorska-Okolow, M. (2013). Significance of podoplanin expression in cancer-associated fibroblasts: A comprehensive review. Int J Oncol *42*, 1849-1857.

Randall, T.D., Carragher, D.M., and Rangel-Moreno, J. (2008). Development of secondary lymphoid organs. Annu Rev Immunol *26*, 627-650.

Randolph, G.J., Angeli, V., and Swartz, M.A. (2005). Dendritic-cell trafficking to lymph nodes through lymphatic vessels. Nature Reviews Immunology *5*, 617-628.

Randolph, G.J., Ochando, J., and Partida-Sanchez, S. (2008). Migration of dendritic cell subsets and their precursors. Annual Review of Immunology *26*, 293-316.

Reilkoff, R.A., Bucala, R., and Herzog, E.L. (2011). Fibrocytes: emerging effector cells in chronic inflammation. Nat Rev Immunol *11*, 427-435.

Repass, J.F., Laurent, M.N., Carter, C., Reizis, B., Bedford, M.T., Cardenas, K., Narang, P., Coles, M., and Richie, E.R. (2009). IL7-hCD25 and IL7-Cre BAC Transgenic Mouse Lines: New Tools for Analysis of IL-7 Expressing Cells. Genesis *47*, 281-287.

Roozendaal, R., and Mebius, R.E. (2011). Stromal Cell-Immune Cell Interactions. Annual Review of Immunology, Vol 29 *29*, 23-43.

Roozendaal, R., Mebius, R.E., and Kraal, G. (2008). The conduit system of the lymph node. International Immunology *20*, 1483-1487.

Roozendaal, R., Mempel, T.R., Pitcher, L.A., Gonzalez, S.F., Verschoor, A., Mebius, R.E., von Andrian, U.H., and Carroll, M.C. (2009). Conduits Mediate Transport of Low-Molecular-Weight Antigen to Lymph Node Follicles. Immunity *30*, 264-276.

Round, J.L., and Mazmanian, S.K. (2009). The gut microbiota shapes intestinal immune responses during health and disease (vol 9, pg 313, 2009). Nature Reviews Immunology *9*, 600-600.

Saada, J.I., Pinchuk, I.V., Barrera, C.A., Adegboyega, P.A., Suarez, G., Mifflin, R.C., Di Mari, J.F., Reyes, V.E., and Powell, D.W. (2006). Subepithelial myofibroblasts are novel nonprofessional APCs in the human colonic mucosa. Journal of Immunology *177*, 5968-5979.

Sakaguchi, S., Yamaguchi, T., Nomura, T., and Ono, M. (2008). Regulatory T cells and immune tolerance. Cell *133*, 775-787.

Sato, A., Hashiguchi, M., Toda, E., Iwasaki, A., Hachimura, S., and Kaminogawa, S. (2003). CD11b(+) Peyer's patch dendritic cells secrete IL-6 and induce IgA secretion from naive B cells. Journal of Immunology *171*, 3684-3690.

Scandella, E., Bolinger, B., Lattmann, E., Miller, S., Favre, S., Littman, D.R., Finke, D., Luther, S.A., Junt, T., and Ludewig, B. (2008). Restoration of lymphoid organ integrity through the interaction of lymphoid tissue-inducer cells with stroma of the T cell zone. Nat Immunol *9*, 667-675.

Schluns, K.S., Kieper, W.C., Jameson, S.C., and Lefrancois, L. (2000). Interleukin-7 mediates the homeostasis of naive and memory CD8 T cells in vivo. Nat Immunol *1*, 426-432.

Schneider, K., Potter, K.G., and Ware, C.F. (2004). Lymphotoxin and LIGHT signaling pathways and target genes. Immunol Rev *202*, 49-66.

Sekirov, I., Russell, S.L., Antunes, L.C.M., and Finlay, B.B. (2010). Gut Microbiota in Health and Disease. Physiol Rev *90*, 859-904.

Senn, K.A., McCoy, K.D., Maloy, K.J., Stark, G., Frohli, E., Rulicke, T., and Klemenz, R. (2000). T1-deficient and T1-Fc-transgenic mice develop a normal protective Th2-type immune response following infection with Nippostrongylus brasiliensis. Eur J Immunol *30*, 1929-1938.

Shapiro-Shelef, M., and Calame, K. (2005). Regulation of plasma-cell development. Nature Reviews Immunology *5*, 230-242.

Shevach, E.M. (2006). From vanilla to 28 flavors: Multiple varieties of T regulatory cells. Immunity *25*, 195-201.

Siegert, S., Huang, H.Y., Yang, C.Y., Scarpellino, L., Carrie, L., Essex, S., Nelson, P.J., Heikenwalder, M., Acha-Orbea, H., Buckley, C.D.*, et al.* (2011). Fibroblastic Reticular Cells From Lymph Nodes Attenuate T Cell Expansion by Producing Nitric Oxide. Plos One *6*.

Sinha, R.K., Park, C., Hwang, I.Y., Davis, M.D., and Kehrl, J.H. (2009). B Lymphocytes Exit Lymph Nodes through Cortical Lymphatic Sinusoids by a Mechanism Independent of Sphingosine-1-Phosphate-Mediated Chemotaxis. Immunity *30*, 434-446.

Sixt, M., Kanazawa, N., Seig, M., Samson, T., Roos, G., Reinhardt, D.P., Pabst, R., Lutz, M.B., and Sorokin, L. (2005). The conduit system transports soluble antigens from the afferent lymph to resident dendritic cells in the T cell area of the lymph node. Immunity *22*, 19-29.

Soderberg, K.A., Payne, G.W., Sato, A., Medzhitov, R., Segal, S.S., and Iwasaki, A. (2005). Innate control of adaptive immunity via remodeling of lymph node feed arteriole. P Natl Acad Sci USA *102*, 16315-16320.

Spadoni, I., Iliev, I.D., Rossi, G., and Rescigno, M. (2012). Dendritic cells produce TSLP that limits the differentiation of Th17 cells, fosters Treg development, and protects against colitis. Mucosal Immunol *5*, 184-193.

Steeber, D.A., Erickson, C.M., Hodde, K.C., and Albrecht, R.M. (1987). Vascular Changes in Popliteal Lymph-Nodes Due to Antigen Challenge in Normal and Lethally Irradiated Mice. Scanning Microscopy *1*, 831-839.

Stein, J.V., Rot, A., Luo, Y., Narasimhaswamy, M., Nakano, H., Gunn, M.D., Matsuzawa, A., Quackenbush, E.J., Dorf, M.E., and von Andrian, U.H. (2000). The CC chemokine thymus-derived chemotactic agent 4 (TCA-4, secondary lymphoid tissue chemokine, 6Ckine, exodus-2) triggers lymphocyte function-associated antigen 1-mediated arrest of rolling T lymphocytes in peripheral lymph node high endothelial venules. J Exp Med *191*, 61-76.

Sun, C.M., Hall, J.A., Blank, R.B., Bouladoux, N., Oukka, M., Mora, J.R., and Belkaid, Y. (2007). Small intestine lamina propria dendritic cells promote de novo generation of Foxp3 T reg cells via retinoic acid. J Exp Med *204*, 1775-1785.

Sun, Z., Unutmaz, D., Zou, Y.R., Sunshine, M.J., Pierani, A., Brenner-Morton, S., Mebius, R.E., and Littman, D.R. (2000). Requirement for RORgamma in thymocyte survival and lymphoid organ development. Science *288*, 2369-2373.

Takahashi-Iwanaga, H., and Fujita, T. (1985). Lamina propria of intestinal mucosa as a typical reticular tissue. A scanning electron-microscopic study of the rat jejunum. Cell Tissue Res *242*, 57-66.

Takeuchi, O., Hoshino, K., Kawai, T., Sanjo, H., Takada, H., Ogawa, T., Takeda, K., and Akira, S. (1999). Differential roles of TLR2 and TLR4 in recognition of gram-negative and gram-positive bacterial cell wall components. Immunity *11*, 443-451.

Tan, K.W., Yeo, K.P., Wong, F.H.S., Lim, H.Y., Khoo, K.L., Abastado, J.P., and Angeli, V. (2012). Expansion of Cortical and Medullary Sinuses Restrains Lymph Node Hypertrophy during Prolonged Inflammation. Journal of Immunology *188*, 4065-4080.

Terstappen, L.W.M.M., Johnsen, S., Segersnolten, I.M.J., and Loken, M.R. (1990). Identification and Characterization of Plasma-Cells in Normal Human Bone-Marrow by High-Resolution Flow-Cytometry. Blood *76*, 1739-1747.

Tew, J.G., Wu, J.H., Fakher, M., Szakal, A.K., and Qin, D.H. (2001). Follicular dendritic cells: beyond the necessity of T-cell help. Trends Immunol *22*, 361-367.

Tezuka, H., Abe, Y., Iwata, M., Takeuchi, H., Ishikawa, H., Matsushita, M., Shiohara, T., Akira, S., and Ohteki, T. (2007). Regulation of IgA production by naturally occurring TNF/iNOS-producing dendritic cells. Nature *448*, 929-U927.

Tomasek, J.J., Gabbiani, G., Hinz, B., Chaponnier, C., and Brown, R.A. (2002). Myofibroblasts and mechano-regulation of connective tissue remodelling. Nat Rev Mol Cell Biol *3*, 349-363.

Tomei, A.A., Siegert, S., Britschgi, M.R., Luther, S.A., and Swartz, M.A. (2009). Fluid Flow Regulates Stromal Cell Organization and CCL21 Expression in a Tissue-Engineered Lymph Node Microenvironment. Journal of Immunology *183*, 4273-4283.

Turley, S.J., Fletcher, A.L., and Elpek, K.G. (2010). The stromal and haematopoietic antigen-presenting cells that reside in secondary lymphoid organs. Nature Reviews Immunology *10*, 813-825.

Tzeng, T.C., Chyou, S., Tian, S., Webster, B., Carpenter, A.C., Guaiquil, V.H., and Lu, T.T. (2010). CD11c(hi) dendritic cells regulate the re-establishment of vascular quiescence and stabilization after immune stimulation of lymph nodes. J Immunol *184*, 4247-4257.

Ushiki, T., Ohtani, O., and Abe, K. (1995). Scanning electron microscopic studies of reticular framework in the rat mesenteric lymph node. Anat Rec *241*, 113-122.

van de Pavert, S.A., Olivier, B.J., Goverse, G., Vondenhoff, M.F., Greuter, M., Beke, P., Kusser, K., Hopken, U.E., Lipp, M., Niederreither, K.*, et al.* (2009). Chemokine CXCL13 is essential for lymph node initiation and is induced by retinoic acid and neuronal stimulation. Nat Immunol *10*, 1193-U1178.

Vega, F., Coombes, K.R., Thomazy, V.A., Patel, K., Lang, W.H., and Jones, D. (2006). Tissue-specific function of lymph node fibroblastic reticulum cells. Pathobiology *73*, 71-81.

Vicente-Suarez, I., Larange, A., Reardon, C., Matho, M., Feau, S., Chodaczek, G., Park, Y., Obata, Y., Gold, R., Wang-Zhu, Y.*, et al.* (2014). Unique lamina propria stromal cells imprint the functional phenotype of mucosal dendritic cells. Mucosal Immunol.

Vogt, T.K., Link, A., Perrin, J., Finke, D., and Luther, S.A. (2009). Novel function for interleukin-7 in dendritic cell development. Blood *113*, 3961-3968.

von Andrian, U.H., and Mempel, T.R. (2003). Homing and cellular traffic in lymph nodes. Nat Rev Immunol *3*, 867-878.

Ware, C.F. (2008). Targeting lymphocyte activation through the lymphotoxin and LIGHT pathways. Immunol Rev *223*, 186-201.

Webster, B., Ekland, E.H., Agle, L.M., Chyou, S., Ruggieri, R., and Lu, T.T. (2006). Regulation of lymph node vascular growth by dendritic cells. Journal of Experimental Medicine *203*, 1903-1913.

Wendland, M., Willenzon, S., Kocks, J., Davalos-Misslitz, A.C., Hammerschmidt, S.I., Schumann, K., Kremmer, E., Sixt, M., Hoffmeyer, A., Pabst, O., and Forstert, R. (2011). Lymph Node T Cell Homeostasis Relies on Steady State Homing of Dendritic Cells. Immunity *35*, 945-957.

Wilting, J., Papoutsi, M., Christ, B., Nicolaides, K.H., von Kaisenberg, C.S., Borges, J., Stark, G.B., Alitalo, K., Tomarev, S.I., Niemeyer, C., and Rossler, J. (2002). The transcription factor Prox1 is a marker for lymphatic endothelial cells in normal and diseased human tissues. Faseb J *16*, 1271-+.

Worbs, T., Mempel, T.R., Bolter, J., von Andrian, U.H., and Forster, R. (2007). CCR7 ligands stimulate the intranodal motility of T lymphocytes in vivo. Journal of Experimental Medicine *204*, 489-495.

Wu, J.F., Chitapanarux, T., Chen, Y.S., Soon, R.K., and Yee, H.F. (2013). Intestinal myofibroblasts produce nitric oxide in response to combinatorial cytokine stimulation. J Cell Physiol *228*, 572-580.

Yamamoto, M., Sato, S., Hemmi, H., Hoshino, K., Kaisho, T., Sanjo, H., Takeuchi, O., Sugiyama, M., Okabe, M., Takeda, K., and Akira, S. (2003). Role of adaptor TRIF in the MyD88-independent toll-like receptor signaling pathway. Science *301*, 640-643.

Yanagawa, Y., and Onoe, K. (2002). CCL19 induces rapid dendritic extension of murine dendritic cells. Blood *100*, 1948-1956.

Yanagawa, Y., and Onoe, K. (2003). CCR7 ligands induce rapid endocytosis in mature dendritic cells with concomitant up-regulation of Cdc42 and Rac activities. Blood *101*, 4923-4929.

Yip, L.D., Su, L., Sheng, D.Q., Chang, P., Atkinson, M., Czesak, M., Albert, P.R., Collier, A.R., Turley, S.J., Fathman, C.G., and Creusot, R.J. (2009). Deaf1 isoforms control the expression of genes encoding peripheral tissue antigens in the pancreatic lymph nodes during type 1 diabetes. Nat Immunol *10*, 1026-U1107.

Zhang, Z.B., Andoh, A., Inatomi, O., Bamba, S., Takayanagi, A., Shimizu, N., and Fujiyama, Y. (2005). Interleukin-17 and lipopolysaccharides synergistically induce cyclooxygenase-2 expression in human intestinal myofibroblasts. J Gastroen Hepatol *20*, 619-627.

Zhu, M.Z., and Fu, Y.X. (2011). The role of core TNF/LIGHT family members in lymph node homeostasis and remodeling. Immunol Rev *244*, 75-84.

Zhu, Y.T., Zhu, M., and Lance, P. (2012). iNOS signaling interacts with COX-2 pathway in colonic fibroblasts. Exp Cell Res *318*, 2116-2127.

7. List of publications during PhD

- Siegert S, Huang HY, **_Yang CY_**, Scarpellino L, Carrie L, Essex S, Nelson PJ, Heikenwalder M, Acha-Orbea H, Buckley CD, Marsland BJ, Zehn D, Luther SA ¨Fibroblastic reticular cells from lymph nodes attenuate T cell expansion by producing nitric oxide¨ *PLoS One 6(11):e27618, 2011*

- **_Yang CY_**, Vogt TK, Favre S, Scarpellino L, Huang HY, Tacchini-Cottier F, Luther SA ¨Trapping of naive lymphocytes triggers rapid growth and remodeling of the fibroblast network in reactive murine lymph nodes¨ *Proc Natl Acad Sci USA, 111(1):E109-18, 2014*